

*Leishmania major* drives host phagocyte death and cell-to-cell transfer depending on intracellular pathogen proliferation rate

**Thesis**

for the degree of

**doctor rerum naturalium (Dr. rer. nat.)**

approved by the Faculty of Natural Sciences of Otto von Guericke University Magdeburg

by M.Sc. Iris Baars

born on January 11, 1994 in De Marne (The Netherlands)

Examiner: Prof. Dr. Andreas Müller

Prof. Dr. Friedrich Frischknecht

submitted on: February 26, 2024 defended on:

December 02, 2024

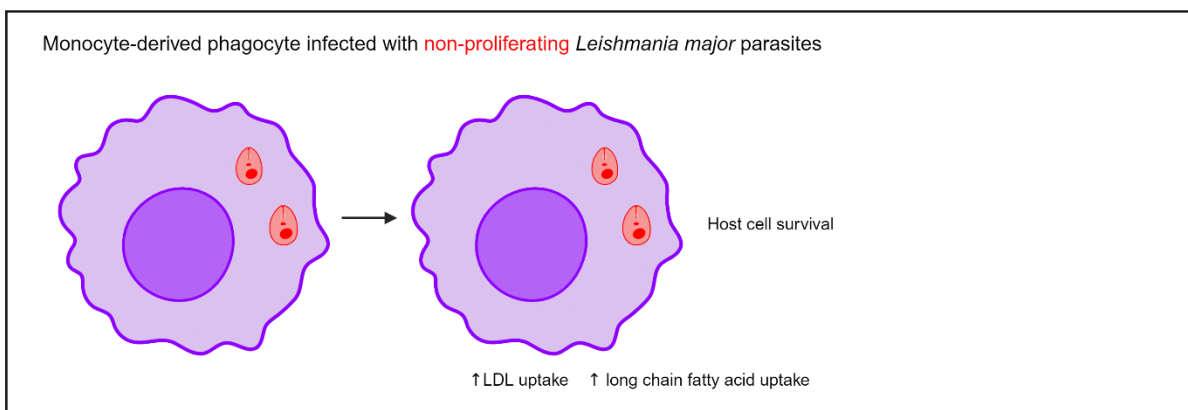
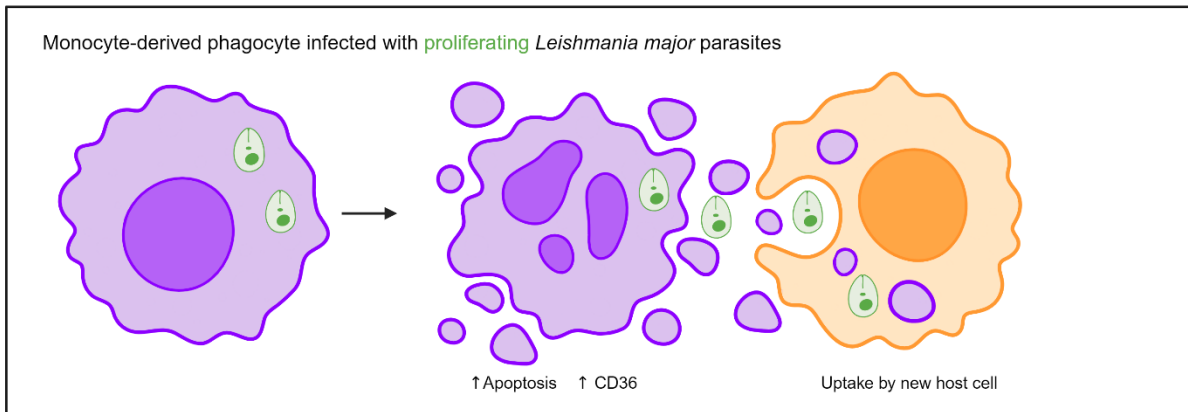
**ABSTRACT**

M. Sc., Baars, Iris: „*Leishmania major* drives host phagocyte death and cell-to-cell transfer depending on intracellular pathogen proliferation rate”

The virulence of intracellular pathogens relies largely on the ability to survive and replicate within phagocytes, but also on the release and transfer into new host cells. Such cell-to-cell transfer could represent a target for counteracting microbial pathogenesis. However, our understanding of the underlying cellular and molecular processes remains woefully insufficient. Therefore, we studied *Leishmania major* (*L. major*) cell-to-cell transfer among monocyte-derived cells and investigated the involvement of monocyte-derived host cell death and altered host cell metabolism in such transfer events. Using depletion of *Leishmania*-permissive CD11c-expressing monocyte-derived host cells in vivo, we were able to show that CD11c<sup>+</sup> cells play a dual role in the ongoing infection, functioning both as host cells for *L. major* parasites and as inducers of iNOS, an important contributor in *Leishmania* clearance. In order to study *L. major* transfer among these monocyte-derived cells, we quantified *L. major* transfer and uptake of host cell material together with the parasite into adoptively transferred cells in vivo using intravital 2-photon microscopy analysis and flow cytometry analysis of CD11c-YFP reporter mice. Transfer of the parasite to new host cells occurred directly without a detectable extracellular state, and was associated with concomitant uptake of cellular material from the original host cell. By visualising cell death using live cell imaging, and using intravital 2-photon imaging of a Förster resonance energy transfer-based (FRET-based) cell-death-biosensor, we next studied whether apoptosis of the original host affects *L. major* transfer. Using intravital 2-photon microscopy of caspase-3 activation in the *L. major*-infected live skin and using a caspase-3 reporter assay in *L. major*-infected human monocyte-derived macrophages, we showed increased apoptosis in cells infected by the parasite. To see whether intracellular parasite proliferation affects the fate of the infected host cell, we studied intracellular *L. major* proliferation in relation to cellular changes in murine intraperitoneal and bone marrow-derived macrophages using a photoconversion-based proliferation biosensor in vitro. In this regard, we observed a relation between high pathogen proliferation and cell death in infected cells, and long-term residency within an infected host cell was only possible for slowly proliferating parasites. Interestingly, using proliferation-modified parasites, we were able to show that *L. major* proliferation induced cell death of the infected host cell and that intracellular parasite proliferation rate modified host cell metabolic pathways. More specifically, intracellular parasite proliferation reduced glucose uptake and increased the expression of CD36, a glycoprotein involved in high fatty acids uptake, in infected host macrophages. Regarding parasite proliferation and the microenvironment, we showed, using intravital imaging of the proliferation biosensor-infected murine ear dermis, that high proliferating parasites were more often observed in close proximity to blood vessels as compared to low proliferating parasites. This

might be due to reduced control by macrophages or by the increased likelihood of newly recruited monocyte-derived host cells present in this area. Lastly, we showed that IL-11 receptor signalling, which is suggested to play a role in phagocytosis, does not play a major role in recruitment and infection of monocytes during *L. major* infection in vivo. Taken together, our results suggest that *L. major* drives its own dissemination to new phagocytes by inducing host cell death in a proliferation-dependent manner. To our knowledge, we are the first to show evidence that *L. major* stimulates dissemination among phagocytes through parasite proliferation-dependent cell death. This newly obtained knowledge can serve as a starting point for the creation of innovative treatments that can inhibit the establishment of intracellular pathogens at their site of infection.

GRAPHICAL ABSTRACT



## ZUSAMMENFASSUNG

M. Sc., Baars, Iris: „*Leishmania major* drives host phagocyte death and cell-to-cell transfer depending on intracellular pathogen proliferation rate”

Die Virulenz intrazellulärer Krankheitserreger hängt weitgehend von ihrer Fähigkeit ab, in Phagozyten zu überleben und zu replizieren, aber auch von der Freisetzung aus solchen Phagozyten und dem Transfer in neue Wirtszellen. Dieser Zell-zu-Zell-Transfer könnte ein Angriffspunkt für die Bekämpfung der mikrobiellen Pathogenese sein, aber die zugrunde liegenden zellulären und molekularen Prozesse sind nach wie vor wenig charakterisiert. Daher wurde in der vorliegenden Arbeit der Zell-zu-Zell-Transfer des Parasiten *Leishmania major* (*L. major*) zwischen monozytenabgeleiteten Wirtszellen und die Beteiligung des Zelltods und Veränderungen im Stoffwechsel von infizierten Wirtszellen an diesen Prozessen untersucht. Mithilfe der Depletion von *Leishmania*-permissiven CD11c-exprimierenden monozytenabgeleiteten Wirtszellen in vivo konnten wir zeigen, dass CD11c<sup>+</sup>-Zellen eine doppelte Rolle bei der laufenden Infektion spielen und sowohl als Wirtszellen für *L. major*, als auch als Induktoren von iNOS, einem wichtiger Faktor bei der Beseitigung von Leishmanien, fungieren. Um den *L. major*-Transfer zwischen monozytenabgeleiteten Zellen zu untersuchen, quantifizierten wir den *L. major*-Transfer und die Aufnahme von Wirtszellmaterial zusammen mit dem Parasiten in adoptiv übertragene Zellen in vivo mithilfe der intravitale 2-Photonen-Mikroskopie und einer Durchflusszytometrie von CD11c-YFP-Reportermause. Die Übertragung des Parasiten auf neue Wirtszellen erfolgte direkt ohne erkennbaren extrazellulären Zustand und war mit der gleichzeitigen Aufnahme von Zellmaterial aus der ursprünglichen Wirtszelle verbunden. Als nächstes untersuchten wir, ob die Apoptose der ursprünglichen Wirtszelle den *L. major*-Transfer beeinflusst, indem wir den Zelltod im lebenden Gewebe visualisierten, wofür wir einen auf Fluoreszenzresonanzenergietransfer basierenden (FRET-basierten) Apoptose-Biosensor für die intravitale 2-Photonen-Bildgebung verwendeten. Mit diesem experimentellen Tiermodell und unter Verwendung eines Caspase-3-Reporter-Assays in mit *L. major* infizierten menschlichen monozytenabgeleiteten Makrophagen zeigten wir eine erhöhte Apoptose in mit dem Parasiten infizierten Zellen. Um herauszufinden, ob die intrazelluläre Parasitenproliferation das Schicksal der infizierten Wirtszelle beeinflusst, untersuchten wir die intrazelluläre *L. major*-Proliferation in Bezug auf zelluläre Veränderungen in murinen intraperitonealen und aus dem Knochenmark differenzierten Makrophagen unter Verwendung eines auf Photokonversion basierenden Proliferationsbiosensors in vitro. In diesem Zusammenhang beobachteten wir einen Zusammenhang zwischen hoher Pathogenproliferation und Zelltod in infizierten Zellen, und ein langfristiger Aufenthalt in einer infizierten Wirtszelle war nur für langsam proliferierende Parasiten möglich. Interessanterweise konnten wir mithilfe proliferationsmodifizierter Parasiten zeigen, dass die Proliferation von *L. major* den Zelltod der infizierten Wirtszelle induzierte und dass die intrazelluläre Parasitenproliferationsrate den Stoffwechsel der Wirtszelle

veränderte. Genauer gesagt reduzierte die intrazelluläre Parasitenvermehrung die Glukoseaufnahme und erhöhte die Expression von CD36, einem Glykoprotein das an der Aufnahme hoher Fettsäuren beteiligt ist. In Bezug auf die Parasitenproliferation zeigten wir außerdem mithilfe intravitaler Mikroskopie, dass stark proliferierende Parasiten häufiger in unmittelbarer Nähe von Blutgefäßen beobachtet wurden als niedrig proliferierende Parasiten, was möglicherweise darauf zurückzuführen ist, dass in diesem Bereich vermehrt neu rekrutierte aus monozytenabgeleiteten Wirtszellen vorhanden sind, für die bekannt ist, dass sie eine hohe Pathogenproliferation begünstigen. Schließlich haben wir gezeigt, dass die Signalübertragung des IL-11-Rezeptors, von dem angenommen wird, dass er eine Rolle bei der Phagozytose spielt, bei der Rekrutierung und Infektion von Monozyten während einer *L. major*-Infektion in vivo keinen Einfluss hat. Zusammenfassend legen unsere Ergebnisse nahe, dass *L. major* seine eigene Verbreitung in neue Phagozyten vorantreibt, indem der Parasit den Zelltod des Wirts in proliferationsabhängiger Weise induziert. Unseres Wissens nach sind wir die ersten, die Beweise dafür vorlegen konnten, dass *L. major* die Ausbreitung zwischen Phagozyten durch den durch die Proliferation des Parasiten bedingten Zelltod stimuliert. Dies kann als Ausgangspunkt für die Entwicklung innovativer Behandlungen dienen, die die Etablierung intrazellulärer Krankheitserreger an ihrem Standort hemmen können Ort der Infektion.

**ABBREVIATIONS**

2-NBDG	2-(N-(7-Nitrobenz-2-oxa-1,3-diazol-4-yl)Amino)-2-Deoxyglucose
AF	Alexa fluor
ALR	Aim2-like receptors
AMT	Aminoethyltrioxsalen
APC	Allophycocyanin
APC	Antigen-presenting cell
BCR	B cell receptor
BMC	Bone marrow chimera
BMDM	Bone marrow-derived macrophages
BV	Brilliant violet
C1/12	Short-/medium-chain fatty acids
C16	Long chain fatty acids
CCR2	C-C-motif chemokine receptor 2
CD	Cluster of differentiation
CFP	Cyan fluorescent protein
CFSE	Carboxyfluorescein succinimidyl ester
CL	Cutaneous Leishmaniasis
CR	Complement receptor
CXCL	Chemokine (C-X-C motif) ligand
DAPI	4',6-Diamidino-2-phenylindole dihydrochloride
DC	Dendritic cell
ddH <sub>2</sub> O	Double distilled water
DISC	Death-inducing signalling complex
dLN	Draining lymph node
VI	

DNA	Deoxyribonucleic acid
DTR	Diphtheria toxin receptor
DTX	Diphtheria toxin
<i>E. coli</i>	<i>Escherichia coli</i>
EDTA	Ethylenediaminetetraacetic acid
EGFP	Enhanced green fluorescent protein
FACS	Fluorescence-activated cell sorting
FAD	Flavin adenine nucleotide
Fas-L	Fas ligand
FCS	Fetal calf serum
FITC	Fluorescein isothiocyanate conjugate
FMN	Flavin mononucleotide
FRET	Förster resonance energy transfer
FSC	Forward Scatter
G-CSF	Granulocyte-colony stimulating factor
GFP	Green fluorescent protein
GLUT1	Glucose transporter 1
gp	Glycoprotein
GSDMD	Gasdermin D
HDGF	Hepatoma-derived growth factor
HMGB1	High mobility group box 1 protein
HSC	Hematopoietic stem cell
i.p.	Intraperitoneally
iNOS	Inducible nitric oxide synthase
IFN	Interferon

Ig	Immunoglobulin
IL	Interleukin
kb	Kilo bases
KBMA	Killed but metabolically active
<i>L. aethiopica</i>	<i>Leishmania (Leishmania) aethiopica</i>
<i>L. amazonensis</i>	<i>Leishmania (Leishmania) amazonensis</i>
<i>L. braziliensis</i>	<i>Leishmania (Viannia) braziliensis</i>
<i>L. chagasi</i>	<i>Leishmania (Leishmania) chagasi</i>
<i>L. donovani</i>	<i>Leishmania (Leishmania) donovani</i>
<i>L. guyanensis</i>	<i>Leishmania (Viannia) guyanensis</i>
<i>L. infantum</i>	<i>Leishmania (Leishmania) infantum</i>
<i>L. major</i>	<i>Leishmania (Leishmania) major</i>
<i>L. mexicana</i>	<i>Leishmania (Leishmania) mexicana</i>
<i>L. panamensis</i>	<i>Leishmania (Viannia) panamensis</i>
<i>L. peruviana</i>	<i>Leishmania (Viannia) peruviana</i>
<i>L. tropica</i>	<i>Leishmania (Leishmania) tropica</i>
<i>L. venezuelensis</i>	<i>Leishmania (Leishmania) venezuelensis</i>
L-NIL	N6-(1-iminoethyl)-L-lysine hydrochloride
LAP	LC3-associated phagocytosis
LdISP2	<i>Leishmania donovani</i> inhibitor of Serine Peptidases 2
LDL	Low-density lipoprotein
LED	Light-emitting diode
<i>Lm</i>	<i>Leishmania (Leishmania) major</i>
LP	Longpass
LPG	Lipophosphoglycan

LPS	Lipopolysachariden
LSM	Laser scanning microscope
M-CSF	Macrophages colony-stimulating factor
MAC	Membrane attack complex
MACS	Magnetic activated cell sorting
MBL	Mannose-binding lectin
MCL	Muco-cutaneous Leishmaniasis
MCL-1	Myeloid cell leukemia 1
MDM	Monocyte-derived macrophages
MFI	Mean fluorescence intensity
MHC	Histocompatibility complex
MIP	Macrophage inflammatory protein
MOI	Multiplicity of infection
MSCV	Mouse stem cell virus
NADPH	Nicotinamide adenine dinucleotide phosphate hydrogen
NE	Neutrophil elastase
NET	Neutrophil extracellular trap
NFκB	NF-kappaB
NK	Natural killer
NLR	Nod-like receptor
NLRP	Nod-like receptor protein
NO	Nitric oxide
NOD	Nucleotide-binding oligomerization domain protein
PAMP	Pathogen-associated molecular pattern
PBS	Phosphate-buffered saline

PCR	Polymerase chain reaction
PD-1	Programmed cell death-1
PE	Phycoerythrin
PerCP	Peridinin chlorophyll protein
PFA	Paraformaldehyde
PGN	Primarily peptidoglycan
PKDL	Post kala-azar dermal leishmaniasis
PRR	Pathogen recognition receptor
PS	Phosphatidylserine
PSM	Phenol-soluble modulin
qRT-PCR	Quantitative reverse transcription polymerase chain reaction
RIP	Receptor interacting protein
RIPK	Receptor interacting protein kinase
RLRs	RIG-I like receptors
RNA	Ribonucleic acid
RNI	Reactive nitrogen intermediate
RNS	Reactive nitrogen species
ROI	Respiratory burst-derived reactive oxygen intermediate
ROS	Reactive oxygen species
rpm	Revolutions per minute
RT	Room temperature
SCF	Stem cell factor
SD	Standard deviation
SSC	Side scatter
TCR	T cell receptor

TH	T helper cell
TLR	Toll-like receptor
TNF	Tumor necrosis factor
TRAIL	TNF-related apoptosis-inducing ligand
Treg	Regulatory T cell
U	Units
V/V	Volume per volume
VL	Visceral Leishmaniasis
w/v	Weight per volume
WT	Wild type
YFP	Yellow fluorescent protein
ZBP1	Z-DNA-binding protein 1
ZTL	Central animal facility

## TABLE OF CONTENTS

ABSTRACT.....	I–II
GRAPHICAL ABSTRACT.....	III
ZUSAMMENFASSUNG.....	IV–V
ABBREVIATIONS.....	VI–XI
TABLE OF CONTENTS.....	XII–XIV
1. INTRODUCTION.....	1–23
1.1 Pathogens.....	1–2
1.2 <i>Leishmania</i> .....	3–5
1.3 Immune response during <i>Leishmania</i> infection.....	6–16
1.3.1 Host cell entry.....	6–8
1.3.2 Innate immune response during <i>Leishmania</i> infection.....	9–12
1.3.3 Adaptive immune response during <i>Leishmania</i> infection.....	13–14
1.3.4 Cytokines and paracrine signalling during <i>Leishmania</i> infection.....	15–16
1.4 Cell-to-cell transmission of <i>Leishmania</i> parasites.....	17–18
1.5 Host cell death during <i>Leishmania</i> infection.....	19–22
1.6 Project aims.....	23
2. MATERIALS AND METHODS.....	24–45
2.1 Materials.....	24–30
2.2 Methods.....	31–45
2.2.1 Parasites, mice and infections.....	31
2.2.2 Preparation of killed but metabolically active parasites.....	32
2.2.3 Adoptive cell transfer.....	33
2.2.4 Generation of bone marrow chimeric mice.....	34–35
2.2.5 Human monocyte-derived macrophages.....	36
2.2.6 Murine macrophages.....	37–38

2.2.7 Flow cytometry .....	39
2.2.8 Proliferation analysis .....	40
2.2.9 Quantitative Reverse Transcription PCR .....	41
2.2.10 Intravital imaging .....	42
2.2.11 Intravital image analysis .....	43
2.2.12 Statistical analysis .....	44
2.2.13 Study approval .....	45
<b>3. RESULTS .....</b>	<b>46–75</b>
3.1 CD11c-expressing cells play dual role during <i>Leishmania</i> infection depending on the infection stage .....	46–48
3.2 Quantification of <i>L. major</i> uptake by newly recruited monocytes in vivo suggests direct cell-to-cell transfer .....	49–50
3.3 Original host cell material is taken up by newly infected cells .....	51–53
3.4 An in vivo cell death reporter system shows higher apoptosis in infected compared to uninfected phagocytes at the site of infection .....	54–57
3.5 <i>L. major</i> -infected cells containing high proliferating pathogens undergo apoptosis and drive cell-to-cell transfer .....	58–60
3.6 Proliferation-competent pathogens induce cell death in infected macrophages .....	61–63
3.7 <i>L. major</i> intracellular proliferation rate modifies host cell metabolic pathways .....	64–69
3.8 High proliferating <i>L. major</i> parasites more likely reside in close proximity to blood vessels .....	70–72
3.9 Ablation of IL-11 receptor signalling does not significantly influence <i>Leishmania</i> infection in monocytes in vivo .....	73–75
<b>4. DISCUSSION .....</b>	<b>76–90</b>
4.1 The role of CD11c-expressing cells during <i>Leishmania</i> infection .....	77–78
4.2 Cellular dissemination of <i>Leishmania</i> .....	79
4.3 Apoptosis as cellular exit strategy for <i>Leishmania</i> .....	80–81

4.4 Other potential cellular exit strategies for <i>Leishmania</i> .....	82–84
4.5 Host cell death and intracellular <i>Leishmania</i> proliferation .....	85–86
4.6 Host cell metabolism and intracellular <i>Leishmania</i> proliferation .....	87–89
4.7 Conclusions and implications.....	90
6. REFERENCES .....	91–132
7. APPENDIX .....	133–134
7.1 Macro for vessel distance analysis.....	133–134

# 1. INTRODUCTION

## 1.1 Pathogens

Apart from containing about  $10^{13}$  human cells, the human body contains about  $10^{14}$  microbes, such as bacteria, viruses, fungi and parasites. Most microbes live in symbiosis with the human body, meaning that both organisms benefit from the interaction (1). However, some microbes are potentially harmful when the host lacks the ability to maintain homeostasis. These harmful microbes are referred to as pathogens.

In order for the host to survive, a strong response against pathogens is required. These responses are executed by the immune system, consisting of an innate and an adaptive part. The innate immune system is fast-acting and consists of physical barriers, such as the skin and mucous membranes, as well as effector cells, including natural killer (NK) cells, mast cells, eosinophils, basophils, macrophages, neutrophils and dendritic cells (DCs). The soluble mediators of the innate system comprise predominantly the complement system and cytokines and chemokines. The adaptive system is slow-acting and highly specific. The main effector cells of the adaptive immune system are B lymphocytes and cytotoxic  $CD8^+$  and  $CD4^+$  T helper lymphocytes, which are further subdivided into T-helper1 (Th1), T-helper2 (Th2), T-helper17 (Th17) and regulatory T (Treg) cells. Soluble factors of the adaptive immune system include cytokines, chemokines and antibodies (see chapter 1.3 for more detail).

Despite the existence of these complex systems, many pathogens have developed strategies to be able to survive inside the host. In order to survive, the pathogen not only needs to avoid or circumvent the host immune responses, but also requires a suitable niche in order to replicate, and needs strategies in order to eventually exit and spread to a new host (2, 3).

Various types of intracellular pathogens exist, which all have co-evolved with their hosts to establish pathogen-host cell interactions, forming the basis of the pathogen's cellular tropism. The most widespread pathogens are viruses and bacteria. It is difficult to treat viral infections, since viruses need the basic transcription and translation machinery of their host cells for their replication (4). Nonetheless, there are antiviral drugs available and vaccination allows us to prevent viral infections (5). Bacterial infections, on the contrary, are relatively easily treatable. Bacteria, which are usually free-living cells, reproduce mainly by binary fission and perform most of their basic tasks themselves, relying on the host primarily for nutrition. Because the basic machinery of bacteria is quite different from that of their host, it enables us to find antibacterial drugs that specifically target the pathogen. Nevertheless, antimicrobial resistance is currently one of the biggest global public health threats (6). The most complex group of pathogens are pathogenic fungi and protozoan parasites, because just like the hosts that they infect, they are eucaryotes. In addition, fungi and parasites take on different forms during their life cycle. It is therefore more difficult to find drugs that will kill the pathogen

without killing the host and that will attack all forms of the pathogen (7). Thus, it is essential to understand the interaction between the host and these pathogens in more detail to be better able to treat the infections caused by them. In this regard, this thesis will focus on further understanding the dynamics between parasites and their hosts.

## 1.2 *Leishmania*

In this thesis, we will focus on the obligate intracellular parasite, *Leishmania*. This parasite causes the disease Leishmaniasis, the second most severe neglected tropical disease next to malaria, with approximately one million new cases annually (8, 9). More than 20 different *Leishmania* spp. are known to cause disease in humans (10), the six major ones being *L. tropica*, *L. major*, *L. donovani*, *L. infantum* and *L. mexicana*, all of the *Leishmania* (*Leishmania*) subgenus and *L. braziliensis*, of the *Leishmania* (*Viannia*) subgenus (11, 12). There are three major forms of Leishmaniasis; cutaneous (CL), mucosal/muco-cutaneous (MCL) and visceral (VL) (10). VL is the most severe form, affecting visceral organs like spleen and liver and can be fatal if left untreated. CL and MCL are less severe, with the former manifesting self-healing ulcers and the latter resulting in partial or total destruction of the mucosal epithelia of the mouth, nose, throat, and associated tissues (Figure 1.1). A fourth form, post kala-azar dermal leishmaniasis (PKDL), usually presents as a complication of VL and is characterised by a macular, maculopapular, and nodular rash and is, in contrast to VL, not fatal (10, 13). The severity of disease progression depends on various factors, including the parasite strain, infecting parasite dose, composition of sand fly saliva, site of infection, extent of tissue damage, host skin microbiome, sand fly gut microbiota and most importantly, the host immune response (14–25). So far, drugs to control Leishmaniasis are limited due to high costs and toxicity, and there is currently no safe and effective vaccine for application in humans (26, 27). The complexity of the host immune response to *Leishmania* is also a key limiting factor for developments in this field (28–30).

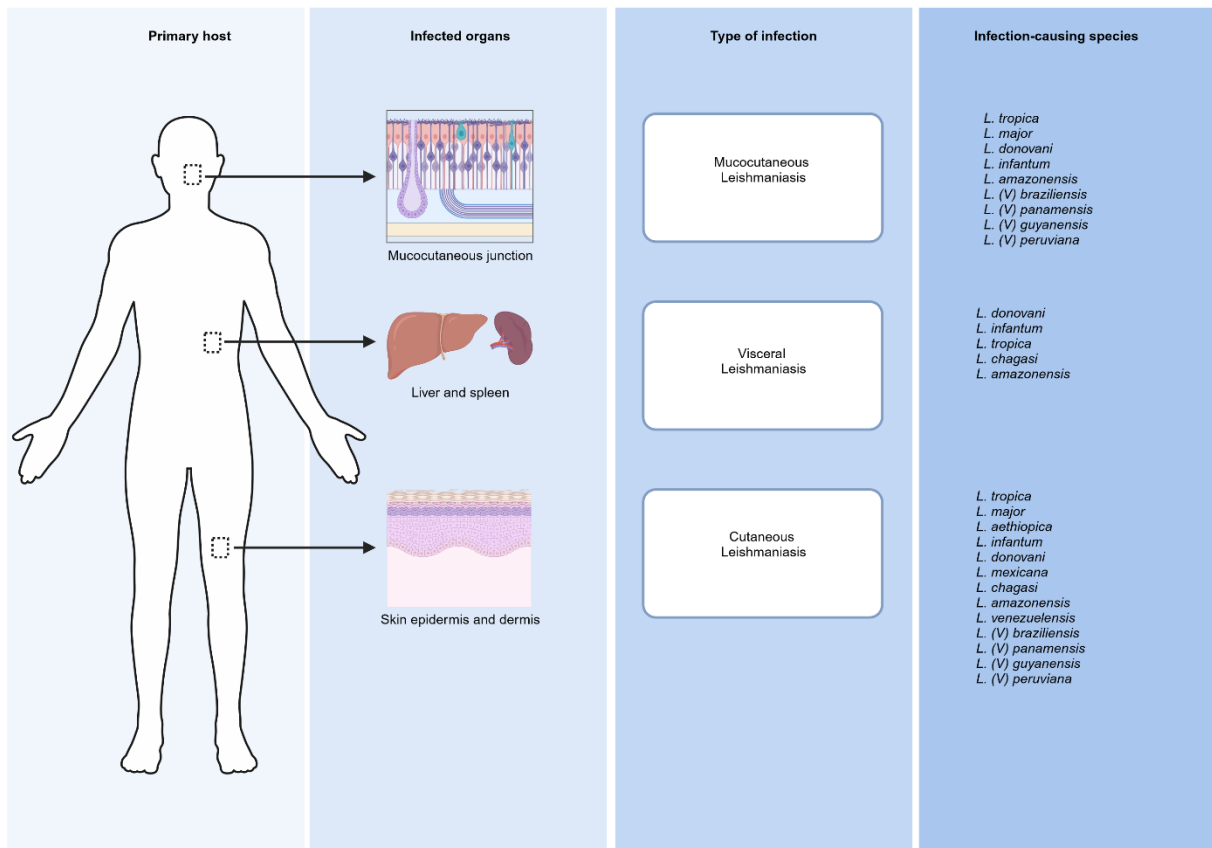


**Figure 1.1: Types of leishmaniasis, affected organs and infection-causing *Leishmania* species.** Mucocutaneous Leishmaniasis affects mucocutaneous junctions, Visceral Leishmaniasis affects liver and spleen, Cutaneous Leishmaniasis affects skin epidermis and dermis. Created with Biorender.

### Life cycle

Leishmaniasis is generally transmitted by female Phlebotomine and Lutzomyia sand flies, but can, sporadically, also be transmitted by syringe sharing, blood transfusions, or from mother to foetus (13, 31, 32). *Leishmania* parasites occur in two forms, the elongated (10–20  $\mu\text{m}$ ) motile promastigote form and the oval-shaped (3–7  $\mu\text{m}$  in diameter) non-motile amastigote form. The promastigote form exists in the sand fly vector, where it undergoes various differentiation steps and transforms into the infective metacyclic promastigote form. When a sand fly vector bites an infected mammal, it ingests the amastigotes, which transform into the flagellated promastigote form in the midgut of the insect. Eventually, the procyclic promastigotes move to the alimentary tract of the insect where they survive extracellularly and multiply by asexual binary fission (13). Although *Leishmania* reproduction is mainly asexual, a nonobligatory sexual reproductive cycle is now known to accompany parasite development in the sand fly vector (33–35). After reproduction in the alimentary tract, the promastigotes migrate towards the salivary glands and oesophagus, transform into infective metacyclic promastigotes and are transmitted along with the insect saliva, containing anticoagulant to prevent blood coagulation, to the mammalian host during the next blood meal (32). After entry into the host, the promastigotes are rapidly taken up by neutrophils and thereafter mainly reside within

macrophages and DCs. Within these professional phagocytes, the parasite-enclosing parasitophorous vacuoles fuse with lysosomes to form phagolysosomes, which are acidic compartments rich in microbicidal peptides and hydrolytic enzymes and wherein *Leishmania* promastigotes transform into and replicate as amastigotes (36, 37). Thereafter, amastigotes can be phagocytosed by new monocyte-derived cells or can be taken up by the sand fly during a blood meal, thereby completing its life cycle (38, 39) (Figure 1.2).

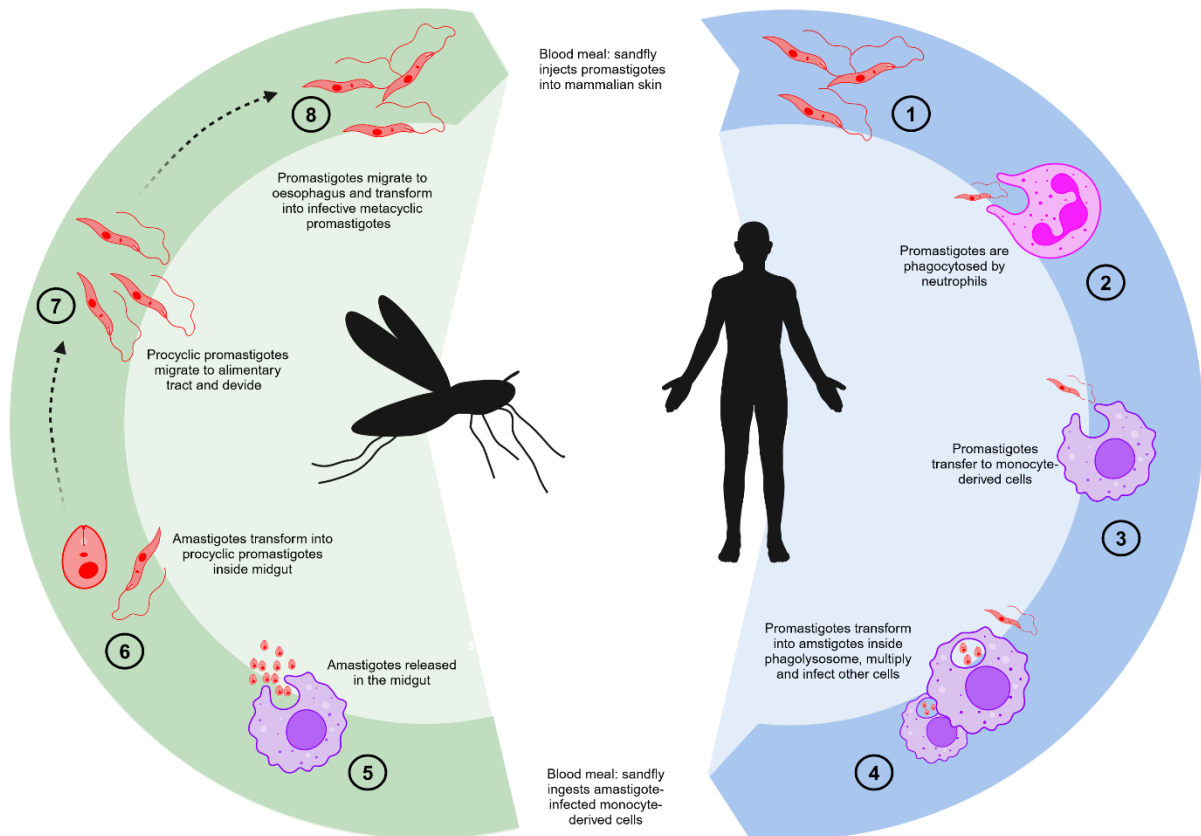


**Figure 1.2: *Leishmania* life cycle.** *Leishmania* parasites maintain their life cycle by residing inside mammalian (blue cycle) and sand fly (green cycle) hosts. Leishmaniasis is transmitted by the bite of infected female phlebotomine sandflies. The sand fly injects promastigotes into the mammalian skin during a blood meal (1). Upon inoculation into the skin, promastigotes are rapidly phagocytised by neutrophils (2) and thereafter transfer to monocyte-derived phagocytes (3). Promastigotes transform into amastigotes inside the phagolysosomes of these professional phagocytes and multiply by simple division (4). Amastigote-infected monocyte-derived cells are ingested by a sand fly during their blood meal and amastigotes are released inside the sand fly midgut (5), where they transform into procyclic promastigotes (6). Procyclic promastigotes migrate towards the alimentary tract (7), divide and migrate towards the oesophagus, where they transform into infective metacyclic promastigotes (8). These metacyclic promastigotes can be ingested into a mammalian host by another blood meal, thereby completing the *Leishmania* life cycle. Created with Biorender.

## 1.3 Immune response during *Leishmania* infection

### 1.3.1 Host cell entry

#### *Complement*

Upon skin infiltration, *Leishmania* promastigotes evade immediate host immune responses by entering different types of host cells, which include neutrophils, macrophages, fibroblasts, keratinocytes and DCs. This intracellular lifestyle provides several advantages, including nutrient accessibility and evasion from the immune system (40). An important regulator in *Leishmania* uptake by professional phagocytes is C3, which is part of the complement system. The complement system represents a network of activators, regulators, effectors and signals that are involved in rapid clearance of invading pathogens (41). There are three distinct pathways through which complement can be activated: the classical, the lectin and the alternative pathway. Whereas the classical and the lectin pathway require antibody or lectin binding respectively, the alternative pathway is directly activated by the pathogens. Activated complement generates various effector molecules. C3a and C5a are involved in immune cell recruitment and activation, whereas C3b, iC3b, and C3d opsonise pathogens, thereby promoting their phagocytosis. The C5b–C6–C7–C8–C9 (C5b–9) membrane attack complex (MAC) directly promotes lysis of the target pathogen (42–45) (Figure 1.3).

*Leishmania* can use deposited C3b to enter macrophages and neutrophils through complement receptor (CR)2 and can be phagocytosed by monocytes through CR1 and CR3, which is associated to a low respiratory burst and therefore to parasite survival (46, 47). *Leishmania* have developed additional strategies to avoid killing by the complement system. The two major virulence factors of *Leishmania* are glycoalyx component lipophosphoglycan (LPG) and the leishmanial metalloprotease GP63. LPG is the major acceptor of C3b and is essential for resistance to killing by the complement system in metacyclic promastigotes (48, 49). Similarly, GP63 converts C3 into iC3b, thereby inhibiting the formation of subsequent MAC (50) (Figure 1.3). Importantly, LPG and GP63 induce phagocytosis through C3b receptor CD11b by C3b opsonisation or through direct binding to cell surface receptors such as the mannose and fibronectin receptor. Thus, LPG and GP63-mediated uptake into host cells protect *Leishmania* from the complement cascade killing. In addition, *L. donovani* inhibitor of Serine Peptidases 2 (LdISP2) inhibits the lectin pathway of complement by inhibiting the formation of MAC and complement-mediated lysis via upregulation of C5aR signalling, which in turns promotes parasite survival inside the host (51).



These receptors are involved in the activation of neutrophils, macrophages, DCs and NK cells and ultimately contribute to driving CD4<sup>+</sup> T cells to Th1 and Th17 cells. Specifically, TLR2 are involved in enhancing the production of cytokines such as Interleukin (IL)-12, tumor necrosis factor alpha (TNF- $\alpha$ ), interferon gamma (IFN- $\gamma$ ), reactive oxygen species (ROS), nitric oxide (NO), nuclear translocation of NF-kappaB (NF $\kappa$ B) and expression of the chemokine CXCL1 (54–56). All these mechanisms contribute to the defence against *Leishmania* infection. However, in some instances LPG binding to TLR2 can lead to a reduction in anti-leishmanial responses, thereby inducing *Leishmania* burden (44, 57, 58). Whether the TLR2-LPG interaction elicits a host-protective or disease-exacerbation response depends on several factors, such as the *Leishmania* species, TLR homodimer or heterodimer formation, tissue tropism, and differential downstream immune signalling (59). While TLR2, as well as TLR4, recognise *Leishmania* outside, TLR3 and TLR9 recognise *Leishmania*-related PAMPs inside the vacuole (44). Similar to TLR2, TLR9 promote the production of IL-12 and IFN- $\gamma$  by DCs and are involved in the activation of NK cells and the recruitment of neutrophils (60–62).

### 1.3.2 Innate immune response during *Leishmania* infection

#### *Neutrophils*

Neutrophils are the first innate immune cells responding upon *Leishmania* inoculation into the skin (19). They are recruited to the site of infection in response to several factors derived from the host, the sand fly, or the parasite itself. Neutrophils rapidly engulf *Leishmania* parasites and contribute to clearance of invading pathogens by formation of neutrophil extracellular traps (NETs) or by the secretion of neutrophil elastase (NE) or ROS (19, 63–65) (Figure 1.4). In addition, neutrophils can contribute to the recruitment of immune cells, such as additional neutrophils, monocytes, immature DCs and T cell subsets through the secretion of cytokines and chemokines (66, 67). Although neutrophils are important contributors to *Leishmania* control, *Leishmania* have developed strategies to survive within neutrophils. Neutrophils have a short lifespan and rapidly undergo cell death, leading to their phagocytosis by macrophages. During *Leishmania* infection, the parasite resides within neutrophils, delaying the apoptosis of their initial host cell by activation of ERK1/2 and induction of anti-apoptotic proteins Bcl-2 and Bfl-1 until macrophages are recruited to the site of infection (68). Thereafter, neutrophil cell death is induced in order to promote transfer into macrophages where the parasite can survive and replicate. In addition, *Leishmania* can evade neutrophil-mediated killing by interfering with NETs. These NETs, released by neutrophils, are composed of nuclear DNA and granular and cytoplasmic proteins that form extracellular filaments, which can ensnare and kill microorganisms (69). *Leishmania* can induce both classical NETosis, which is ROS-dependent and concludes with the death of the neutrophil, and early NETosis, which is ROS-independent, does not result in neutrophil death and is associated with the trapping of microorganism by chromatin (70–73). Some *Leishmania* promastigotes have been shown to be resistant to NET-mediated killing by the expression of LPG on the promastigote cell surface (74). Also, 3'-nucleotidase/nuclease, a class I nuclease member expressed by *Leishmania* promastigotes, as well as the endonuclease Lundep present in the vector's saliva are able to cleave NET-DNA, allowing parasites to escape the trapping and killing by NETs (75, 76). Moreover, NET formation has been shown to interfere with monocyte-derived DC differentiation and function, thereby promoting parasite survival (77, 78). In addition, *L. major*-infected neutrophils were shown to have enhanced uptake of apoptotic cells, thereby decreasing nicotinamide adenine dinucleotide phosphate (NADPH) oxidase and ROS production. This in turn also results in increased parasite survival (79).

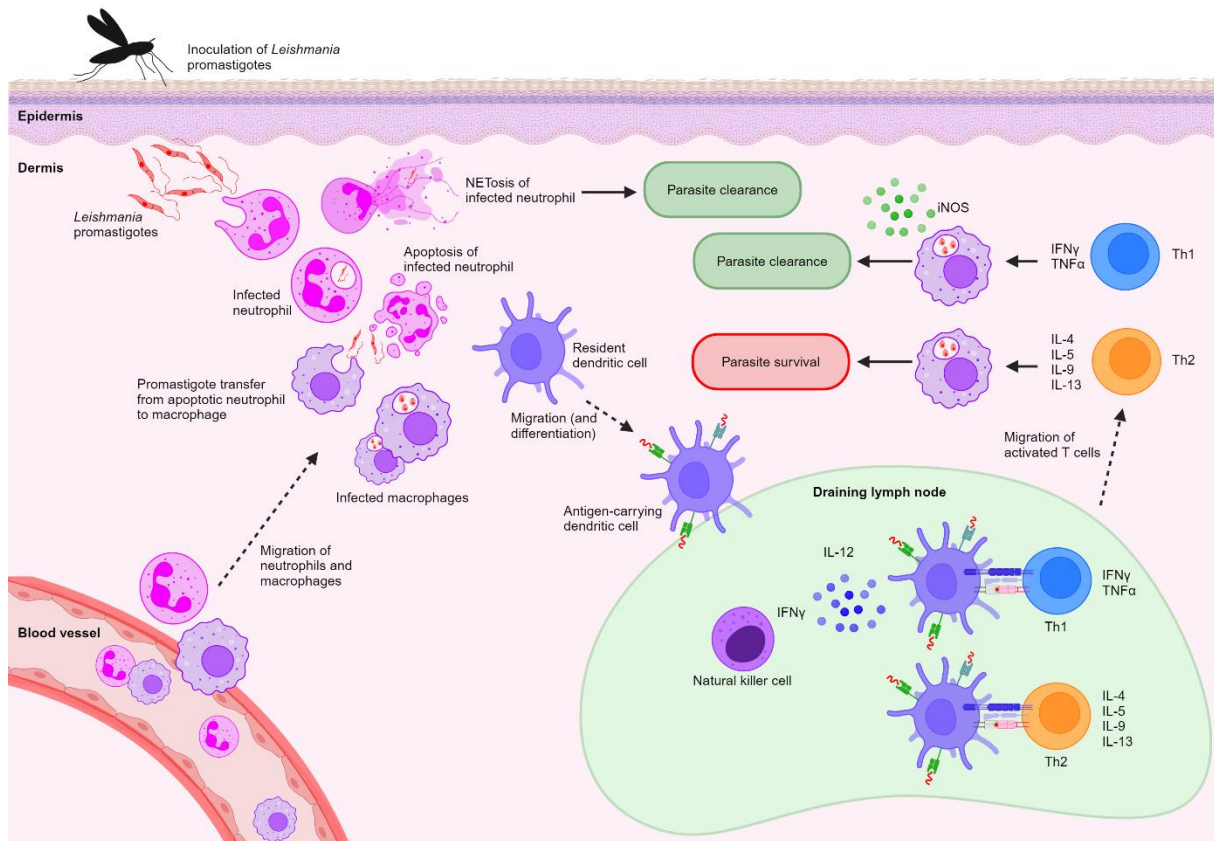


**Figure 1.4: Immune response against *Leishmania* infection.** Upon *Leishmania* entry into the skin dermis, different phagocytic cells infiltrate to the infection site. Infiltrating neutrophils rapidly engulf *Leishmania* parasites and contribute to clearance of the parasite by formation of neutrophil extracellular traps (NETs) or by the secretion of neutrophil elastase (NE) or reactive oxygen species (ROS). Additionally, infected neutrophils can become apoptotic, thereby promoting parasite phagocytosis by macrophages. Parasites can also be engulfed antigen-presenting cells (APCs), such as resident dendritic cells (DC) and monocyte-derived cells, which migrate to the draining lymph carrying *Leishmania* antigens. Inside the draining lymph node, parasite antigens are presented by such APCs. This antigen presentation, together with the production of Interleukin (IL)-12 by DCs and natural killer (NK) cells, induces CD4<sup>+</sup> Th1 cell differentiation. Th1 cells migrate to the infection site and finally produce and secrete Interferon (IFN)- $\gamma$  and Tumor necrosis factor (TNF)- $\alpha$ . This in turn induces the production macrophage-derived iNOS and thereby of nitric oxide (NO), which promotes *Leishmania* killing. A Th1-mediated immune response is therefore associated to parasite clearance. Additionally, the differentiation of CD4<sup>+</sup> Th2 cell inside the draining lymph node and the subsequent migration of Th2 cells to the site of infection leads to the production of IL-4, IL-5, IL-9 and IL-10 and does not induce iNOS production by macrophages. A Th2-mediated immune response is therefore associated with parasite survival. Created with Biorender.

### Monocyte-derived cells

Although neutrophils are the initial host cell of *Leishmania* parasites, monocyte-derived cells, and more specifically macrophages, are the primary resident cell of the parasite and the major effector cells to kill the parasite (19, 80). *Leishmania* infect macrophages directly after being released from neutrophils or following the phagocytosis of apoptotic neutrophils containing

intact parasites, with *Leishmania* parasites using the neutrophils as “Trojan horses” before they enter macrophages (19, 81, 82) (Figure 1.4). In vivo imaging revealed that parasites can also escape dying neutrophils to infect macrophages, which was termed the ‘Trojan rabbit’ strategy (83). Macrophage inflammatory protein (MIP)-1 $\beta$  secretion by infected neutrophils has been suggested to be involved in the recruitment of macrophages to the site of the infection (82). Once the parasite is recognised by the macrophage, host cell vesicles originating from endosomes, lysosomes and the endoplasmic reticulum fuse with the plasma membrane to contribute to parasite engulfment and formation of the promastigote-containing phagosomes, which subsequently fuse with further lysosomes (84–86). The result of this fusion is the formation of a phagolysosomal parasitophorous vacuole, where *Leishmania* develop into amastigotes.

The phagocytic effect of macrophages is usually initiated following their activation by DCs and by opsonisation (87, 88). There are different activation and maturation states of recruited monocyte-derived phagocytes that can be found inside the infected dermis of the mouse skin, which can be distinguished based on their Ly6C and major histocompatibility complex (MHC)-II expression (89). Previous findings have indicated an important role of such inflammatory monocytes as a niche for the parasite during primary infection and for efficient containment of *L. major* during secondary infections (90). More recently, our group has shown that CD11c-expressing Ly6C<sup>+</sup>CCR2<sup>+</sup> monocytes, resembling an inflammatory phenotype, constitute a reservoir for efficient *Leishmania* proliferation and cell-to-cell transmission (91).

While macrophages are the main effector cells during *Leishmania* infection, strategies to circumvent the anti-microbial effects of macrophages are of utmost importance for *Leishmania* to spread and survive. Therefore, the parasite has developed several of such strategies. First, *Leishmania* use GP63 to interfere with macrophage signalling pathways to overcome the microbicidal effect of the host and use LPG to inhibit the fusion of the parasitophorous vacuole with host cell lysosomes (92–96). In addition, *Leishmania* amastigotes are able to survive in the harsh highly acidic environment of the phagolysosome and are even able to hijack its anti-microbial defence mechanisms (97–99). Lastly, *Leishmania* are able to interfere with macrophage functioning by modulating the adhesion and migratory capability of mononuclear phagocytes (100, 101).

### *Dendritic cells*

DCs are antigen-presenting cells (APCs) that are able to take up, process and present pathogen-derived material, called antigens, to T cells via antigen presentation platforms, called MHC molecules (102). They form the link between the innate and the adaptive immune system. Following the recognition and internalisation of pathogens, DCs migrate to secondary lymphoid organs to present processed antigens to naïve T cells (103) (Figure 1.4). Subsequently, the adaptive immune response is activated via the presentation of small endogenous peptides

through MHC class I molecules, recognised by cytotoxic CD8<sup>+</sup> T cells, or via the presentation of small exogenous peptides through MHC class II molecules, recognised by CD4<sup>+</sup> T helper cells. DCs are also able to take up, process and present exogenous antigens with MHC class I molecules to cytotoxic CD8<sup>+</sup> T cells, a process known as cross-presentation (104). Additionally, co-stimulatory molecules, such as CD40, CD80, and CD86, provide secondary signals for T cell expansion and differentiation and are therefore critical for effective antigen presentation (105). The infection of DCs with *Leishmania* results in the production of Interleukin-12p70 (IL-12), which facilitates the deployment of a so-called Th1 response (see chapter 1.3.3 –1.3.4 for more detail) and enhances protective immunity through activation of NK cells and subsequent IFN- $\gamma$  production (60, 61, 92). DCs are therefore considered to play a central role in facilitating an effective immune response against *Leishmania* (106–108). Dermal monocyte-derived DCs were shown to be especially important in the induction of protective Th1 responses against *Leishmania*. These dermal monocyte-derived DCs, which differentiate inside the dermis and subsequently migrate into the draining lymph nodes (dLNs), differ from lymph node monocyte-derived DCs, which are recruited directly to the dLNs (107).

### 1.3.3 Adaptive immune response during *Leishmania* infection

#### *B and T lymphocytes*

As mentioned previously, the main factor influencing the severity of Leishmaniasis is the immune response developed by the host, and, more specifically, the adaptive immune response (25). The functions of the adaptive immune response are executed by lymphocytes, the B and T cells. B cells are responsible for the humoral response of the adaptive immune system and are characterised by the production of pathogen-neutralising antibodies, also known as immunoglobulins, upon antigen recognition via a membrane-bound B-cell receptor (BCR). Additionally, B cells are involved in chemokine and cytokine secretion and function as antigen-presenting cells via MHC-II-dependent antigen presentation (109). On the other hand, T cells possess exclusive surface receptors, called T cell receptors (TCRs), that recognise antigens bound to MHC on the surface of APCs. Naïve T cells become activated through recognition of the MHC-bound antigen by the TCR and binding of co-stimulatory molecules on the surface of APCs with co-stimulatory receptors expressed on T cells. This in turn leads to the secretion of cytokines and an antigen-specific T cells response (110). Furthermore, the proliferating CD4<sup>+</sup> T helper cells, which later develop into effector T cells, differentiate into the T helper (Th) subtypes, Th1 and Th2 (110–112) (Figure 1.4).

A Th2 response is most typically associated with IL-4, IL-5, IL-9 and IL-13 production, which drives B cell proliferation and immunoglobulin class-switching to immunoglobulin E (IgE) and basophil and mast cells activation (111, 113). Because *Leishmania* are obligate intracellular parasites and are therefore not efficiently neutralised by antibodies, individuals with a predominantly humoral response, mediated by Th2 cells, are unable to control the infection and exhibit a severe form of the disease, called diffuse cutaneous leishmaniasis (25, 114). Successful control of *Leishmania* infection is associated with a strong Th1 response, in which Th1 cells activate macrophages through IFN- $\gamma$  production (115–118). Activated T cells also upregulate CD40L, which bind CD40 on macrophages and act as a secondary activation signal (119). Activated macrophages in turn express inducible nitric oxide synthase (iNOS), an enzyme that produces NO, which is needed for clearance of intracellular *Leishmania* parasites (90, 107, 118, 120, 121) (Figure 1.4). However, an exaggerated T cell response accompanied by the production of high levels of proinflammatory cytokines, such as IFN- $\gamma$  and TNF- $\alpha$ , as well as a decreased production of IL-10 and transforming growth factor  $\beta$  (TGF- $\beta$ ) can also lead to immunopathology, which, in severe cases, can lead to mucosal leishmaniasis (122).

To evade an effective Th1 response, *Leishmania* employ several mechanisms that interfere with the antigen presentation machinery. For example, *L. donovani* was suggested to disrupt membrane rafts, which are important for antigen presentation and efficient activation of effector T cells, in infected macrophages (123, 124). In addition, *Leishmania* GP63 can cleave the CD8 molecule on T cells to suppress proper recognition of exogenous *Leishmania* antigens

on MHC-I, also known as cross-presentation (125). With these mechanisms, *Leishmania* are able to suppress both CD4<sup>+</sup> and CD8<sup>+</sup> T cell activation. However, paracrine secretion of IFN- $\gamma$  by T cells has been shown to activate infected macrophages even without direct cell-to-cell contact, suggesting that CD4<sup>+</sup> T cells can exert their protective activity by engaging a minority of infected cells (126).

Importantly, the adaptive immune response is essential for immunity against secondary *Leishmania* infections. That is, it has been shown that upon resolution of primary *Leishmania* infections, a small pool of parasites remains at the primary infection site and in the dLNs. These parasites are responsible for a long-lasting memory CD4<sup>+</sup> T cell-dependent immunity to reinfection and were mainly found in iNOS<sup>+</sup> macrophages (127, 128). Two distinct populations of persistently-infected macrophages have been described in the skin. One subset contained parasites that remain quiescent, whereas parasites in another subset continued to replicate in a manner similar to those during the acute stage of the infection (128). The fact that slowly proliferating, persistent parasites can remain within iNOS<sup>+</sup> host cells suggest that these parasites can somehow circumvent killing by iNOS. A possible explanation is that cells expressing NO are activated by, and preferentially kill, metabolically active parasites. Another explanation is that persistent parasites are generally resistant to killing by NO produced in the tissue. In addition to the importance of CD4<sup>+</sup> T cells and iNOS<sup>+</sup> macrophages, Foxp3<sup>+</sup> Treg cells, immune cells that play an important role in homeostasis via suppressing aberrant immune responses, also seem to play an important role during *Leishmania* persistence and help maintaining efficient immunity against reinfection (129–134).

### 1.3.4 Cytokines and paracrine signalling during *Leishmania* infection

#### *Type 1-related cytokines*

Cytokines related to an efficient Th1 response are IL-12, IFN- $\gamma$  and TNF- $\alpha$ . IL-12, predominantly produced by macrophages, DCs and NK cells, is essential for differentiation of IFN- $\gamma$ - and TNF- $\alpha$ -producing Th1 cells, which in turn are responsible for the activation of inflammatory macrophages (135, 136) (Figure 1.4). These inflammatory macrophages are crucial for the killing of *Leishmania* parasites via the triggering of a respiratory burst. This burst is associated with enhanced production of ROS and reactive nitrogen species (RNS), including superoxide, hydrogen peroxide, hydroxyl radicals, and NO, which exhibit high microbicidal capacity (25, 137, 138). Especially NO, which is produced by iNOS under consumption of L-arginine and in the presence of cofactors NADPH, tetrahydrobiopterin, flavin adenine nucleotide (FAD) and flavin mononucleotide (FMN), is essential for the resolution of *Leishmania* infection (139–141). In addition to the antimicrobial effect of respiratory burst-derived reactive oxygen intermediates (ROIs) and reactive nitrogen intermediates (RNIs) alone, NO together with superoxide can form the even more reactive peroxynitrite, which has been shown to be an effective antimicrobial compound (142). Thus, peroxynitrite formation might be a way of concentrating the antimicrobial effect of ROIs and RNIs to the site where it is needed, and NO production could be more effective at sites with high oxygen availability.

#### *Type 2-related cytokines*

In contrast to Th1-related cytokines, IL-4 and IL-13, produced by Th2 lymphocytes, induce the anti-inflammatory phenotype (143). Anti-inflammatory macrophages are characterised by polyamine biosynthesis via activation of the enzyme arginase and the production of urea and L-ornithine, which are beneficial for *Leishmania* proliferation and survival inside macrophages (137, 144, 145). In addition, infection of macrophages by *Leishmania* also enhances the production of other immuno-regulatory cytokines, such as IL-10 and TGF- $\beta$ , which deactivate macrophage functions (11). IL-10 also inhibits the respiratory burst and the production of inflammatory cytokines, particularly TNF, by macrophages and thus inhibits the anti-microbial mechanisms of the infected host cell (143) (Figure 1.4).

#### *Interleukin-11*

Although IFN- $\gamma$ , TNF- $\alpha$  and IL-12 are known to be the main players in *Leishmania* clearance, other cytokines also play role. As such, IL-6 is expressed in experimental cutaneous and visceral *Leishmania* infections of the mouse (146–151), and was shown to be present also in cutaneous, mucosal, and visceral human leishmaniasis (152–161). However, evidence exists that IL-6 might either promote, suppress, or leave unaltered intracellular antileishmanial host defence mechanisms, leaving the role of this cytokine during *Leishmania* infection unclear (162–168). In addition, recent studies have suggested a role for IL-11, another member of the

IL-6 family of cytokines, during *Leishmania* infection. IL-11 activates its target cells by first binding to the membrane-bound IL-11 receptor (IL-11R), which subsequently results in the recruitment of two molecules glycoprotein 130 (gp130), the formation of a gp130 homodimer and the activation of intracellular signalling cascades, most notably the Jak/STAT signalling pathway (169, 170). Furthermore, it can bind to soluble forms of the IL-11R (sIL-11R), which also induce gp130 homodimerization and activate intracellular signalling (171). Although the biological functions of IL-11 are under intense investigation, it is established that it mediates proliferation, production of cytokines, immunity to infection, and inflammatory response (172–175). IL-11 has important immunomodulatory functions by acting on macrophages/monocytes, CD4<sup>+</sup> T cells and B cells and has been shown to be upregulated in bacterial and viral infection (176–178). In human, IL-11 has been implied to play a role in cancers, tuberculosis, and multiple sclerosis and inhibition of IL-11 signalling has been proposed as a therapeutic strategy for a number of diseases, including cancer, cardiovascular and lung diseases (179–182). Furthermore, a role for IL-11 has been implied in phagocytosis. In more detail, IL-11 was suggested to affect phagocytic functions in osteoclasts and was shown to reduce myelin phagocytosis by microglia, macrophage-like immune cells of the central nervous system (183, 184). Also, CsIL-11, a teleost IL-11 homologue, was shown to increase the phagocytic capacity of peripheral blood leukocytes (185). Interestingly, increased levels of IL-11 mRNA in the lesions of *L. donovani*-infected patients have been reported (186). However, a role for IL-11 on the monocyte recruitment and pathogen uptake during *Leishmania* infection has not been investigated so far.

## 1.4 Cell-to-cell transmission of *Leishmania* parasites

Host cell exit of intracellular pathogens, such as *Leishmania*, and subsequent infection of new cells represents a fundamental step in infection, and might represent an Achilles' heel of microbial pathogenesis (40). Although the mechanisms by which *Leishmania* parasites enter into and exit from neutrophils have been intensely studied (82, 83), the exit from and transfer among monocyte-derived cells remains largely uncharacterised. While very early studies in mice postulated that the unrestricted replication of the intracellular amastigotes causes host cell rupture and release of the parasites (187), more recent findings suggested that the release of *Leishmania* from the infected host cells is strictly regulated. For example, Rittig and colleagues found evidence that *L. major* is released by murine peritoneal macrophages through exocytosis (188, 189). Furthermore, *L. amazonensis* was shown to use a pore-forming cytolyisin to exit host cells (190–192). Despite these findings, the mechanisms involved in efficient parasite exit and transmission in vivo are still largely unknown. Unravelling these mechanisms is however of utmost importance, since *Leishmania* amastigotes, which are proliferating intracellularly, have to leave infected macrophages to infect other cells in order to persist and propagate at the site of infection. Pathogens can exit their host cells either by lytic or non-lytic mechanisms. Non-lytic mechanisms include exocytosis, extrusion, budding, protrusion and apoptotic programmed cell death, whereas lytic mechanisms include cell lysis and necrotic and pyroptotic programmed cell death (Figure 1.5). The majority of intracellular pathogens most likely utilises more than one of these strategies, depending on life-cycle stage, environmental factors and host cell type (193–197). One possible mechanism involved in the spread of *Leishmania* parasites among phagocytic subsets is cell death of the infected host cell.

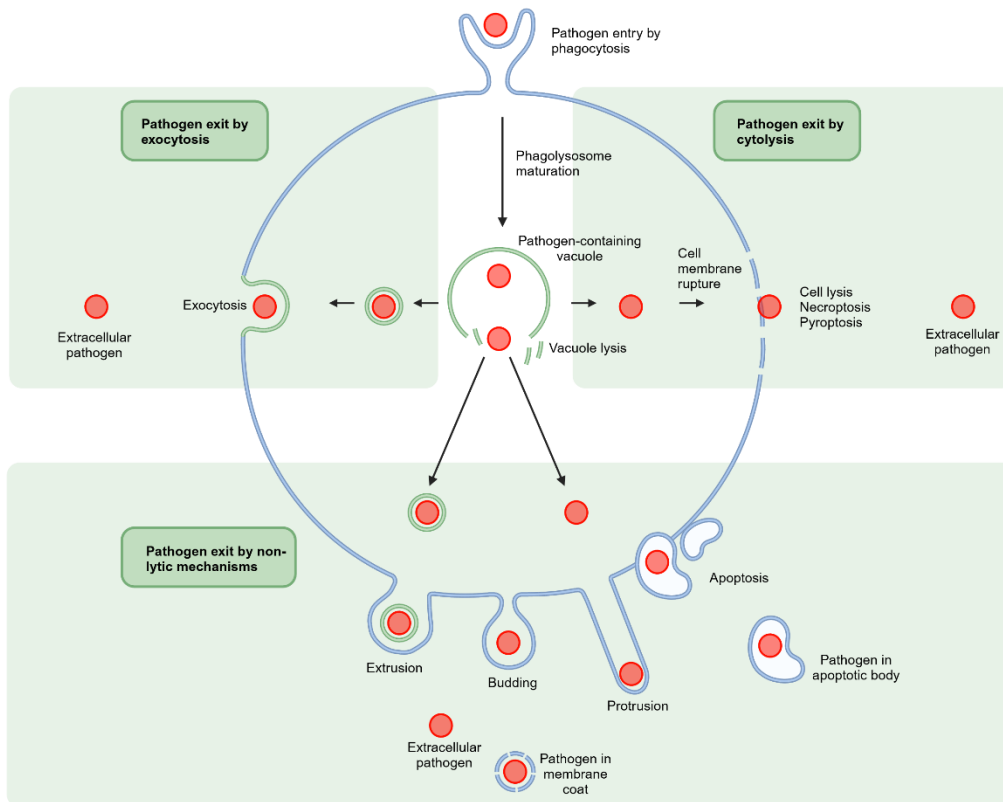


**Figure 1.5: Pathogen exit strategies.** Pathogens can exit host cells by various exit strategies. After pathogen entry, pathogens reside within a vacuole inside the host cell cytoplasm. Pathogens can exit their host cell while remaining within a vacuole by exocytosis (upper left section). Pathogens can also exit the vacuole and translocate into the cytosol by promoting vacuole lysis. After vacuole exit, pathogens can exit their host cell by cell lysis, necroptosis or pyroptosis, which are all associated with cell membrane rupture (upper right section) or by non-lytic mechanisms, thereby leaving the host cell intact. These mechanisms include extrusion, budding, protrusion, and apoptosis (lower section). Created with Biorender.

## 1.5 Host cell death during *Leishmania* infection

Cell death is critical for homeostatic maintenance and plays an important role during inflammation (198). Cells can be removed either in a controlled manner, by programmed cell death, or in a lytic poorly controlled manner. The most well characterised and prevalent form of controlled cell death, apoptosis, involves specific molecular machinery that ensures non-lytic removal of cells (199). Other forms of regulated cell death include autophagy, necroptosis and pyroptosis, each with specific regulatory factors and effects on the surrounding, whereas the uncontrolled lysis of cells, also known as necrosis, results in the unspecific spilling of the cellular contents into surrounding tissues (200).

### *Autophagy*

Autophagic cell death is characterised by the appearance of large intracellular vesicles. Although autophagy is officially considered a cell death pathway, it is predominantly a survival process associated with the maintenance of cellular and tissue homeostasis (201, 202). The pathway is activated in response to a metabolic crisis or in order to remove damaged organelles and protein aggregates via lysosome-mediated degradation and therefore usually accompanies rather than promotes cell death (203). A specific autophagic pathway, known as LC3-associated phagocytosis (LAP), plays a role in eliminating intracellular pathogens (204). LAP results in lysosomal fusion and maturation of the LAPosome, which engulfs pathogenic particles (205). Although the relevance of autophagic cell death in *Leishmania* infection remains poorly understood, enhanced LC3 labelling, suggesting autophagy induction, was observed in various in vitro and in vivo *Leishmania* infection models (206–213). Furthermore, *L. major* GP63 was shown to inhibit LC3 recruitment to the phagosomal membrane, resulting in parasite escape from LAP-promoted engulfment and therefore potentially in enhanced intracellular survival (210, 214).

### *Necrosis and necroptosis*

Necrosis and necroptosis are characterised by swelling of cell organelles, plasma membrane rupture and eventual lysis of the cell. This in turn results in spillage of intracellular contents into the surrounding tissue and is therefore associated to tissue damage (215, 216). Necrotic and necroptotic cell death are triggered by extracellular toxic stimuli, including hypoxia, extreme temperatures, radiation, drugs, and pathogens, and are generally accompanied by an inflammatory response (217). Although necrosis is mainly associated with caspase-independent uncontrolled cell death occurring as a consequence of irreparable cell damage, necroptosis occurs in a regulated manner. Necroptosis is initiated by several signalling pathways and occurs due to the activation of the kinase domain of the receptor-interacting protein 1 (RIP1) and the assembly of the RIP1/RIP3-containing signalling complex. It is triggered by members of the TNF family, requires caspase-8 inhibition, and assembly of the necrosome (RIPK1–RIPK3

complex IIb) (218, 219). When looking at *Leishmania* infection, previous studies have demonstrated that RIPK1–RIPK3–MLKL-associated necroptosis is important for neutrophil death during *L. infantum* infection and for macrophage death during *L. braziliensis*, *L. amazonensi* and *L. major* infection (220–222). In case of necrosis, high mobility group box 1 protein (HMGB1) and hepatoma-derived growth factor (HDGF) released from necrotic cells activate nod-like receptor protein 3 (NLRP3), resulting in inflammasome activation and release of the pro-inflammatory cytokine IL-1 $\beta$ . NLRP3 inflammasome activation in bystander cells is triggered mainly through ATP produced by mitochondria released from damaged cells (223). With regard to *Leishmania*, the inflammasome, although playing a more central role in pyroptotic cell death, was shown to be important for restriction of parasite replication during infection with *L. amazonensis*, *L. braziliensis*, and *L. infantum chagasi*, but not during *L. major* infection (224).

### *Pyroptosis*

Pyroptosis is a form of programmed cell death, which, unlike apoptosis, is pro-inflammatory (225). This form of cell death relies on caspase-1 activation and is intended to remove pathogens through massive induction of inflammatory signalling. Caspase-1-dependent pore formation results in rapid rupture of the plasma membrane and the release of the pro-inflammatory cytokines, IL-1 $\beta$  and IL-18 (226–228). Pyroptosis is initiated by activation of the NLRs, mainly NLRP3 or NLRC4, upon detection of danger signals during infection (229). NLRs then promote the formation of the inflammasome and the activation of caspase-1 through inflammasome adaptor protein ASC (230–233). Sequentially, activated caspase-1 is able to cleave the pore forming Gasdermin D (GSDMD) proteins, which are essential for the pyroptosis-mediated cytokine release (227, 234, 235). Thus far, the role of pyroptosis during *Leishmania* infection remains inconclusive. Recently, we were able to demonstrate that *L. major* spread in macrophages is diminished upon impairment of the pyroptosis pathway in vitro, implicating pyroptotic cell death as a possible exit mechanism from infected macrophages (236). Another recent study showed that *L. amazonensis* infection triggered GSDMD activation in macrophages, leading to transient pore formation, potassium efflux and NLRP3 inflammasome activation, although it did not lead to cell death (237). Moreover, other studies have suggested that host macrophage pyroptosis may contribute to *Leishmania* dissemination and that *L. amazonensis* and *L. donovani* infection suppress macrophage pyroptosis (94, 238–241).

### *Apoptosis*

During this thesis, we will mainly focus on apoptotic cell death, the most common type of programmed cell death. This evolutionarily conserved form of cell death contributes to organ development and tissue homeostasis and also plays an important role in preventing pathogen reproduction, as previously observed during viral infections (242). Apoptosis focusses on removing cellular debris in a highly regulated and controlled manner without causing collateral

damage to surrounding tissues. It is characterised by cell shrinkage, phosphatidylserine (PS) exposure, membrane blebbing, DNA fragmentation, and packaging of cell contents into apoptotic bodies and usually results in phagocytosis of such apoptotic bodies (200, 243–245). Phagocytosis of pathogen-containing apoptotic bodies prevents the release of intracellular pathogens to the extracellular space, often facilitating the re-uptake of pathogens and thus their cell-to-cell spread (246). Apoptosis is dependent on the activation of a series of cysteine-aspartate proteases known as caspases and can be initiated through two distinct signalling pathways (247). The intrinsic, or mitochondrial, pathway is usually initiated in a cell-autonomous manner. This pathway is predominantly mitochondrial-mediated and is triggered by various extra- and intra-cellular stresses, which include oxidative stress, irradiation, and treatment with cytotoxic drugs (248, 249). Additionally, the pathway can be initiated by the absence of pro-survival signals, such as cytokines, hormones and growth factors in the immediate environment of the cell. The intrinsic pathway is controlled by the Bcl2 protein family and more specifically, by the insertion of Bax/Bak into the mitochondrial outer membrane, which results in cytochrome c release from the mitochondrial intermembrane space into the cytosol and eventually in apoptosis (250, 251). On the contrary, cytochrome c release is blocked by the anti-apoptotic proteins, Bcl-2 and Bcl-xL (252).

The extrinsic, or death receptor, pathway involves a classical ligand-cell-surface-receptor interaction. This pathway is critical for immune system function and homeostasis and is engaged when extracellular ligands such as TNF, Fas ligand (Fas-L), and TNF-related apoptosis-inducing ligand (TRAIL) bind their corresponding transmembrane receptors (253, 254). This binding subsequently results in the formation of a death-inducing signalling complex (DISC) and eventually leads to a cascade of caspase activation and death of the cell (255).

Both the intrinsic and the extrinsic pathway converge at the execution phase, a phase mainly mediated by caspases (256). These caspases have been subclassified into initiator caspases (caspase-8 and -9) and executioner caspases (caspase-3, -6, and -7). The initiator caspases are activated through “induced proximity” when adaptor proteins interact with the pro-domains and promote caspase dimerization (257, 258). In contrast to the initiator caspases, the executioner caspases are activated due to proteolytic cleavage. Cleavage of caspase-6 is mediated by caspase-3 and -7, whereas activation of caspase-3 and -7 is generally carried out by the initiator caspases, caspases-8 and -9 (259). The activation of the executioner caspases initiates a cascade of events that results in endonuclease-mediated DNA fragmentation, destruction of the nuclear proteins and cytoskeleton, crosslinking of proteins, the expression of ligands for phagocytic cells and the formation of apoptotic bodies (260, 261).

Findings regarding host cell apoptosis and *Leishmania* infection so far remain inconclusive. A number of previous studies have suggested that *Leishmania* inhibit apoptosis. For example, *L. donovani* infection was suggested to inhibit the programmed cell death-1 (PD-1) receptor or to activate the anti-apoptotic AKT signalling pathway, or the anti-apoptotic protein myeloid

cell leukemia 1 (MCL-1) (262–267). Additionally, *L. donovani* and *L. infantum* promastigotes have been suggested to increase anti-apoptotic Bcl-2 in macrophages (268, 269). Moreover, camptothecin-induced apoptosis of monocyte-derived DCs was inhibited by infection with *L. mexicana* promastigotes and amastigotes and Akarid and colleagues showed that *L. major* inhibits apoptosis in murine bone marrow-derived macrophages (270–275). On the contrary, there are also a number of reports showing that *Leishmania* induce apoptosis. DaMata and colleagues demonstrated that *L. amazonensis*-induced macrophage apoptosis was associated with activation of caspases-3, -8 and -9 (276). Furthermore, parasite viability was shown to be an essential criterion for apoptosis induction in infected macrophages in vitro and *L. aethiopica*, but not *L. mexicana*, was shown to induce caspase-3-dependent host macrophage apoptosis and cell-to-cell spreading in vitro (277, 278). This suggests that host cell apoptosis might be *Leishmania* state and strain dependent, which is in line with another study showing that *Leishmania* infection protects murine macrophages from cycloheximide-induced apoptosis in a species and strain specific manner (279). Recently, we and others showed that *Leishmania* cell-to-cell transmission among phagocytes might be associated to host cell death (38, 91). Also, in a human in vitro infection model, *L. major* promastigotes, hiding inside apoptotic neutrophils, were demonstrated to transfer to macrophages, using the neutrophils as Trojan horses (82). Finally, increased apoptosis in CD4<sup>+</sup> lymphocytes and monocytes was observed in patients with acute visceral leishmaniasis (280).

## 1.6 Project aims

Despite the above-described findings about *Leishmania* cell-to-cell transmission and host cell death, transfer mechanisms remain enigmatic. So far, studies have mainly focused on the connection between infection-related inflammation and cell death and not on the link between infection and cell death on a cellular level. Therefore, we aimed to investigate host cell death in relation to *L. major* exit from and uptake into monocyte-derived phagocytes during ongoing infection in vivo.

Using intravital 2-photon microscopy of the infected skin, we show here an increased apoptosis rate in *L. major* infected phagocytes in the ongoing infection, and direct cell-to-cell transfer to newly recruited phagocytes. This transfer involved the uptake of cell material from the original infected host cell both in vivo and in isolated human cells. In addition, our findings indicated that *L. major* proliferation specifically modulates host cell metabolism and drives cell death, thereby enabling the efficient dissemination of the pathogen to new phagocytes.

As cell-to-cell transfer of *L. major* seems to be linked with pathogen proliferation, we furthermore analysed the microenvironment of cells infected with high- and low-proliferating pathogens. We could show by intravital 2-photon microscopy that pathogen proliferation in the proximity of blood vessels is higher, indicating a specific distribution of cell-to-cell transfer into monocytes newly recruited from the bloodstream.

Moreover, since IL-11 has been suggested to play a role in phagocytosis and increased levels of IL-11 mRNA were observed in the lesions of *L. donovani*-infected patients, the contribution of IL-11 signalling on monocyte-derived cell recruitment and infection by *L. major* in a mouse model of cutaneous leishmaniasis was established. In this regard, we show using flow cytometry analysis of murine *L. major*-infected ear tissue that ablation of IL-11R signalling does not influence monocyte recruitment in *Leishmania*-infected ear tissue and does not affect *Leishmania* infection in monocytes in vivo.

## 2. MATERIALS AND METHODS

### 2.1 Materials

**Table 2.1.1: Mouse lines.**

Mouse line	Supplier/Source
B6.129(ICR)-Tg(CAG-ECFP)CK6Nagy/J	Jackson Laboratories
B6.129S7-Rag1 <sup>tm1Mom</sup> /J	Jackson Laboratories
B6.Cg-Tg(Itgax-Venus)1Mnz/J	Jackson Laboratories
B6N-TyrcBrdCrCl	Charles River
B6.FVB-Tg(ITGAX-DTR/EGFP)57Lan/J	Jackson Laboratories
B6.SJL-Ptprca <sup>a</sup> Pepcb <sup>b</sup> /BoyJ	Jackson Laboratories
C57BL/6J	Charles River
IL11R <sup>+/+</sup>	Christoph Garbers, University of Magdeburg
IL11R <sup>-/-</sup>	Christoph Garbers, University of Magdeburg

**Table 2.1.2: Biological agents.**

Agents	Supplier/Source
<i>Leishmania major</i> line	
LRC-L137 V121 wild type	(Handman et al., 1983)
LRC-L137 V121, dsRed expressing	(Misslitz et al., 2000)
Lm <sup>SWITCH</sup> , mKikume expressing	(Müller et al., 2013)
MHOM/IL/81/FEBNI, dsRed expressing	(Wenzel et al., 2012)
Cell line	
294T	Stefanie Kliche, University of Magdeburg
Plasmid/construct	
pLC-ECO	Stefanie Kliche, University of Magdeburg
pLEXY-hyg2	Jena Bioscience
CFP-DEVD-YFP	Philippe Bousso, Institut Pasteur, Paris
CFP-DEVG-YFP	Philippe Bousso, Institut Pasteur, Paris

**Table 2.1.3: Basic buffers.**

Buffer	Reagents	Concentration/amount
Flow cytometry/MACS in PBS	FCS	0.5% (w/v)
	EDTA	2.5 mM

<b>PBS</b> in ddH <sub>2</sub> O, pH 7.4	NaCl	140 mM
	KCl	2.7 mM
	Na <sub>2</sub> HPO <sub>4</sub>	8 mM
	KH <sub>2</sub> PO <sub>4</sub>	1.8 mM
<b>TAP</b> in 100 mL ddH <sub>2</sub> O	Tris	242 g
	Acidic acid	57.1 mL
	EDTA	37.3 g

**Table 2.1.4: Primer sequences.**

Gene	Forward primer	Reverse primer
<i>SHERP</i>	GACGCTCTGCCCTTCACATAC	TCTCTCAGCTCTCGGATCTTGTC
<i>ABC</i>	CGGGTTTGTCTTTCAGTCGT	CACCAGAGAGCATTGATGGA
<i>NMT</i>	CCGTCGACTGTGATTGGGAA	GTGAATGCGCCACGATCAAA

**Table 2.1.5: Antibiotics.**

Antibiotic	Stock concentration	Supplier
Ciprofloxacin (Ciprobay)	50 mg/mL in ddH <sub>2</sub> O	Bayer
Hygromycin B	50 mg/mL in PBS	Thermo Fisher Scientific
Neomycin sulfate	50 mg/mL in ddH <sub>2</sub> O	Sigma–Aldrich
Penicillin/Streptomycin	10000 U, 10000 µg/mL	Biochrom AG Carl Roth

**Table 2.1.6: Kits.**

Kit	Supplier
CF® 640R TUNEL Assay Apoptosis Detection Kit	Biotium
High–Capacity cDNA reverse Transcription Kit	Applied Biosystems™
LIVE/DEAD™ Fixable Violet Dead Cell Stain Kit	Thermo Fisher Scientific
SYBR™ Green PCR Master Mix	Applied Biosystems™

**Table 2.1.7: Biochemical and chemical reagents.**

Reagent	Source/Supplier
2–Mercaptoethanol	Carl Roth
2–Mercaptoethanol	Sigma–Aldrich
2–NBDG (2–(N–(7–Nitrobenz–2–oxa–1,3–diazol–4–yl)Amino)–2–Deoxyglucose)	Invitrogen
Accutase	BioLegend
Acepromazin	CEVA GmbH
Adenine	Sigma–Aldrich
Agarose Standard	Carl Roth
AlexaFluor405SE	Molecular Probes
AmBisome	Gilead Sciences

Aminoethyltrioxsalen (AMT, psoralen)	Sigma-Aldrich
BD FACS Flow™ Sheath Fluid	BD Bioscience
BD FACST™ Clean Solution	BD Bioscience
BD FACST™ Rinse Solution	BD Bioscience
Biotin	Sigma-Aldrich
Biotin MicroBeads	Miltenyi Biotech
Biopterin	Sigma-Aldrich
BODIPY™ 500/510 C1, C12 (4,4-Difluoro-5-Methyl-4-Bora-3a,4a-Diaza-s-Indacene-3-Dodecanoic Acid)	Invitrogen
BODIPY™ FL C16 (4,4-Difluoro-5,7-Dimethyl-4-Bora-3a,4a-Diaza-s-Indacene-3-Hexadecanoic Acid)	Invitrogen
BODIPY™ FL LDL (Low Density Lipoprotein from Human Plasma, BODIPY™ FL complex)	Invitrogen
Bovine serum albumin (BSA)	Sigma-Aldrich
Calcium chloride (CaCl <sub>2</sub> )	Carl Roth
Caspase-3 reporter dye NucView405	Biotium
Carboxyfluorescein succinimidyl ester (CFSE)	Molecular Probes
Chloroform	Sigma-Aldrich
Chloroquine	Sigma-Aldrich
Collagenase	Sigma-Aldrich
4',6-Diamidino-2-phenylindole dihydrochloride (DAPI)	Sigma-Aldrich
Diphtheria toxin (DTX)	Sigma-Aldrich
DMEM medium	Sigma-Aldrich
DNase I	Invitrogen
Endotoxin-Free Ultra Pure Water	Merck
Ethanol (99% v/v)	Carl Roth
Ethidium bromide	Carl Roth
Ethylenediaminetetraacetic acid (EDTA)	Carl Roth
Fetal Calf Serum (FCS)	Pan Biothech GmbH
Fetal Calf Serum (FCS)	Sigma-Aldrich
Gamma-interferon	R&D Systems
Glycerol	Carl Roth
Glycogen	Sigma-Aldrich
Heat-inactivated fetal bovine serum	PAN Biotech
Hemin	Sigma-Aldrich
4-(2-hydroxyethyl)-1-piperazineethanesulfonic acid (HEPES)-Buffer	Gibco
4-(2-hydroxyethyl)-1-piperazineethanesulfonic acid (HEPES)-Buffer	Biochrom AG

Isoflurane	CP Pharma
Isopropanol	Carl Roth
IVISense Vascular NP 680 Fluorescent Nanoparticles (AngioSPARK)	PerkinElmer
Ketamine	Ratiopharm
L-Glutamin	Gibco
L-Glutamin	Biochrom AG
Liberase™ TL	Roche/Sigma-Aldrich
N6-(1-iminoethyl)-L-lysine hydrochloride (L-NIL)	Sigma-Aldrich
LPS	Sigma-Aldrich
Macrophages colony-stimulating factor (M-CSF)	PeProTech
Macrophages colony-stimulating factor (M-CSF)	R&D systems/bio-technie
Magnesium chloride (MgCl <sub>2</sub> )	Carl Roth
<i>Medium</i> 199	Sigma-Aldrich
Mouse Interleukin-3	R&D Systems
Mouse Interleukin-6	R&D Systems
Mouse serum	Recovered from mice
Natriumchloride (NaCl)	Carl Roth
Paraformaldehyde (PFA)	Sigma-Aldrich
PBS Dulbecco (phosphate-buffered saline, without (w/o) Ca <sup>2+</sup> , Mg <sup>2+</sup> )	Biochrom AG
Perm/Wash buffer	BD Biosciences
Polybrene	Sigma-Aldrich
Quick-Load 1 kb DNA Ladder	New England Biolabs
Random hexamer primers	Thermo Fisher Scientific
Retronectin	Takara
RPMI 1640 medium	PAN Biotech
RPMI 1640 medium	Sigma-Aldrich
SOC-medium	New England Biolabs
Sodium chloride (NaCl)	Carl Roth
Sodiumpyrovat	Gibco
Stem cell factor (SCF)	Sigma-Aldrich
StemSpan™ SFEM	Stemcell
Sucrose	Carl Roth
Tris (hydroxymethyl)-aminomethan (Tris)	Carl Roth
Triton X-100	Sigma-Aldrich
TRIZOL	Invitrogen
Trypan Blue Solution (0.4%)	Sigma-Aldrich

Trypsin/EDTA	Merck Millipore
Xylazine (Rompun 2%)	Bayer

**Table 2.1.8: Antibodies for negative hematopoietic stem cell selection via MACS.** All antibodies are biotin-labelled and diluted in MACS buffer.

Antibody specificity	Clone	Supplier	Dilution from commercial stock
CD127 (IL-7R $\alpha$ )	SB/199	BioLegend	1:500
CD19	6D5	BioLegend	1:500
CD3 $\epsilon$	145-2C11	BioLegend	1:500
CD4	GK1.5	BioLegend	1:500
CD45R/B220	RA3-6B2	BioLegend	1:500
CD8a	53-6.7	BioLegend	1:500
Ly-6G/Ly-6C (Gr-1)	RB6-8C5	BioLegend	1:500
TER119	TER-119	BioLegend	1:500

**Table 2.1.9: Antibodies for hematopoietic stem cell sorting using Aria III Cell Sorter.**

Antibody specificity	Clone	Supplier	Dilution from commercial stock	Label
cKIT	2B8	BioLegend	1:500	AF647
Sca-1	D7	BioLegend	1:500	FITC
Streptavidin	n/a	BioLegend	1:500	BV421

**Table 2.1.10: Antibodies for flow cytometry analysis.**

Antibody specificity	Clone	Supplier	Dilution from commercial stock	Label
AnnexinV	n/a	BioLegend	1:40	APC
AnnexinV	n/a	BioLegend	1:40	AF647
CD11b	M1/70	BioLegend	1:200	APC
CD11c	N418	BioLegend	1:200	APC-Cy7
CD16/32	93	BioLegend	1:100	None (Fc-block)
CD36	CRF D-2712	BioLegend	1:200	APC
CD36	CRF D-2712	BioLegend	1:200	FITC
CD45	30-F11	BioLegend	1:200	BV510
CD45.1	A20	BioLegend	1:200	APC-Cy7
CD45.1	30-F11	BioLegend	1:200	PerCP-Cy5
CD45.2	104	BioLegend	1:200	PE-Cy7

F4/80	BM8	BioLegend	1:200	BV421
Glut1	SA0377	Invitrogen	1:200	APC
iNOS	CXNFT	Invitrogen	1:200	APC
Ly6C	HK1.4	BioLegend	1:200	Pe-Cy7
Ly6C	HK1.4	BioLegend	1:200	BV785
Ly6G	1A8	BioLegend	1:200	BV421
MHC class II (IA/IE)	M5/114.15.2	BioLegend	1:200	BV510

**Table 2.1.11: Laboratory equipment.**

Equipment	Supplier
24-well Nunc™ UpCell plates	Thermo Fisher Scientific
μ-Dish 35 mm, high Grid-500 Glass Bottom	ibidi
ABI PRISM 7000	Applied Biosystems
Aria III Cell Sorter	BD Biosciences
AutoMACS Pro Separator	Miltenyi Biotech
Centrifuge 1-16K	Sigma
FACS Fortessa	BD Biosciences
FACS Symphony	BD Biosciences
FACS ARIA III	BD Biosciences
Gel Doc XR+ System	Bio-Rad
Gene Pulser II System	BioRad
HeraSafe HS 12	Heraeus
Incubating orbital shaker	VWR
Incubator	Gesellschaft für Labortechnik
LED diodes 375 nm	Strato
LED diodes 405 nm	Thorlabs
MicroAmp™ Fast Optical 96-Well Reaction Plate with Bar-code, 0.1 mL	Applied Biosystems™
(Wide) Mini-sub® Cell GT	BioRad
Multifuge 1 SR/3 SR	Heraeus
NanoDrop ND-1000 Spectrophotometer	Thermo Fisher Scientific
Thermocycler	Bio-Rad
Thermomixer comfort	Eppendorf
Tube Revolver	Thermo Fisher Scientific
qTOWER3 G RT-PCR Cycler	Analytik Jena

**Table 2.1.12: Microscopes.**

Equipment	Supplier
<b>2-photon microscope</b>	
LSM 700 confocal laser scanning microscope	Zeiss
Mai Tai DeepSee Ti:Sa laser	Spectra-Physics
W Plan-Apochromat 20x/1.0 DIC VIS-IR dipping objective	Zeiss
<b>Inverted transmitted light microscope</b>	
Wilovert S	Helmut Hund GmbH
<b>Widefield microscope</b>	
Leica DMI8 inverted microscope	Leica Microsystems
20x dry objective	Leica Microsystems

**Table 2.1.13: Software.**

Software	Supplier
Ape (A plasmid Editor)	M. Wayne Davis
BD FACS Diva	BD Biosciences
Deconvolution/deblurring algorithm	XCOSM software package
DiscIT	(Moreau et al., 2012)
Fiji software	NIH, <a href="http://rsb.info.nih.gov/ij/">http://rsb.info.nih.gov/ij/</a>
FlowJo X software	FlowJo, LLC
GraphPad Prism 8	GraphPad Inc. Software
Imaris	Oxford Instruments
Las X Navigator	Leica microsystems
NxT Software	Thermo Fisher Scientific
ZEN acquisition software	Zeiss

## 2.2 Methods

### 2.2.1 Parasites, mice and infections

All mice were bred and housed under specific pathogen-free conditions in the central animal facility (ZTL) of the Medical Faculty at the Otto von Guericke University of Magdeburg (Table 2.1.1). Wild type CD45.1 (B6.SJL-*PtprcaPepcb*/BoyJ), Actin-ECFP (B6.129(ICR)-Tg(CAG-ECFP)CK6Nagy/J), CD11c-DTR-GFP<sup>t9</sup> (B6.FVB-Tg(ITGAX-DTR/EGFP)57Lan/J), *Rag1*<sup>-/-</sup> (B6.129S7-*Rag1*<sup>tm1Mom</sup>/J) and CD11c-EYFP (B6.Cg-Tg(Itgax-Venus)1Mnz/J) mice were purchased from Jackson Laboratories (Bar Harbor, MA), wild type C57BL/6J and B6N-TyrcBrdCrCrl (B6 albino wild type) mice were obtained from Charles River (Sulzfeld, Germany) and mice deficient for IL-11R have been described previously (281). Mice were used at an age of 8–10 weeks for bone marrow recipients, and up to 16 weeks for infection and as donors. All mice had been backcrossed for at least 10 generations onto a C57/BL6 background by the commercial suppliers. Age- and sex-matched animals were used as controls.

For all murine in vivo and in vitro experiments, *L. major* LRC-L137 V121 wild type, DsRed or mKikume expressing *Lm*<sup>SWITCH</sup> parasites were previously described (282–284) (Table 2.1.2). Parasites were grown in M199 medium completed with 10% heat-inactivated fetal calf serum (FCS), 0.1 mM adenine, 1 mg/mL biotin, 5 mg/mL hemin, and 2 mg/mL biopterin (all from Sigma) for maximally 6 passages.

For the infection of human monocyte-derived macrophages (MDM), *L. major* (MHOM/IL/81/FEBNI) DsRed parasites were cultured on Novy-McNeal-Nicolle modified medium and axenic amastigotes were generated from logarithmic phase promastigotes as described previously (285). Axenic amastigotes were resuspended in complete medium, centrifuged (2400 g, 8 min, at room temperature (RT)) and adjusted to  $10 \times 10^6$  parasites per mL.

For the infection of mice, stationary phase promastigote parasites were centrifuged (600 g, 5 min, RT) and resuspended in PBS. For flow cytometry analysis,  $2 \times 10^6$  and for intravital imaging,  $2 \times 10^5$  parasites were subsequently injected in 10  $\mu$ L into the ear dermis. Analysis was performed 3 weeks post infection. Photoconversion of the *Lm*<sup>SWITCH</sup> parasites in the mouse ear was performed with a 405 nm wavelength, 665 mW/cm<sup>2</sup> collimated high power LED (Thorlabs). Ears of anesthetized mice were illuminated from each side for 30 seconds at 20 cm distance and analysed after 48h by flow cytometry.

### 2.2.2 Preparation of killed but metabolically active parasites

To prepare the KBMA *L. major*,  $12.5 \times 10^6$  parasites were opsonized with RPMI 1640 containing 25% naïve mouse serum and  $10 \mu\text{M}$  4'aminomethyl-4,5',8-trimethyl psoralen (AMT) (Sigma-Aldrich) for 30 min at  $26^\circ\text{C}$ . Parasites were illuminated for 10 minutes with 375 nm UV-A-light using an assembly of  $3 \times 3$  LED diodes (Strato, half-viewing angle:  $10^\circ$ ; Radiant Power: 10 mW) at a distance of 0.8 cm. The KBMA parasites were washed once with pre-warmed RPMI for 10 min at 2500 rpm,  $4^\circ\text{C}$  and used for the infection of murine intraperitoneal or murine bone marrow-derived macrophages.

Proliferation competence was tested by comparing  $5 \times 10^6$  *Lm<sup>DsRed</sup>* proliferation-competent and KBMA promastigotes which were seeded in pre-warmed M199 medium completed with 10% heat-inactivated FCS, 0.1 mM adenine, 1 mg/mL biotin, 5 mg/mL hemin, and 2 mg/mL biopterin (all from Sigma) into each well of an uncoated 24-Well plate and incubated at  $26^\circ\text{C}$ . The parasite concentration of each sample was determined after counting using a Neubauer chamber at day 0, 1, 2 and 3.

### 2.2.3 Adoptive cell transfer

For bone marrow isolation, bone marrow cells from CD45.1<sup>+</sup> or constitutively CFP-expressing Actin-CFP wild type mice were flushed out of tibia and femur with ice cold non-supplemented RPMI medium and filtered through 100-micron cell strainers. Cells were washed with non-supplemented PBS, and  $8 \times 10^7$  cells per recipient were resuspended in PBS and injected intravenously into the tail vein of CD45.2<sup>+</sup> C57BL/6 or CD11c-YFP reporter mice. 5 days post transfer, immune cells isolated from the infected ears were analysed via flow cytometry.

For Carboxyfluorescein succinimidyl ester (CFSE) staining, CD45.1<sup>+</sup> wild type, IL-11R<sup>+/+</sup> and IL-11R<sup>-/-</sup> bone marrow cells mice were mixed in a 1:1 ratio and labelled with CFSE for 20 minutes at 37°C in non-supplemented PBS. Thereafter, cells were washed with PBS supplemented with 10% FCS, and  $8 \times 10^7$  cells per recipient were resuspended in PBS and injected intravenously into the tail vein of CD45.2<sup>+</sup> C57BL/6 mice. As a control for IL-11R deficiency, CFSE-labelled CD45.1<sup>+</sup> WT and CD45.2<sup>+</sup> IL-11R<sup>+/+</sup> cells were injected intravenously into the tail vein of CD45.2<sup>+</sup> C57BL/6 mice. Immune cells isolated from the infected ears were analysed via flow cytometry 5 days post transfer.

## 2.2.4 Generation of bone marrow chimeric mice

In order to study the effect of CD11c cell depletion during *Leishmania* infection, bone marrow chimeric mice were generated. To this end, we made use of cells containing a diphtheria toxin receptor (DTR)–Enhanced Green Fluorescent Protein (EGFP, Stratagene) fusion protein under the control of the CD11c promoter. These cells allowed us to deplete CD11c cells by intraperitoneal application of diphtheria toxin (DTX) (Sigma–Aldrich). For generation of bone marrow chimeric mice,  $20 \times 10^6$  CD11c–DTR/GFP bone marrow cells were used to reconstitute lethally irradiated 9–10–week–old wild type CD45.1<sup>+</sup> (B6.SJL–*Ptprca<sup>a</sup>Pepc<sup>b</sup>*/BoyJ) or C57BL/6J recipient mice, resulting in animals that expressed the DTR on CD11c cells specifically in the non–lymphocyte immune cell compartment. Drinking water was supplemented with neomycin sulfate (2 g/L Sigma–Aldrich) for two weeks following transplantation to prevent infection with opportunistic pathogens. Nine weeks post transplantation, mice were infected with  $2 \times 10^6$  DsRed–expressing *L. major*. Mice were then exposed to either 96 h or 48 h of CD11c cell depletion. Mice undergoing the 96 h depletion were injected intraperitoneally with 4 µg/kg body weight DTX (dissolved at 1 µg/mL in PBS) 96 h and 48 h before analysis and mice undergoing the 48 h depletion were injected with 4 µg/kg body weight DTX (dissolved at 1 µg/mL in PBS) 48 h before analysis with flow cytometry.

In order to visualise apoptosis in myeloid cells, we employed a genetically encoded reporter based on a Förster Resonance Energy Transfer (FRET)–based CFP–DEVD–YFP construct for Caspase–3 activity or a non–cleavable CFP–DEVG–YFP control construct (286–288) (Table 2.1.2). For virus production, the constructs, encoded on mouse stem cell virus (MSCV) vectors (kindly provided by Philippe Bousso, Institut Pasteur, Paris) were transfected into 294T cells (kindly provided by Stefanie Kliche, University of Magdeburg) together with the pLC–ECO helper plasmid (Addgene plasmid # 12371, kindly provided by Stefanie Kliche, University of Magdeburg) (Table 2.1.2) in DMEM medium with 10% FCS and 1:1000 (V/V) Chloroquine (Sigma–Aldrich). Bone marrow–derived hematopoietic stem cells (HSCs) from 8–16 week old *Rag1<sup>-/-</sup>* donor mice were isolated by negative magnetic selection after incubation at 4° C for 30 min with lineage biotinylated antibodies anti–CD45R/B220 (clone RA3–6B2), anti–Ly–6G/Ly–6C (Gr–1) (clone RB6–8C5), anti–TER119 (clone TER–119), anti–CD3ε (clone 145–2C11), anti–CD19 (clone 6D5), anti–CD4 (clone GK1.5), anti–CD8a (clone 53–6.7) and anti–CD127 (IL–7Rα) (clone SB/199), which were all purchased from BioLegend. Cells were washed once with 1x PBS/2% EDTA and incubated with 1:10 Biotin MicroBeads in 1x PBS/2% EDTA for 15 min at 4° C. Removal of lineage–positive cells was performed using an autoMACS Pro Separator (Miltenyi Biotech). The purified cells were stained with BV421 conjugated anti–Streptavidin (Biolegend), AF647 conjugated anti–cKIT (Biolegend, clone 2B8) and FITC conjugated anti–Sca–1 (Biolegend, clone D7) at 4° C. Lin–cKit<sup>+</sup>Sca1<sup>+</sup> HSCs were FACS sorted on an Aria III Cell Sorter (BD Biosciences) with a flow rate < 5 into a 10% BSA–coated collection tube containing 1 mL StemSpan™ SFEM (Stemcell) + 2 mg Ciprobay (Bayer). Cells, with a final concentration of

$2 \times 10^6$  cells/mL, were resuspended in StemSpan™ SFEM (Stemcell) + 2 mg/mL Ciprobay + 10 ng/mL mIL-3 + 30 ng/mL mIL-6 + 50 ng/mL Stem cell factor (SCF) and 100  $\mu$ L cell suspension was added to each well of a 50  $\mu$ g/mL retronectin-coated (Takara) 96-well. Cells were incubated overnight at 37 °C and 5% CO<sub>2</sub>. For transfection of the HSCs, the CFP-DEVD-YFP and CFP-DEVG-YFP encoding retroviral particles were added to retronectin-coated wells containing StemSpan™ SFEM + 2 mg/mL Ciprobay + 10 ng/mL mIL-3 + 30 ng/mL mIL-6 + 50 ng/mL SCF + 4  $\mu$ g/mL Polybrene and 1:20 HSC suspension was added with a final concentration of 1:2. Thereafter, plates were centrifuged at 700 g, 90 min, 30 °C and incubated at 37 °C, 5% CO<sub>2</sub> overnight. The transfection procedure was repeated the next day. After overnight incubation, transfection efficiency was determined using flow cytometry analysis by measuring the percentage of YFP<sup>+</sup> cells. For generation of bone marrow chimeric mice,  $1 \times 10^5$  transfected *Rag1*<sup>-/-</sup>-HSCs together with  $1 \times 10^5$  wild type CD45.1<sup>+</sup> supporter bone marrow cells were used to reconstitute lethally irradiated 10-week-old B6N-Tyrc BrdCrCrl recipient mice, resulting in animals that expressed the reporter constructs specifically in the non-lymphocyte immune cell compartment. Drinking water was supplemented with neomycin sulfate (2 g/L Sigma-Aldrich) for two weeks following transplantation to prevent infection with opportunistic pathogens. After two weeks, blood of CFP-DEVD-YFP and CFP-DEVG-YFP bone marrow chimeras was isolated and FRET was measured by flow cytometry analysis in order to test whether the bone marrow chimeric mice were successfully reconstituted with our DEVD and DEVG (control) construct. Four weeks later, mice were infected with  $2 \times 10^5$  DsRed-expressing *L. major* and imaged three weeks later using intravital 2-photon microscopy.

### 2.2.5 Human monocyte-derived macrophages

Human peripheral blood mononuclear cells were isolated from buffy coats of anonymised donors (DRK-Blutspendedienst Hessen GmbH) as previously described (289). Human MDM were generated by cultivation in complete medium composed of RPMI 1640, 10% FCS, 50  $\mu$ M  $\beta$ -mercaptoethanol (all from Sigma), 2 mM L-glutamine, 100 U/mL penicillin, 100  $\mu$ g/mL streptomycin and 10 mM HEPES (all from Biochrom AG), supplemented with 50 ng/mL macrophages colony-stimulating factor (M-CSF) (R&D systems / bio-technie) for 5–7 days at 37°C, 5% CO<sub>2</sub>. If not stated otherwise, all incubation and infection steps with cultured human MDM were performed at 37°C, 5% CO<sub>2</sub> using complete medium.

For co-incubation experiments, human MDM were harvested, centrifuged at 147 g, 8 min, RT and stained using 5  $\mu$ M AlexaFluor405SE in PBS (Molecular Probes) according to manufacturer's instructions. Cells were seeded into 12-well culture plates with  $3 \times 10^5$  human MDM per well, infected with axenic amastigotes (MOI 5) for 3 h and washed twice. 24 h post-infection, uninfected human MDM were stained using 5  $\mu$ M CFSE in PBS (Molecular Probes) according to manufacturer's instructions and added to infected macrophages in a ratio of 1:1. After 18 h of co-incubation, cells were harvested, centrifuged at 500 g, 5 min, RT and resuspended in MACS buffer composed of PBS, 0.5% BSA, 0.5 mM EDTA for analysis by flow cytometry.

For the caspase-3 reporter staining, human MDM were harvested, centrifuged at 147 g, 8 min, RT and seeded into 24-well Nunc™ UpCell plates (Thermo Fisher Scientific) with  $2 \times 10^5$  cells per well. Adhered cells were infected with axenic amastigotes (MOI 2) and incubated for 24 h. Subsequently, the caspase-3 reporter dye NucView405 (Biotium) was added to the culture with a final concentration of 2.5  $\mu$ M and incubated for additional 20 h. Cells were then resuspended in the supernatant, centrifuged at 500 g, 5 min, RT and resuspended in MACS buffer for analysis by flow cytometry.

### 2.2.6 Murine macrophages

For isolation of peritoneal macrophages, mice were sacrificed and subsequently 5 mL cold PBS (Sigma–Aldrich) was injected intraperitoneally. The cell suspension was aspirated and cells were seeded in RPMI 1640 (PAN Biotec) supplemented with 10% heat–inactivated fetal bovine serum (PAN Biotec) and 1% Penicillin–Streptomycin (10.000 U/mL, Biochrom) for infection and live cell imaging. For infection, peritoneal macrophages were cultured for 24 h at 37°C, 5% CO<sub>2</sub> and stationary phase non–photoconverted, green fluorescent proliferation–competent *Lm<sup>SWITCH</sup>* (MOI 10) and red fluorescent *Lm<sup>DsRed</sup>* KBMA (MOI 80) promastigotes (opsonised with 25% mouse immune serum for 30 min at 26°C) were added for 2 h. After 24 h of infection, cells were induced with gamma–interferon (0.01 ng/μL, R&D Systems), LPS (1 μg/mL, E. coli O26:B6, Sigma–Aldrich) and the nitric oxide synthase iNOS was inhibited by addition of N6–(1–iminoethyl)–L–lysine hydrochloride (L–NIL) (0.023 μg/μL, Sigma–Aldrich) as described previously (282). TUNEL staining was performed using the CF<sup>®</sup> 640R TUNEL Assay Apoptosis Detection Kit (Biotium) according to the manufacturer's instructions and staining with 0.2 μg/mL DAPI (Sigma–Aldrich). For analysis of parasite proliferation rate during microscopy, *Lm<sup>SWITCH</sup>* parasites were photoconverted for 5 sec at maximum intensity under a 20x dry objective using the 405 nm excitation of a Leica DMI8 inverted microscope (Leica Microsystems) which was also used for all time–lapse microscopy of cell culture infections. 490 nm excitation and 500/550 nm emission was used for detecting non–photoconverted mKikume, 550 nm excitation and 573/647 nm emission for photoconverted mKikume and DsRed, 635 excitation and 662 nm for detection of TUNEL staining and 385 excitation and 425 nm for detection of DAPI staining. Images were automatically acquired every 10 min for a total of 48 h and movies were processed with the Fiji software (NIH, <http://rsb.info.nih.gov/ij/>).

For preparation of bone marrow–derived macrophages (BMDM), bone marrow cells from CD45.1<sup>+</sup> wild type mice were flushed out of tibia and femur with ice cold non–supplemented RPMI medium and filtered through 100–micron cell strainers. Cells were washed with non–supplemented PBS, and 8 × 10<sup>7</sup> cells seeded in RPMI 1640 supplemented with 10% heat–inactivated fetal bovine serum, 1% Penicillin–Streptomycin (10.000 U/mL), 1% 100 mM Sodium pyruvate (Gibco), 1 μg/mL M–CSF (PeProTech) and 50 μM 2–mercaptoethanol (Carl Roth) into each well of an uncoated 6–Well plate (TPP–92406). The medium was changed every three days. After seven days of differentiation, the cells were used in further experiments. For infection, stationary phase *Lm<sup>DsRed</sup>* proliferation–competent (MOI 20) and proliferation–incompetent KBMA (MOI 50) promastigotes (opsonized with 25% mouse immune serum for 30 min at 26°C) were added for 2 h, washed three times with pre–warmed medium and cultivated for 48 h. Cells were then detached using 1 mL of Accutase (BioLegend) and incubation for 15 minutes at 37 °C, and removed by pipetting.

Uptake of short– or medium–chain fatty acids was determined by incubation with 0.5 μg/mL 4,4–Difluoro–5–Methyl–4–Bora–3a,4a–Diaza–s–Indacene–3–Dodecanoic Acid (C<sub>1</sub>–BODIPY

500/510 C<sub>12</sub>, Invitrogen) in PBS for 15 min, RT. Long-chain fatty acid uptake was quantified by incubation with 0.1 µg/mL 4,4-Difluoro-5,7-Dimethyl-4-Bora-3a,4a-Diaza-s-Indacene-3-Hexadecanoic Acid (BODIPY™ FL C<sub>16</sub>, Invitrogen) in PBS for 15 min, RT. LDL uptake was measured by incubation with 20 µg/mL Low Density Lipoprotein from Human Plasma, BODIPY™ FL complex (BODIPY™ FL LDL, Invitrogen) in PBS for 30 min, RT. Glucose uptake was determined using incubation of 100 µM 2-(N-(7-Nitrobenz-2-oxa-1,3-diazol-4-yl)Amino)-2-Deoxyglucose (2-NBDG, Invitrogen) in glucose-free medium (290) for 90 min at 37°C, 5% CO<sub>2</sub>.

APC conjugated anti-Glut1 (clone SA0377) or anti-CD36 (clone CRF D-2712), BV421 conjugated anti-F4/80 (clone BM8), and BV510 conjugated anti-CD45 (clone 30-F11), which were all purchased from BioLegend, were used for surface staining. For live/dead staining, antibodies were diluted in FACS Buffer containing 1:500 LIVE/DEAD™ Fixable Violet Dead Cell Stain Kit (Thermo Fisher Scientific). For AnnexinV staining, cells were resuspended AnnexinV binding buffer (H<sub>2</sub>O, 10 mM 4-(2-hydroxyethyl)-1-piperazineethanesulfonic acid (HEPES)-Buffer (Gibco), 50mM NaCl, 10mM CaCl<sub>2</sub> (Carl Roth), sterile filtered) containing 1:40 APC-labelled AnnexinV (BioLegend) or AF647-labelled AnnexinV (BioLegend). Cells were incubated for 15 minutes on ice in the dark and washed once with AnnexinV binding buffer for 5 minutes at 900 g, 4 °C before analysis.

DsRed fluorescence was read out at 558 nm excitation and 585/15 nm emission and autofluorescence was recorded at 488 nm excitation and 695/40 nm emission. Samples were Fc-blocked using anti-CD16/32 antibody (clone 93) (BioLegend) before antibody staining. Analysis was performed with a Fortessa or FACS ARIA III (BD Biosciences) using 355, 405, 488 and 633 nm lasers. Data were analysed using the FlowJo X software (FlowJo, LLC).

### 2.2.7 Flow cytometry

For the analysis of *in vivo* experiments, ears of mice were separated into two sheets (ventral and dorsal) using forceps and enzymatically digested in RPMI 1640 medium containing 0.1 mg/mL Liberase™ TL (Sigma) and 4 µg/mL DNase (Sigma–Aldrich) for 60 min shaking at 600 rpm and 37°C, and passed through a 70 µm cell strainer. Surface staining of cells was done using APC conjugated anti-CD11b (clone M1/70), APC conjugated anti-iNOS (clone CXNFT), APC–Cy7 conjugated anti-CD11c (clone N418), APC–Cy7 conjugated anti-CD45.1 (clone A20), PE–Cy7 conjugated anti-CD45.2 (clone 104), PerCP–Cy5.5 conjugated anti-CD45 (clone 30–F11), BV421 conjugated anti-Ly6G (clone 1A8), BV421 conjugated anti-F4/80 (clone BM8), BV510 conjugated anti-MHC class II (IA/IE, clone M5/114.15.2), FITC- or APC-conjugated anti-CD36 (clone CRF D-2712) and PE–Cy7 or BV785 conjugated anti-Ly6C (clone HK1.4), which were all purchased from BioLegend. DsRed fluorescence was read out at 558 nm excitation and 585/15 nm emission. An autofluorescence signal was recorded at 488 nm excitation and 695/40 nm emission. Samples were Fc-blocked using anti-CD16/32 antibody (clone 93) (BioLegend) before antibody staining. Analysis was performed with a Fortessa or FACS ARIA III (BD Biosciences) using 355, 405, 488, 561 and 640 nm lasers. For *in vitro* experiments using human MDM, analysis was performed with FACS Symphony or FACS Fortessa (both BD) with laser lines 402 nm (VioFluor405SE, 410LP 431/28), 405 nm (NucView405, 450/50), 488 nm (CFSE, 505LP 530/30 and autofluorescence, 685LP 710/50) and 561 nm (DsRed, 570LP 586/15). Data were analysed using the FlowJo X software (FlowJo, LLC).

### 2.2.8 Proliferation analysis

For widefield microscopy analysis, the proliferation index of *L. major* was calculated based on the fluorescence signals of mKikume Green and mKikume Red in parasite regions of interest defined in a combined total mKikume channel without any proliferation information. In each image analysed, at least five background regions of interest were defined, and their average fluorescence was subtracted from the respective parasite signals. Parasite proliferation index values were defined as

$$10 - \frac{mKikume\ Red_{parasite} - mKikume\ Red_{background}}{mKikume\ Green_{parasite} - mKikume\ Green_{background}}$$

For photoconversion in vivo and subsequent flow cytometry analysis, a 405 nm wavelength, 665 mW/cm<sup>2</sup> collimated high power LED (Thorlabs) was used. Ears of anesthetized mice were fixed and illuminated from each side for 30 seconds at a distance of 20 cm and cells isolated from the infected tissues were analysed after 48 h by flow cytometry. The proliferation index of *L. major* for flow cytometry was calculated based on the MFI of mKikume Green and mKikume Red as described previously (91). In brief, for visualising qualitative comparisons within the same sample using the FlowJo X software (FlowJo, LLC), values were plotted as

$$100 - 10 * \left( \frac{mKikume\ Red}{mKikume\ Green} \right)_{cell}$$

For inter-sample comparison of flow cytometry data, the proliferation index was calculated as

$$\frac{1 - \left( \frac{mKikume\ Red}{mKikume\ Green} \right)_{mean\ (cell\ population\ of\ interest)}}{1 - \left( \frac{mKikume\ Red}{mKikume\ Green} \right)_{mean\ (all\ infected\ cells)}}$$

and represented as percent deviation from the total infected cell population within one sample.

### 2.2.9 Quantitative Reverse Transcription PCR

A quantitative Reverse Transcription Polymerase Chain Reaction (qRT-PCR) was performed to measure promastigote (SHERP) and amastigote (ABC) gene expression in BMDM infected with *Lm<sup>DsRed</sup>* proliferation-competent and KBMA proliferation-incompetent parasites. Extracellular promastigotes were used as a positive control for promastigote gene expression. Ribonucleic acid (RNA) was isolated from infected BMDM and extracellular promastigotes 48 h post-infection. Samples were transferred to 1.5 mL Eppendorf tubes, washed once with PBS and incubated in 1 mL TRIzol reagent (Invitrogen) for 5 min, RT. For RNA extraction, 200  $\mu$ L Chloroform (Sigma-Aldrich) was added and samples were mixed by shaking vigorously and incubated for 2–3 min, RT. Subsequently, samples were centrifuged for 15 minutes at 12000 g, 4 °C and 500  $\mu$ L clear aqueous phase was carefully transferred into a fresh 1.5 mL Eppendorf tube. Thereafter, 1  $\mu$ L Glycogen and 500  $\mu$ L isopropanol were added and samples were incubated for 20 min, –80 °C. After centrifugation for 20 min at 12000g, 4°C, samples were washed with 1 mL 75% cold ethanol for 15 min at 7400g, 4°C. After removal of 75% Ethanol, samples were incubated in 10  $\mu$ L PCR water for 2–3 min, RT, resuspended and total RNA concentration was measured using a NanoDrop ND-1000 Spectrophotometer (Thermo Fisher Scientific).

cDNA was synthesised using random hexamer primers and the High-Capacity cDNA reverse Transcription Kit (Applied Biosystems™) according to the manufacturer's instructions starting from 500 ng total RNA and amplified using a thermocycler (Bio-Rad). PCR products were analysed on a 3% agarose gel and agarose gel pictures were captured using Gel Doc XR+ System (Bio-Rad).

For RT-qPCR analysis of infected BMDM and extracellular promastigotes, the SYBR™ Green PCR Master Mix (Applied Biosystems™) was used according to the manufacturer's instructions to measure SHERP and ABC expression (Table 2.1.4). RT-qPCR was run on a qTOWER3 G RT-PCR Cycler (Analytik Jena). Samples were analysed in triplicates and  $C_T$  values were exported from the ABI PRISM 7000 (Applied Biosystems) sequence detection system. For normalization, the NMT gene expression was included as a reference (Table 2.1.4).

### 2.2.10 Intravital imaging

For intravital 2-photon microscopy, mice were anaesthetised and prepared as described previously (91). Two-photon imaging was performed with a W Plan-Apochromat 20x/1,0 DIC VIS-IR objective (Zeiss) on a LSM 700 confocal laser scanning microscope (Zeiss) and Mai Tai DeepSee (tuned to 840 nm or 920 nm).

For intravital analysis of cell-to-cell transmission, CFP, YFP and DsRed fluorescence as well as harmonics were split with 555 nm long pass, 495 nm long pass, and 510 nm long pass dichroic mirrors and filtered with 600/40 (DsRed), 465/15 (second harmonics), 519/49 (CFP) and 560/25 (YFP) nm bandpass filters.

For analysis of host cell apoptosis *in vivo*, the emitted FRET signal and second harmonics were split with 555 nm long pass, 445 nm long pass, and 510 nm long pass dichroic mirrors and filtered with 465/15 (second harmonics), 519/49 (FRET CFP), 560/25 (FRET YFP) and 600/40 (DsRed) nm bandpass filters before collection with nondescanned detectors.

For blood vessel distance studies, photoconversion of the proliferation biosensor containing *Lm*<sup>SWITCH</sup> parasites in the mouse ear was performed with a 405 nm wavelength, 665 mW/cm<sup>2</sup> collimated high power LED (Thorlabs). Ears of anaesthetised mice were fixed and illuminated from each side for 30 seconds at a distance of 20 cm and were analysed after 48 h by intravital imaging. Mice were injected intravenously with 50 µL IVISense Vascular NP 680 Fluorescent Nanoparticles (AngioSPARK) (PerkinElmer), 15 minutes before intravital 2-photon imaging to visualise the vascularity during *Leishmania* infection in order to determine *Leishmania* proliferation in relation to blood vessel distance *in vivo*. For analysis of parasite proliferation *in vivo*, the emitted mKikume signal, Angiospark signal and second harmonics (all excited at 920 nm) were split with 625 nm long pass, 495 nm long pass, 525 nm long pass, and 555 nm long pass dichroic mirrors and filtered with 470/20 (second harmonics), 525/50 (mKikume green), 600/40 (mKikume red), and 665/80 (Angiospark) nm bandpass filters before collection with nondescanned detectors.

Imaging volumes of 0.8 mm<sup>3</sup> for automated analysis were obtained by collecting 3–4 µm spaced z stacks using the ZEN acquisition software (Zeiss). Images were colour corrected using the channel arithmetics function, superimposed and analysed using the Imaris software (Oxford Instruments), 3D projections and slices were extracted using the Fiji software (NIH, <http://rsb.info.nih.gov/ij/>).

### 2.2.11 Intravital image analysis

Intravital imaging data were rough segmented using the split objects function of the Imaris software (Versions 9 and 10, Oxford Instruments) on the basis of the YFP channel (for FRET analysis) or a combined mKikume red and green channel (for proliferation analysis). Data were then converted to .fcs flow cytometry files using the DiscIT software (291) for further analysis using FlowJo, in which all spectral filtering and gating was performed. Spectral filtering of mKikume parasites was performed on the basis of 625+ nm autofluorescence as described previously (292), and as indicated in chapter 3.8. Distance to blood vessels was calculated using an ImageJ macro employing positional lists of parasite and blood vessel objects (see chapter 7.1 for ImageJ macro).

### 2.2.12 Statistical analysis

Statistical analysis was carried out with GraphPad Prism 8 (GraphPad Software, San Diego, CA, USA). To compare multiple samples pairwise analysis within datasets with more than two experimental groups were performed, one-way analysis of variance (ANOVA) were done for datasets that had passed a Shapiro–Wilk normal distribution test, Kruskal–Wallis tests were performed for datasets with non-normal distribution. Appropriate multiple comparison post-tests (Bonferroni's in ANOVA, Dunn's test for Kruskal–Wallis analyses) were employed as indicated in the respective figure legends. Two-group comparisons were made by two-sided, unpaired or paired t tests for data with normal distribution and Mann–Whitney tests for datasets for which a Shapiro–Wilk normal distribution suggested non-normal distribution. Representation of the mean, median and error (in cases in which not all samples are shown individually) are indicated together with sample size in the figure legends.

### **2.2.13 Study approval**

All animal experiments were reviewed and approved by the Ethics Committee of the Office for Veterinary Affairs of the State of Saxony-Anhalt, Germany (permit license numbers IMKI/G/01-1314/15 and IMKI/G/01-1575/19) in accordance with legislation of both the European Union (Council Directive 499 2010/63/EU) and the Federal Republic of Germany (according to § 8, Section 1 TierSchG, and TierSchVersV). Human monocytes to generate primary macrophages were isolated from buffy coat of healthy volunteers and commercially obtained from the blood bank of the University of Frankfurt, with ethical allowance # 329/10.

### 3. RESULTS

#### 3.1 CD11c-expressing cells play dual role during *Leishmania* infection depending on the infection stage

We recently showed that CD11c-expressing cells constitute an important reservoir for efficient *Leishmania* proliferation and for cell-to-cell transmission (91). We therefore aimed to further study the role of these cells during *L. major* infection by assessing the impact of CD11c<sup>+</sup> cell depletion during ongoing infection in the murine ear dermis.

In order to do so, we generated bone marrow chimeras that were reconstituted with CD11c-DTR/GFP cells to allow us to deplete CD11c cells in the hematopoietic cell compartment upon DTX injection (Figure 3.1.1).



**Figure 3.1.1: Experimental strategy for DTX-mediated CD11c cell depletion during *L. major* infection.** In vivo flow cytometry analysis of *Lm*<sup>DsRed</sup>-infected CD11c-DTR/GFP-reconstituted bone marrow chimeras.

First, to confirm efficient depletion of GFP-expressing CD11c<sup>+</sup> cells upon DTX treatment, the GFP fluorescence in CD45<sup>+</sup> monocyte-derived phagocytes isolated from the infected ear dermis was determined by flow cytometry analysis (Figure 3.1.1 – 3.1.3). Although we observed a reduction in GFP fluorescence upon both 48 h and 96 h of DTX treatment as compared to untreated mice, the difference was not significant, (Figure 3.1.3B).

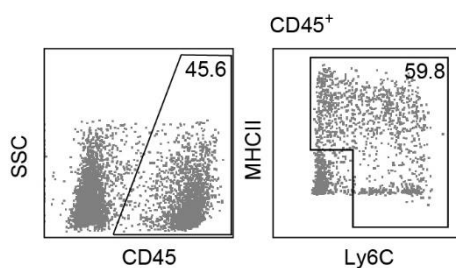


**Figure 3.1.2: Analysis of cells isolated from the infected ear dermis.** Gating strategy for CD45<sup>+</sup> phagocytes in cells isolated from the infected ear dermis of CD11c-DTR/GFP-reconstituted bone marrow chimeras.

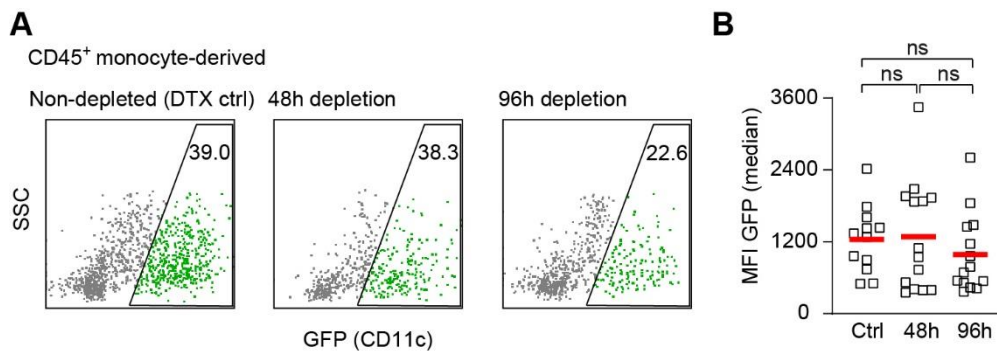


**Figure 3.1.3: DTX-mediated CD11c cell depletion during *L. major* infection in vivo.** (A) Gating strategy for GFP<sup>+</sup> CD11c-expressing cells (green) in non-treated (left plot), 48 h DTX-treated (middle plot) and 96 h DTX-treated (right plot) bone marrow chimeric mice within the CD45<sup>+</sup> phagocytes shown in (Figure 3.1.2). (B) Quantification of median GFP mean fluorescence intensity according to the gating shown in (Figure 3.1.2) and (A). Each dot represents one mouse ear. Horizontal bars denote the mean. Data pooled from two independent experiments. ns, not significant according to one-way ANOVA with Bonferroni post-test.

When looking at the DsRed fluorescence, we observed a reduction upon 48 h depletion of CD11c<sup>+</sup> cells, indicating a decrease in *L. major* burden if CD11c-expressing cells were depleted. In contrast, upon 96 h of depletion, we observed higher DsRed fluorescence than upon 48 h depletion, indicating a *L. major* burden comparable to the control situation (Figure 3.1.4A-B).

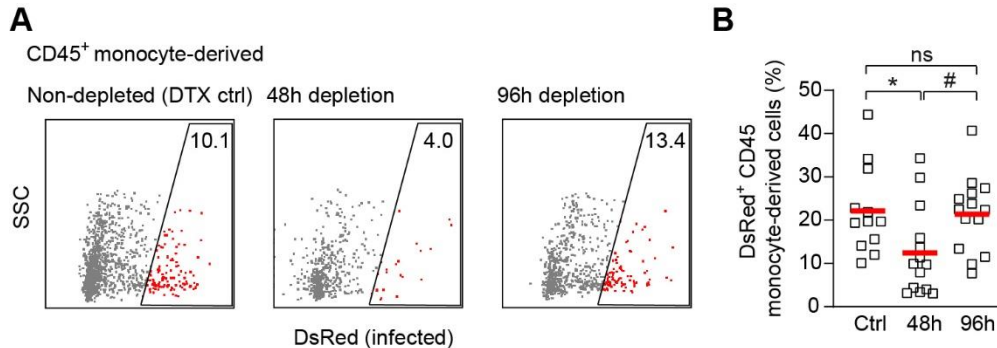


**Figure 3.1.4: CD11c cells as reservoir for *L. major* parasites in vivo.** (A) Gating strategy for DsRed<sup>+</sup> infected cells (red) in non-treated (left plot), 48 h DTX-treated (middle plot) and 96 h DTX-treated (right plot) bone marrow chimeric mice within the CD45<sup>+</sup> phagocytes shown in (Figure 3.1.2). (B) Quantification of percentage of DsRed<sup>+</sup> cells according to the gating shown in (Figure 3.1.2) and (A). Each dot represents one mouse ear. Horizontal bars denote the mean. Data pooled from two independent experiments. \*,  $p < 0.05$ ; #,  $p < 0.1$ ; ns, not significant according to one-way ANOVA with Bonferroni post-test.

Interestingly, the higher *L. major* burden at 96 h post depletion was accompanied with a trend towards decreased iNOS production (Figure 3.1.5A-B), suggesting that reduced pathogen clearance by iNOS might compensate the effects of the missing CD11c<sup>+</sup> cells as hosts for the parasite. Taken together, these results underlined that CD11c<sup>+</sup> cells might play a dual role in the ongoing infection, functioning both as host cells for *L. major* parasites and as inducers of iNOS production.

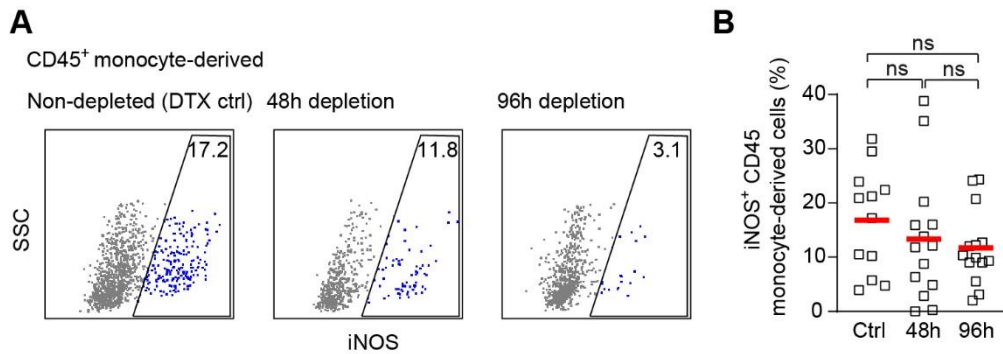


**Figure 3.1.5: CD11c cells as iNOS–producers during *L. major* infection in vivo. (A)** Gating strategy for iNOS<sup>+</sup> cells (blue) in non–treated (left plot), 48 h DTX–treated (middle plot) and 96 h DTX–treated (right plot) bone marrow chimeric mice within the CD45<sup>+</sup> phagocytes shown in (Figure 3.1.2). **(B)** Quantification of percentage of iNOS<sup>+</sup> cells according to the gating show in (Figure 3.1.2) and (A). Each dot represents one mouse ear. Horizontal bars denote the mean. Data pooled from two independent experiments. ns, not significant according to one–way ANOVA with Bonferroni post–test.

Chapter 3.2 – 3.7 published in: Baars I et al., *Leishmania major* drives host phagocyte death and cell-to-cell transfer depending on intracellular pathogen proliferation rate. *JCI Insight*. 2023.

### 3.2 Quantification of *L. major* uptake by newly recruited monocytes in vivo suggests direct cell-to-cell transfer

To study the role of CD11c<sup>+</sup> cells during ongoing *L. major* infection in more detail, we next investigated the transfer of *Leishmania* parasites from these cells. We had recently found evidence that *L. major* parasites can transfer directly from one host cell to the next and therefore aimed to further investigate and quantify *L. major* cell transmission in vivo (91). Importantly, previous studies have shown that phagocytosis of parasites reduces the motility of cells, making intravital 2-photon imaging of *Leishmania* cell-to-cell spread over several hours possible (19).

To this end, we infected CD11c-YFP reporter mice with  $2 \times 10^5$  DsRed-expressing *L. major* (*Lm<sup>DsRed</sup>*) in the ear dermis for 16 days, then adoptively transferred bone marrow cells from constitutively CFP-expressing Actin-CFP mice, and subjected the mice to intravital 2-photon imaging after five days (Figure 3.2.1).

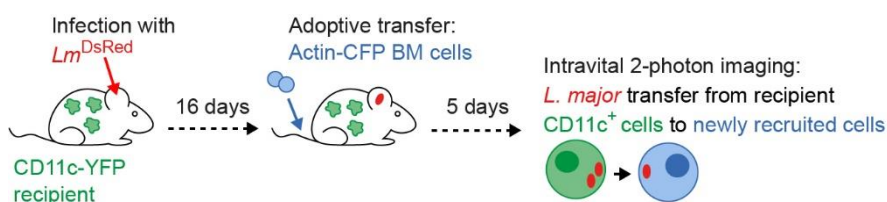


**Figure 3.2.1: Experimental strategy for *Lm<sup>DsRed</sup>* cell-to-cell transfer in vivo.** In vivo intravital 2-photon microscopy of *Lm<sup>DsRed</sup>* transfer from recipient CD11c-YFP cells into newly recruited actin-CFP bone marrow (BM) cells.

We could readily observe the transfer of DsRed-expressing parasites from CD11c-YFP-expressing recipient cells into newly recruited CFP-expressing cells (Figure 3.2.2A). When quantifying the YFP and CFP fluorescence surrounding a parasite during cell-to-cell transfer over time, we observed an immediate drop in YFP fluorescence concomitantly with CFP fluorescence increase, leading to an immediate increase in the CFP/YFP ratio over time (Figure 3.2.2B).

Quantification of all transition events detected, revealed that YFP fluorescence around the parasite did not significantly change before the uptake by CFP-expressing cells, but only at the time point of the most pronounced increase in CFP fluorescence (Figure 3.2.3A–B). These observations suggested that the transfer of *L. major* parasites from one host cell to the next is direct, with no extracellular phase detectable in vivo.

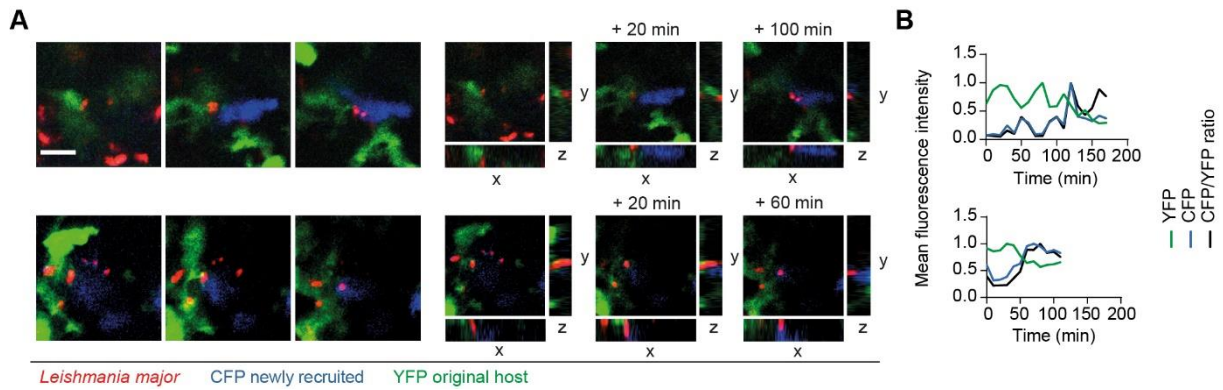


**Figure 3.2.2: Intravital 2-photon imaging of *Lm<sup>DsrRed</sup>* cell-to-cell transfer in vivo. (A–B) Z-projections (left) and single XY image planes (XY) with XZ/YZ reconstructions (right) showing two examples (A) with quantification (B) of an *L. major* (red) cell-to-cell transfer event from an original infected (green) into a newly recruited (blue) cell inside the ear dermis of an anesthetised mouse. Projections consist of 3  $\mu\text{m}$ -spaced z-stacks taken longitudinally every 10 minutes of 8 and 5 slices, respectively. Scale bar, 15  $\mu\text{m}$ .**

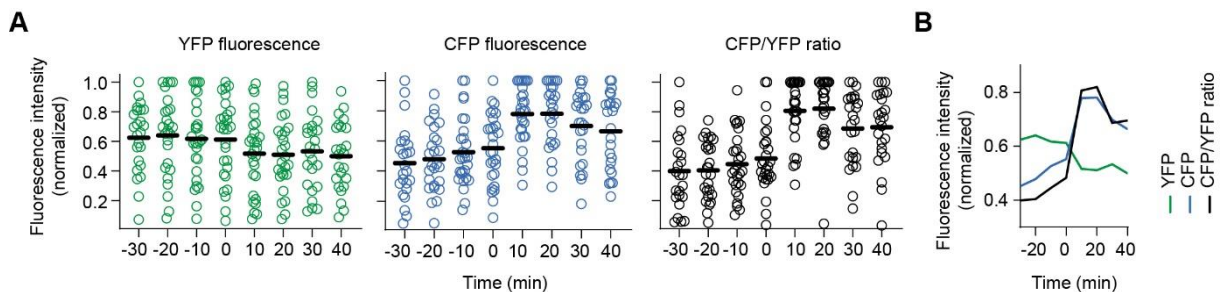


**Figure 3.2.3: *L. major* cell-to-cell transfer is direct in vivo. (A) Fluorescence intensity of YFP (green), CFP (blue) and CFP/YFP ratio (black) around parasites undergoing cell-to-cell transfer over time of all transfer events obtained from 6 animals imaged. Mean fluorescence intensity normalised to the minimum and maximum of each parasite track is shown. Each dot represents one time point of a transfer event. Horizontal bars represent the mean. (B) Overlay of mean values data shown in (A). Data pooled from two independent experiments.**

### 3.3 Original host cell material is taken up by newly infected cells

We next sought to analyse possible mechanisms of cell-to-cell transfer in vivo. We and others had found evidence that *L. major* transfer to new host cells might occur from dying phagocytes in vitro (38, 91). However, in vivo, this has only been shown for infected neutrophils at the very early phase of the infection (19). Therefore, we next examined whether the uptake of original host cell material is accompanied by the uptake of the parasite into newly recruited cells in vivo.

To this end, we infected CD45.2<sup>+</sup> CD11c-YFP reporter mice with  $2 \times 10^6$  DsRed-expressing *L. major* in the ear dermis for 16 days, and then adoptively transferred bone marrow cells from CD45.1<sup>+</sup> wild type mice. Five days after transfer, cells isolated from the infected ears were analysed by flow cytometry (Figure 3.3.1 –3.3.2).

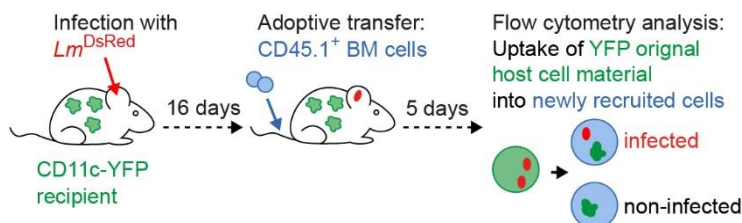


**Figure 3.3.1: Experimental strategy for original host cell material transmission in vivo.** In vivo flow cytometry analysis of YFP<sup>+</sup> original host cell material uptake into newly recruited *Lm*<sup>DsRed</sup>-infected and non-infected bone marrow (BM) cells.

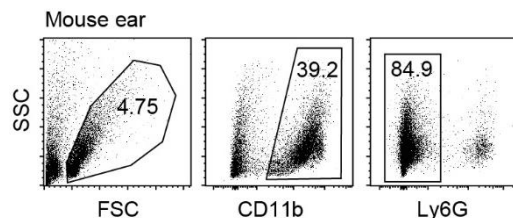


**Figure 3.3.2: Analysis of original host cell material uptake in vivo.** Gating strategy for CD11b<sup>+</sup>Ly6G<sup>-</sup> cells in cells isolated from the infected ear dermis of the mouse.

Newly recruited monocytes could be identified according to their CD45.1 expression (Figure 3.3.3A), and exhibited an increase in YFP fluorescence as compared to those transferred into CD45.2 non-fluorescent recipients, suggesting they had taken up YFP at the site of infection (Figure 3.3.3B).

Interestingly, we observed significantly more YFP fluorescence in infected compared to non-infected CD45.1<sup>+</sup> cells, both by fraction of YFP<sup>+</sup> cells (Figure 3.3.4A) and mean fluorescence (Figure 3.3.4B). The higher YFP fluorescence in infected compared to non-infected cells was observed both in all CD45.1<sup>+</sup> cells (Figure 3.3.4A–B, left panels) and in CD45.1<sup>+</sup> Ly6G<sup>-</sup> phagocytes (Figure 3.3.4A–B, right panels). As expected, mean YFP fluorescence was negligible in YFP<sup>-</sup> control recipient mice, both in infected and non-infected CD45.1<sup>+</sup> cells (Figure 3.3.4B, left panels) and Ly6G<sup>-</sup> phagocytes (Figure 3.3.4B, right panels).

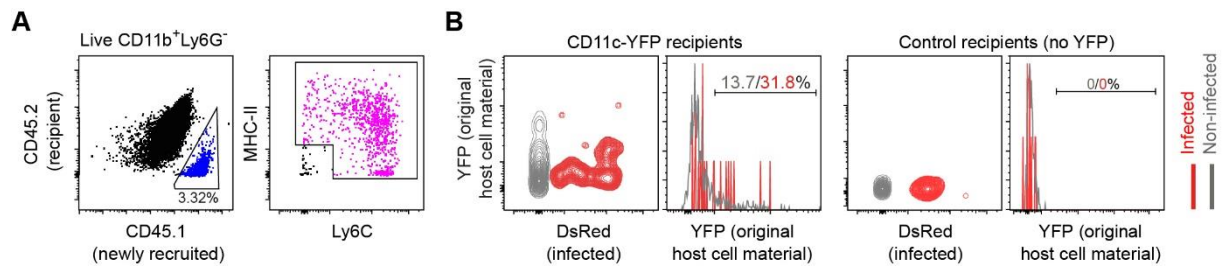


**Figure 3.3.3: Analysis of cellular transmission into newly recruited infected and non-infected phagocytes in vivo.** (A) Gating on CD45.1<sup>+</sup> (newly recruited, blue) and CD45.2<sup>+</sup> (recipient, black) cells and Ly6G<sup>-</sup> phagocytes (pink). (B) Gating on median YFP fluorescence in newly recruited CD45.1<sup>+</sup> infected (red) and non-infected (grey) cells for CD11c-YFP (left plots) and control (right plots) recipient mice.

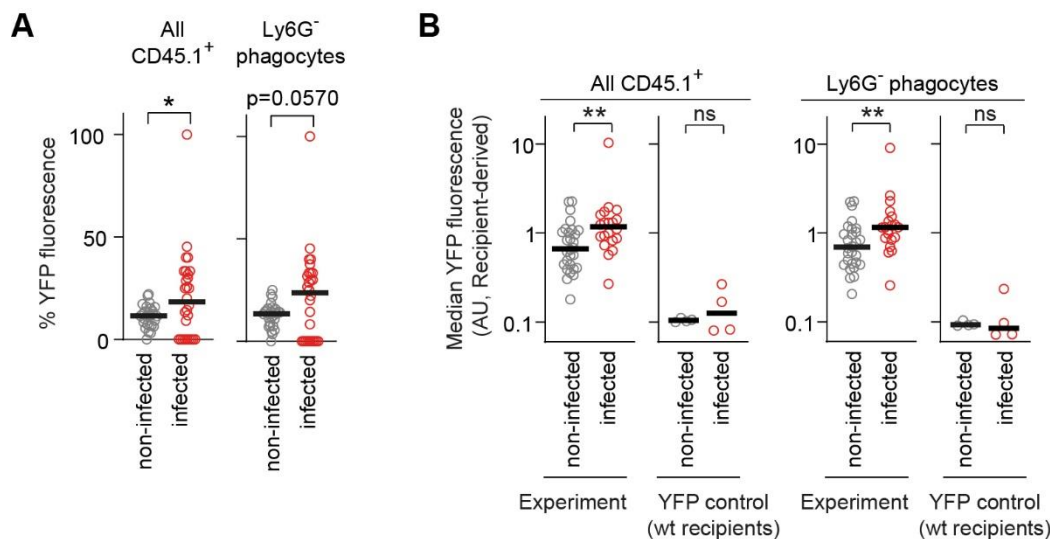


**Figure 3.3.4: *L. major*-infected newly recruited cells take up more YFP<sup>+</sup> original host cell material compared to uninfected cells in vivo.** (A–B) Quantification of percentage of YFP fluorescence (A) and median YFP fluorescence (B) in all CD45.1<sup>+</sup> cells (left panels) and Ly6G<sup>-</sup> phagocytes (right panels) within live CD11b<sup>+</sup>Ly6G<sup>-</sup> newly recruited bone marrow cells for CD11c-YFP and control recipient mice (B only). Each dot represents one mouse ear. Horizontal bars denote the median. Data pooled from three independent experiments. \*\*,  $p < 0.01$ ; \*,  $p < 0.05$ ; ns, not significant according to paired t test.

To test for human relevance, we studied the transfer of cellular material using an in vitro co-incubation assay with human MDM. To this end, AlexaFluor405SE-labelled *Lm*<sup>DsRed</sup>-infected human MDM were co-incubated with CFSE-labelled uninfected human MDM for 18 h and the transfer of cellular material into CFSE-labelled uninfected human MDM was analysed by flow cytometry (Figure 3.3.5 – 3.3.6).

Infected cells could be clearly distinguished into cells that were primary infected (AlexaFluor405SE<sup>+</sup> CFSE<sup>-</sup>) newly infected without uptake of cellular material (AlexaFluor405SE<sup>-</sup> CFSE<sup>+</sup>) and newly infected with uptake of cellular material (AlexaFluor405SE<sup>+</sup> CFSE<sup>+</sup>) (Figure 3.3.7A). In line with our in vivo data, the percentage of infected human MDM was significantly higher for cells containing cellular material of the primary infected host as compared to cells

containing no cellular material of the primary infected host (Figure 3.3.7B). These results indicate that uptake of the parasite by newly recruited monocytes is occurring concomitantly with the uptake of material from the originally infected host cell.

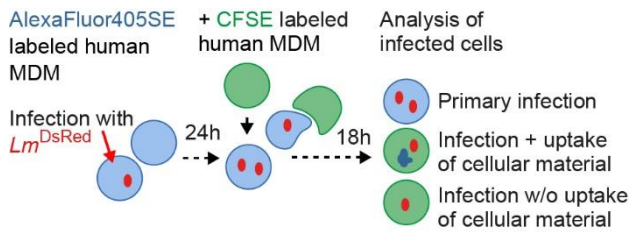


**Figure 3.3.5: Experimental strategy for transmission of cellular material in vitro.** In vitro analysis to determine AlexaFluor405SE<sup>+</sup> material uptake from primary *Lm*<sup>DsRed</sup>-infected human MDM into newly infected CFSE<sup>+</sup> human MDM. MDM, monocyte-derived macrophages.

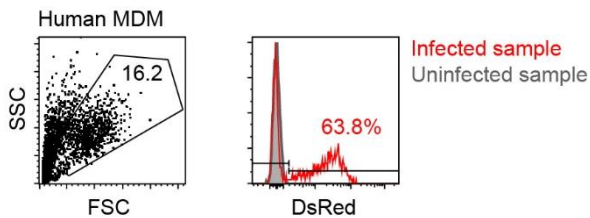


**Figure 3.3.6: Analysis of cellular material transmission in vitro.** Gating strategy for single live human MDM (left plot) and for infected (red) and uninfected (grey) single live human MDM (right plot). MDM, monocyte-derived macrophages. Data obtained in collaboration with van Zandbergen G, Jaedtka M, Bagola K and Volkmar K (Division of Immunology, Paul-Ehrlich-Institut Langen, Langen, Germany).

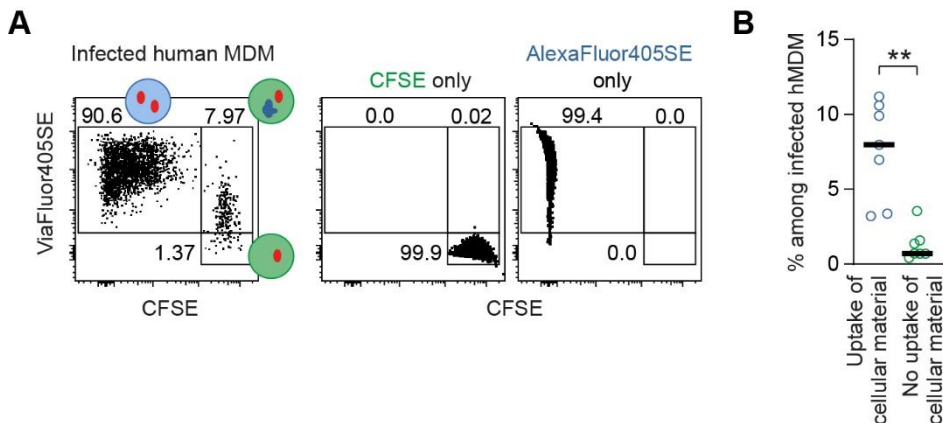


**Figure 3.3.7: *L. major*-infected cells take up cellular material in vitro.** (A) Gating on primary infected (AlexaFluor405SE<sup>+</sup> CFSE<sup>-</sup>), newly infected without cellular material uptake (ViaFluor405SE<sup>-</sup> CFSE<sup>+</sup>) and newly infected with cellular material uptake (AlexaFluor405SE<sup>+</sup> CFSE<sup>+</sup>) human MDM (left plot). Uninfected cells stained with either CFSE or AlexaFluor405SE are shown as controls (right plots). (B) Quantification of percentage of infected human MDM cells without cellular material uptake and with cellular material uptake. Each dot represents one sample. Horizontal bars denote the median. \*\*,  $p < 0.01$  according to paired t test. MDM, monocyte-derived macrophages. Data obtained in collaboration with van Zandbergen G, Jaedtka M, Bagola K and Volkmar K (Division of Immunology, Paul-Ehrlich-Institut Langen, Langen, Germany).

### 3.4 An in vivo cell death reporter system shows higher apoptosis in infected compared to uninfected phagocytes at the site of infection

To investigate the fate of host cells in real-time in the context of parasite infection, we aimed to determine the dynamics of programmed cell death induction during intravital 2-photon imaging of the *L. major* infection site in the ear dermis of the mouse. For this, we retrovirally transduced *Rag1*<sup>-/-</sup> hematopoietic stem cells (HSCs) with a CFP-DEVD-YFP construct in order to express a genetically encoded reporter system in inflammatory cells recruited to the skin (286, 287). This construct is sensitive to cleavage by caspase-3 at the specific Asp-Glu-Val-Asp site linking a Förster Resonance Energy Transfer (FRET) donor (CFP) and acceptor (YFP). Upon the induction of apoptosis, active caspase-3 is expected to cleave the donor from the acceptor, resulting in an increased CFP to FRET ratio (Figure 3.4.1A). A non-cleavable CFP-DEVG-YFP control construct was used to determine specificity of the reporter for caspase-3-dependent cleavage (288). The transfected *Rag1*<sup>-/-</sup> HSCs together with wild type supporter bone marrow were used to reconstitute lethally irradiated recipient B6 albino wild type mice, resulting in animals that expressed the reporter constructs specifically in the non-lymphocyte immune cell compartment. After 10 weeks of recovery from irradiation and bone marrow transfer, mice were infected with  $2 \times 10^5$  DsRed-expressing *L. major* (*Lm*<sup>DsRed</sup>) and imaged three weeks later using intravital 2-photon microscopy (Figure 3.4.1B).

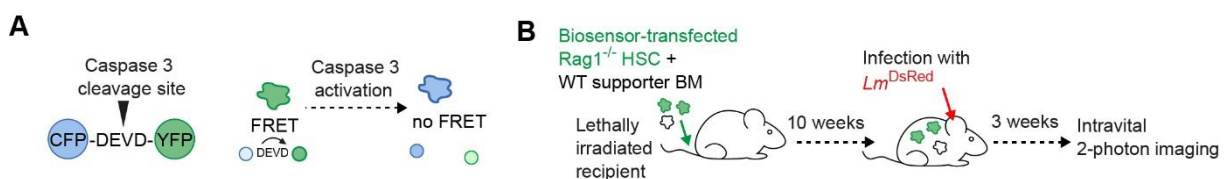


**Figure 3.4.1: Experimental strategy for analysis of host cell apoptosis during *L. major* infection in vivo.**

**(A)** In vivo quantification of cell death dynamics using a FRET-based caspase-3 reporter. DEVD, caspase-3 recognition site. **(B)** *Rag1*<sup>-/-</sup> hematopoietic stem cells transduced with caspase-3 reporter (DEVD) or non-cleavable control (DEVG) were FACS sorted and transferred into lethally irradiated recipient mice. FRET, Foerster Resonance Energy Transfer; HSC, hematopoietic stem cell; WT, wild type; BM, bone marrow.

When analysing the whole blood isolated from the bone marrow chimeric mice, cells positive for both CFP (donor fluorophore) and YFP (acceptor fluorophore) were detectable in CD45.2<sup>+</sup> transferred cells (Figure 3.4.2A). This was the case for both CFP-DEVD-YFP and control CFP-DEVG-YFP bone marrow chimeric mice. We could show that reporter-expressing cells exhibited a small fraction of cells with FRET loss in the CFP-DEVD-YFP bone marrow chimeric mice, but not in the bone marrow chimeric mice containing the CFP-DEVG-YFP control construct (Figure 3.4.2B).

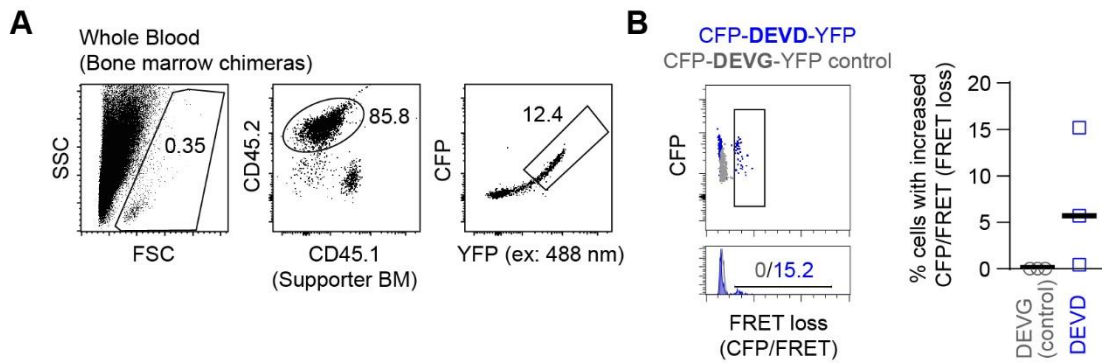


**Figure 3.4.2: Analysis of apoptosis biosensor reconstitution in bone marrow chimeric mice. (A)** Gating strategy for live CD45.2<sup>+</sup> CFP-DEVD-YFP and CFP-DEVG-YFP control cells in whole blood isolated from biosensor-transfected bone marrow chimeric mice. BM, bone marrow. **(B)** Gating strategy (upper left panel), histogram plots (lower left panel) and percent of cells (right panel) showing increased CFP/FRET ratio, indicating FRET loss, in cells expressing the CFP-DEVD-YFP (blue) and CFP-DEVG-YFP control (grey) construct as measured by flow cytometry analysis according to gating shown in (A-B). Each symbol represents one mouse. Horizontal bars denote the median. FRET, Foerster Resonance Energy Transfer.

As expected, time-lapse imaging using 2-photon microscopy at the site of infection showed an accumulation of reporter-expressing bone-marrow derived cells. Automated segmentation and tracking of these cells over time enabled us to map, identify and localise infected and FRET-losing cells by converting the extracted imaging data to cytometry datasets using the DisClT software (291). This revealed FRET loss, indicating apoptosis, in reporter-expressing cells for the CFP-DEVD-YFP (Figure 3.4.3, left panels), but not the CFP-DEVG-YFP control construct (Figure 3.4.3, right panels). Of note, we were also able to localise individual cells undergoing FRET loss over time (Figure 3.4.4A-B).

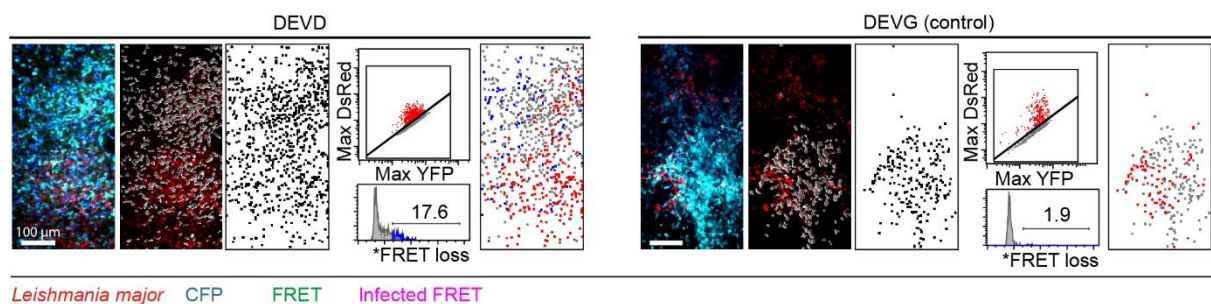


**Figure 3.4.3: Intravital 2-photon imaging of host cell apoptosis during *L. major* infection in vivo.** Z-projections of infected ear dermis of CFP-DEVD-YFP (left) and CFP-DEVG-YFP control (right) mice. 18 slices of 3  $\mu\text{m}$ -spaced z-stacks are projected. Scale bar, 100  $\mu\text{m}$ . 3D surface plot of detected reporter-expressing cells, grey. Mapped cell positions, black; infected cells, red; cells with increased CFP to FRET ratio, blue; infected cells exhibiting FRET loss (map only), pink. FRET, Foerster Resonance Energy Transfer.

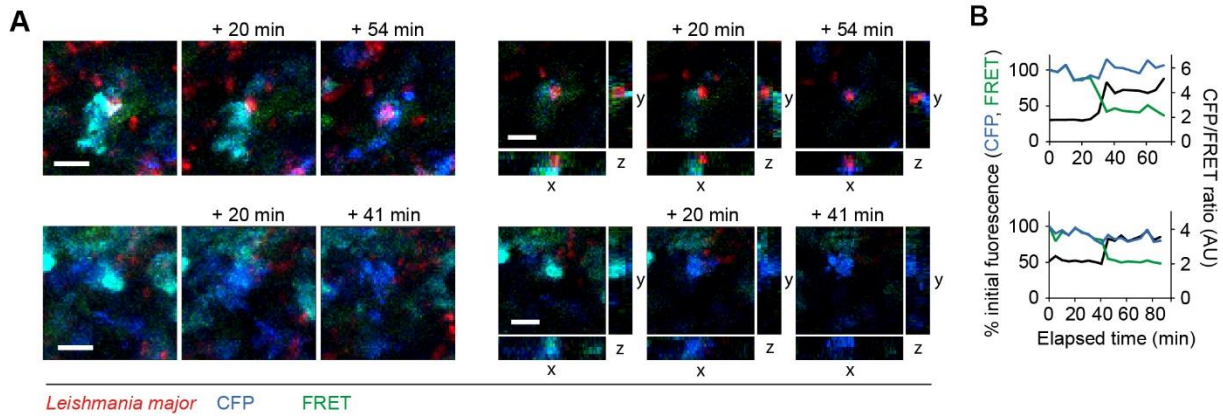


**Figure 3.4.4: Intravital 2-photon imaging of host cell apoptosis during *L. major* infection in vivo.** (A) Z-projections (left) and XY/XZ/YZ sections (right) of an *Lm*<sup>DsRed</sup>-infected (upper panels) and a non-infected (lower panels) apoptotic cell over time. Projections consist of 3  $\mu\text{m}$ -spaced z-stacks taken longitudinally of 11 and 14 slices, respectively. Scale bar, 10  $\mu\text{m}$  (B) Percent of initial CFP and FRET fluorescence and normalised CFP/FRET ratio over time of cells shown in (A). FRET, Foerster Resonance Energy Transfer.

Strikingly, when we compared cells infected by DsRed-expressing *L. major* with non-infected cells (Figure 3.4.5A), we found progressive FRET loss in the infected cell population, which was higher compared to the non-infected cell population (Figure 3.4.5B). Additionally, significantly higher maximum FRET loss was observed in infected as compared to non-infected cells when looking at individual tracks (Figure 3.4.5C) and significantly higher relative FRET loss was observed in infected as compared to non-infected cells when looking at individual mice (Figure 3.4.5D). Again, no FRET loss was observed in the control CFP-DEVG-YFP bone marrow chimeras (Figure 3.4.5A-D). Thus, these data indicate that *L. major*-infected cells undergo more apoptosis as compared to uninfected cells.

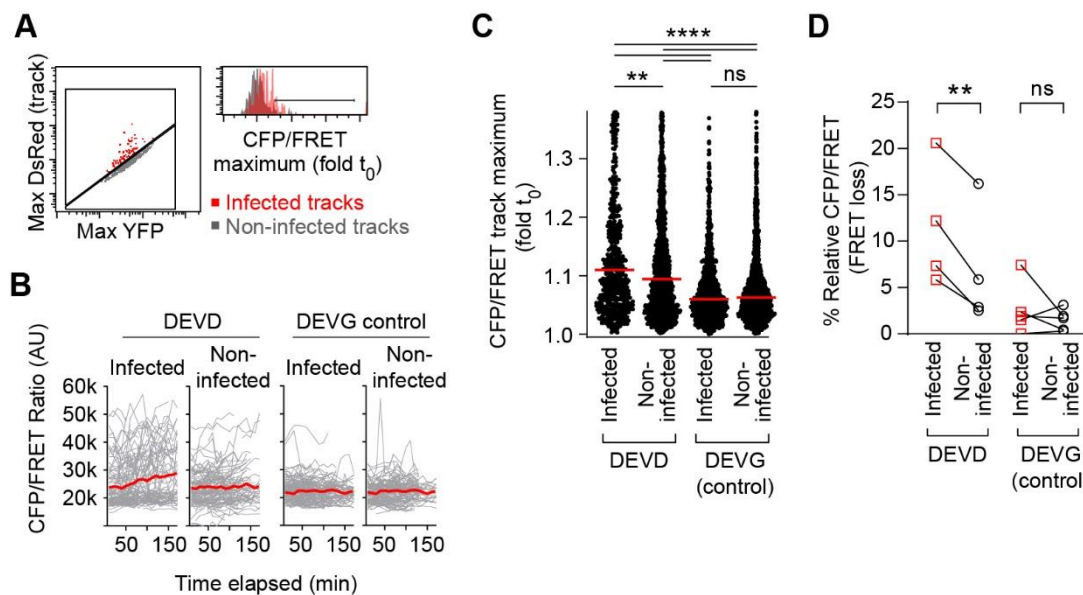


**Figure 3.4.5: More apoptosis in *L. major*-infected cells in vivo.** (A) Gating strategy for infected (red) and non-infected (grey) cell tracks. (B) FRET loss in infected (left panels) and non-infected (right panels) cells for CFP-DEVD-YFP (left) and CFP-DEVG-YFP control (right) mice. 50 randomly selected tracks of at least

200 tracks analysed per condition are shown. (C) FRET loss in infected and non-infected CFP-DEVD-YFP and CFP-DEVG-YFP control mice. Each symbol represents one track. Horizontal bars denote the median. (D) FRET loss in infected and non-infected cell populations from 4–5 animals imaged. Each symbol pair represents one mouse ear. \*\*\*\*,  $p < 0.0001$ ; \*\*,  $p < 0.01$ ; ns, not significant according to Kruskal–Wallis with Dunn post-test in (C), and paired two-way ANOVA with Bonferroni post-test in (D). FRET, Foerster Resonance Energy Transfer.

To support these findings, we made use of a caspase-3 reporter assay to measure caspase-3 activity in *Lm<sup>DsRed</sup>*-infected and uninfected human MDM by flow cytometry (Figure 3.4.6 – 3.4.7). Indeed, we observed significantly higher NucView405 mean fluorescence, indicating caspase-3, in infected compared to uninfected human MDM. Strikingly, the increase in NucView405 mean fluorescence was already observed directly after staining with the caspase-3 reporter, but was even more apparent 20 h post incubation with the reporter (Figure 3.4.7). Therefore, our data indicated that *L. major* infection is related to caspase-3 activity and thereby to apoptosis both in vivo and in vitro.

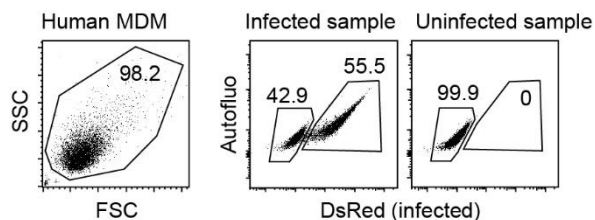


**Figure 3.4.6: Analysis of caspase-3 activity in vitro.** Gating strategy for single live human MDM (left plot) and for DsRed expression (right plots) in infected (left) and non-infected (right) human MDM. MDM, monocyte-derived macrophages. Data obtained in collaboration with van Zandbergen G, Jaedtka M, Bagola K and Volkmar K (Division of Immunology, Paul-Ehrlich-Institut Langen, Langen, Germany).

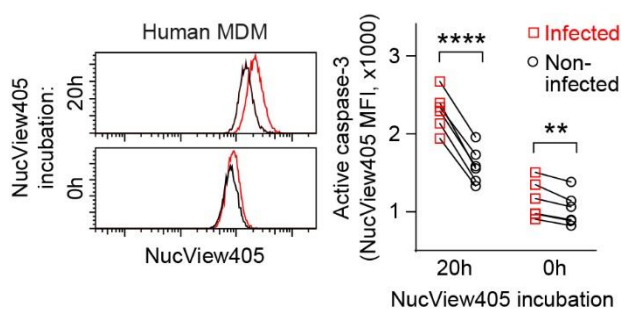


**Figure 3.4.7: More active caspase-3 in *L. major*-infected human monocyte-derived macrophages.** NucView405 (caspase-3 activity), in *Lm<sup>DsRed</sup>*-infected (red) and uninfected (black) human MDM 0 h and 20 h post incubation. Each symbol pair represents one donor. \*\*\*\*,  $p < 0.0001$ ; \*\*,  $p < 0.01$  according to paired two-way ANOVA with Bonferroni post-test. MDM, monocyte-derived macrophages. Data obtained in collaboration with van Zandbergen G, Jaedtka M, Bagola K and Volkmar K (Division of Immunology, Paul-Ehrlich-Institut Langen, Langen, Germany).

### 3.5 *L. major*-infected cells containing high proliferating pathogens undergo apoptosis and drive cell-to-cell transfer

Our previous findings had suggested that high proliferating *L. major* parasites undergo more cell-to-cell transmission than low proliferating parasites (91). Since we had observed enhanced apoptosis in infected cells, we next aimed to investigate *L. major* proliferation rate in relation to cell death of the infected host cells in vitro.

To do so, we infected murine intraperitoneal macrophages with mKikume-expressing *Lm*<sup>SWITCH</sup> parasites, which express a photoconvertible proliferation biosensor (282). In brief, the parasites in the infected macrophages were photoconverted from green to red and imaged by widefield microscopy for 48 h. This enabled us not only to track cell-to-cell transfer of the parasites, but also to determine pathogen proliferation as a function of recovery from photoconversion (91). Furthermore, the use of gridded microscopy dishes allowed us to fix the cells and identify and localise apoptotic macrophages by TUNEL staining following live cell imaging (Figure 3.5.1).

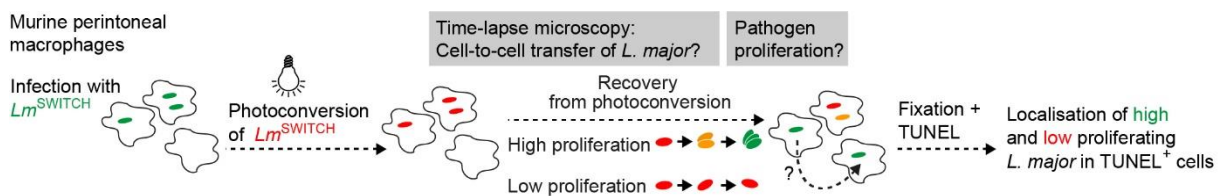


**Figure 3.5.1: Experimental setup for in vitro analysis of parasite proliferation and host cell death.** In vitro analysis of murine peritoneal macrophages infected with a photoconversion-based pathogen proliferation biosensor (*Lm*<sup>SWITCH</sup>) using widefield imaging.

We detected higher *L. major* proliferation in TUNEL<sup>+</sup> compared to TUNEL<sup>-</sup> macrophages (Figure 3.5.2A–C), suggesting that high parasite proliferation is correlated to cell death of the original host cell. Time-resolved analysis of cell-to-cell transfer events prior to fixation (Figure 3.5.3A) revealed that parasite proliferation was high not only in TUNEL<sup>+</sup> cells, but also in TUNEL<sup>-</sup> cells that had been infected only recently (< 800 min, Figure 3.5.3B). In contrast, TUNEL<sup>-</sup> cells found infected for longer periods of time (> 800 min) harboured parasites with significantly lower proliferation (Figure 3.5.3B).

As shown previously in vivo (91), we did not detect any correlation between pathogen burden and intracellular pathogen proliferation rate (Figure 3.5.4A–B), indicating that the differences of intracellular residence time before apoptosis were attributable to pathogen proliferation, and not pathogen burden. Taken together, these data suggested that long-term residency of *L. major* parasites within macrophages is related to low parasite proliferation.

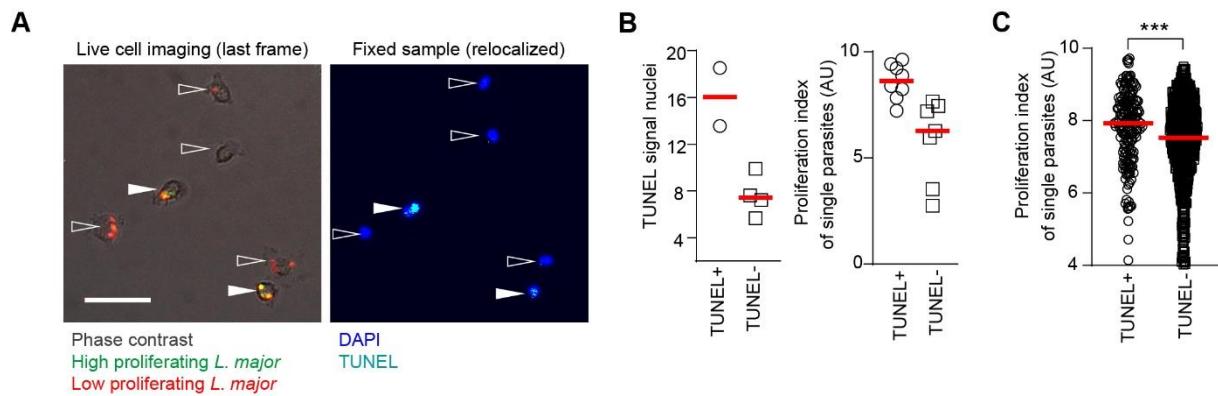


**Figure 3.5.2: Intracellular *L. major* proliferation rate affects host cell death in vitro.** (A) One example of high proliferating (green) *Lm<sup>SWITCH</sup>* parasites co-localising with TUNEL<sup>+</sup> (cyan) murine peritoneal macrophages. One frame at the end of live cell imaging (left panel) and TUNEL staining after fixation (right panel) of the same site are shown. TUNEL<sup>+</sup> cells are marked with closed arrows and TUNEL<sup>-</sup> cells are marked with open arrows. Scale bar, 50  $\mu$ m. (B) Quantification of TUNEL signal (left panel) and proliferation index (right panel) within the peritoneal macrophages shown in (A). Each symbol represents one individual cell (left panel) or parasite (right panel). Horizontal bars denote the median. (C) Quantification of proliferation index in all TUNEL<sup>+</sup> and TUNEL<sup>-</sup> murine peritoneal macrophages analysed. Each symbol represents one individual parasite. Data were pooled from two independent microscopy experiments. Horizontal bars denote the median. \*\*\*,  $p < 0.001$  according to Mann-Whitney test.

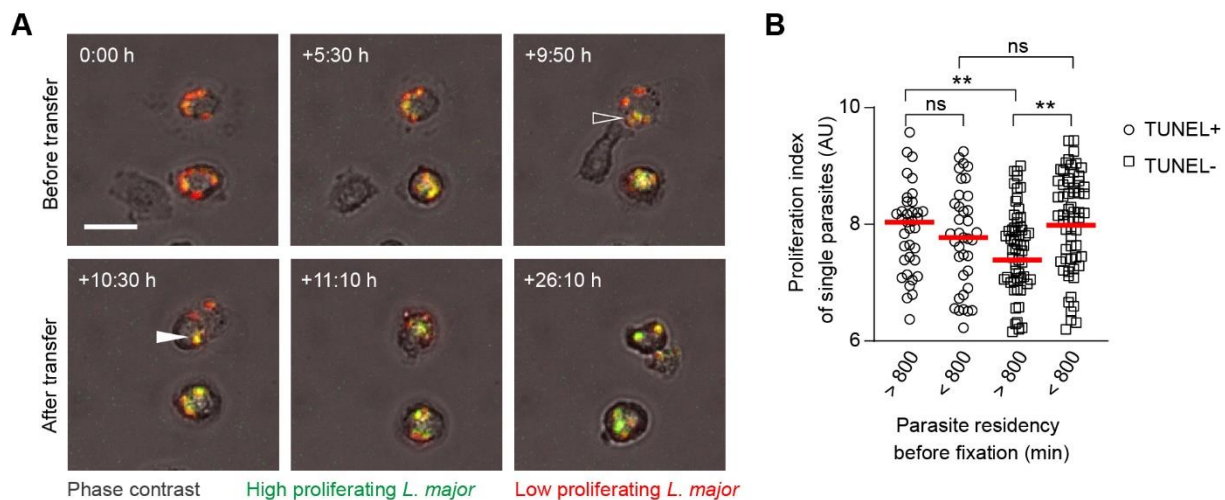


**Figure 3.5.3: Intracellular *L. major* proliferation rate and time affects the fate of the infected host cell in vitro.** (A) One example of an *Lm<sup>SWITCH</sup>* cell-to-cell transfer event between two murine peritoneal macrophages. The transferring *Lm<sup>SWITCH</sup>* parasites are indicated with an open arrow in the donor host macrophage and with a closed arrow in the recipient macrophage. Scale bar, 20  $\mu$ m. (B) Quantification of proliferation index in TUNEL<sup>+</sup> and TUNEL<sup>-</sup> murine peritoneal macrophages distinguished based on long-term (> 800 min before fixation) and recent (< 800 min before fixation) parasite residency. Note that long-term intracellular residency in TUNEL<sup>-</sup> cells involves low parasite proliferation. Each symbol shows one individual parasite. Data were pooled from two independent microscopy experiments. Horizontal bars denote the mean. \*\*,  $p < 0.01$ ; ns, not significant according to Mann-Whitney test.

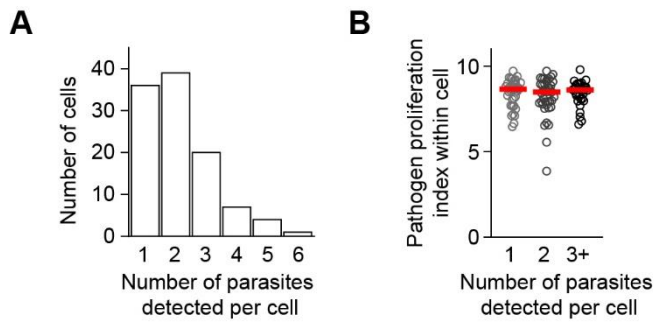


**Figure 3.5.4: Intracellular *L. major* proliferation does not correlate with intracellular pathogen burden in vitro.** (A) Number of parasites per infected macrophage determined in >100 cells infected with *Lm*<sup>SWITCH</sup> 48 h after photoconversion and imaged by widefield microscopy. (B) Pathogen proliferation determined by widefield microscopy for *Lm*<sup>SWITCH</sup> 48 h after photoconversion in macrophages infected with 1, 2 or more than 2 parasites. Each symbol represents one cell. Data pooled from 10 independently imaged fields of view. Horizontal bars denote the median. No significant differences were found according to Kruskal–Wallis test.

### 3.6 Proliferation-competent pathogens induce cell death in infected macrophages

The observation that high proliferating *L. major* parasites were found mainly in apoptotic or newly infected cells raised the question if pathogen proliferation might induce cell death in infected macrophages, or is a result of cell death. In order to investigate whether a predefined parasite proliferation affects the fate of the infected host in a direct manner, we aimed to modify parasite proliferation for infection of murine intraperitoneal macrophages and murine bone marrow-derived macrophages.

To do so, we made use of Killed but Metabolically Active (KBMA) *L. major* parasites (293–295). These parasites are not able to proliferate due to low-grade DNA crosslinking (Figure 3.6.1), but largely retained their fluorescence (Figure 3.6.2) and could be shown by qPCR to switch to amastigote-specific gene expression upon infection of macrophages (Figure 3.6.3). These findings together suggested that KBMA *L. major* parasites indeed lack proliferation capacity, but predominantly maintain essential *Leishmania*-related properties and could therefore be used to investigate whether parasite proliferation affects the fate of infected macrophages in a direct manner.

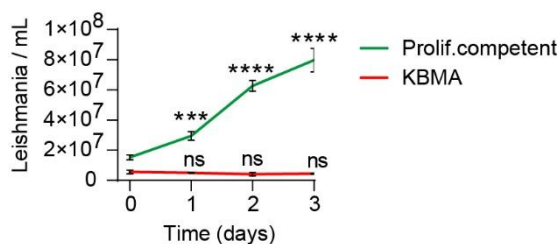


**Figure 3.6.1: Killed but metabolically active *L. major* parasites do not proliferate.** (A) Plot of mean error with standard deviation displaying the growth curve of proliferation-competent (green) and KBMA proliferation-incompetent (red) parasites. Data represent three independent samples for each condition. Vertical bars denote the standard deviation. \*\*\*\*,  $p < 0.0001$ ; \*\*\*,  $p < 0.001$ ; ns, not significant according to paired two-way ANOVA with Sidak post-test. KBMA, killed but metabolically active. Data obtained in collaboration with Dewitz L-A (Institute of Molecular and Clinical Immunology, Medical Faculty, Otto von Guericke University Magdeburg, Magdeburg, Germany).

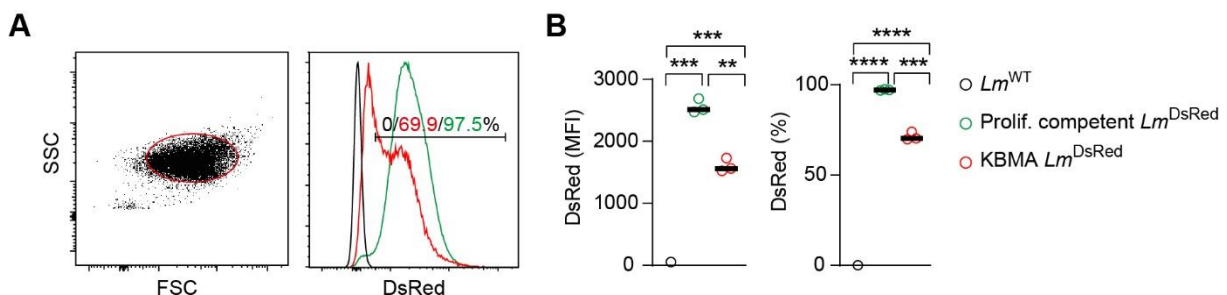


**Figure 3.6.2: Killed but metabolically active *L. major* parasites largely retain DsRed fluorescence.** (A) Gating strategy for single live cells (left) and histogram plots showing DsRed fluorescence (right) in BMDM infected with non-fluorescent *Lm*<sup>WT</sup> (black), proliferation-competent *Lm*<sup>DsRed</sup> (green) and proliferation-incompetent KBMA *Lm*<sup>DsRed</sup> (red) parasites. (B) DsRed mean fluorescence intensity (left) and percent of DsRed<sup>+</sup> cells (right) in BMDM infected with non-fluorescent *Lm*<sup>WT</sup> (black), proliferation-competent

*Lm*<sup>DsRed</sup> (green) and proliferation–incompetent KBMA *Lm*<sup>DsRed</sup> (red) parasites. Each symbol represents one independent sample. Horizontal bars denote the median. \*\*\*\*,  $p < 0.0001$ ; \*\*\*,  $p < 0.001$ ; \*\*,  $p < 0.01$  according to one–way analysis of variance (ANOVA). KBMA, killed but metabolically active; WT, wild type. Data obtained in collaboration with Dewitz L–A (Institute of Molecular and Clinical Immunology, Medical Faculty, Otto von Guericke University Magdeburg, Magdeburg, Germany).

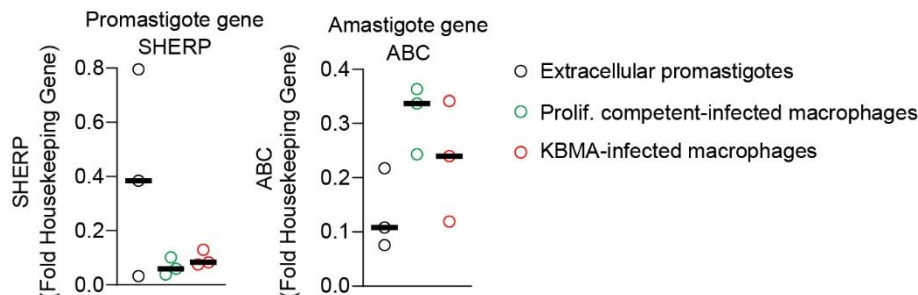


**Figure 3.6.3: Killed but metabolically active *L. major* parasites maintain differentiation–related *Leishmania* properties.** Promastigote (*SHERP*) and amastigote (*ABC*) gene expression (normalised to *NMT* as a housekeeping gene) in extracellular promastigotes (black), proliferation–competent (green) and KBMA proliferation–incompetent (red) parasites as measured by qPCR. Each symbol represents one sample. Data represent three independent samples for each condition. Horizontal bars denote the median. KBMA, killed but metabolically active; WT, wild type. Data obtained in collaboration with Dewitz L–A (Institute of Molecular and Clinical Immunology, Medical Faculty, Otto von Guericke University Magdeburg, Magdeburg, Germany).

To study the fate of KBMA–*L. major*–infected macrophages versus macrophages infected with proliferation–competent parasites side–by–side, DsRed–expressing KBMA parasites and mKikume green–expressing non–treated parasites were used to co–infect murine intraperitoneal macrophages. The infected macrophages were imaged by widefield microscopy for 48 h using gridded microscopy dishes to identify and localise apoptotic macrophages by TUNEL staining after the live cell imaging (Figure 3.6.4).

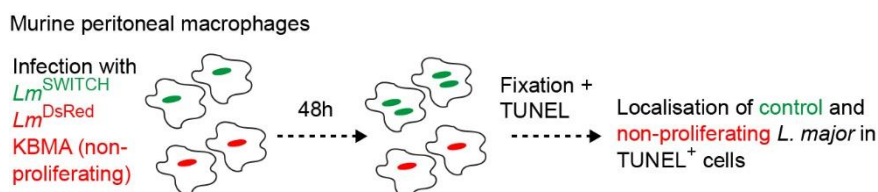


**Figure 3.6.4: Experimental setup for in vitro analysis of host cell death upon modification of intracellular pathogen proliferation.** Widefield imaging of host cell death using murine peritoneal macrophages infected with *Lm*<sup>mKikumeGreen</sup> proliferation–competent and *Lm*<sup>DsRed</sup> proliferation–incompetent KBMA parasites. KBMA, killed but metabolically active.

We observed cell death both by TUNEL staining and by visual signs of cell death (membrane blebbing, figure 3.6.5A). Significantly more proliferation–competent, mKikume green–expressing parasites were observed in the TUNEL<sup>+</sup> compared to the TUNEL<sup>–</sup> macrophages (Figure 3.6.5B–C), suggesting that *L. major* proliferation induces cell death of the infected host.

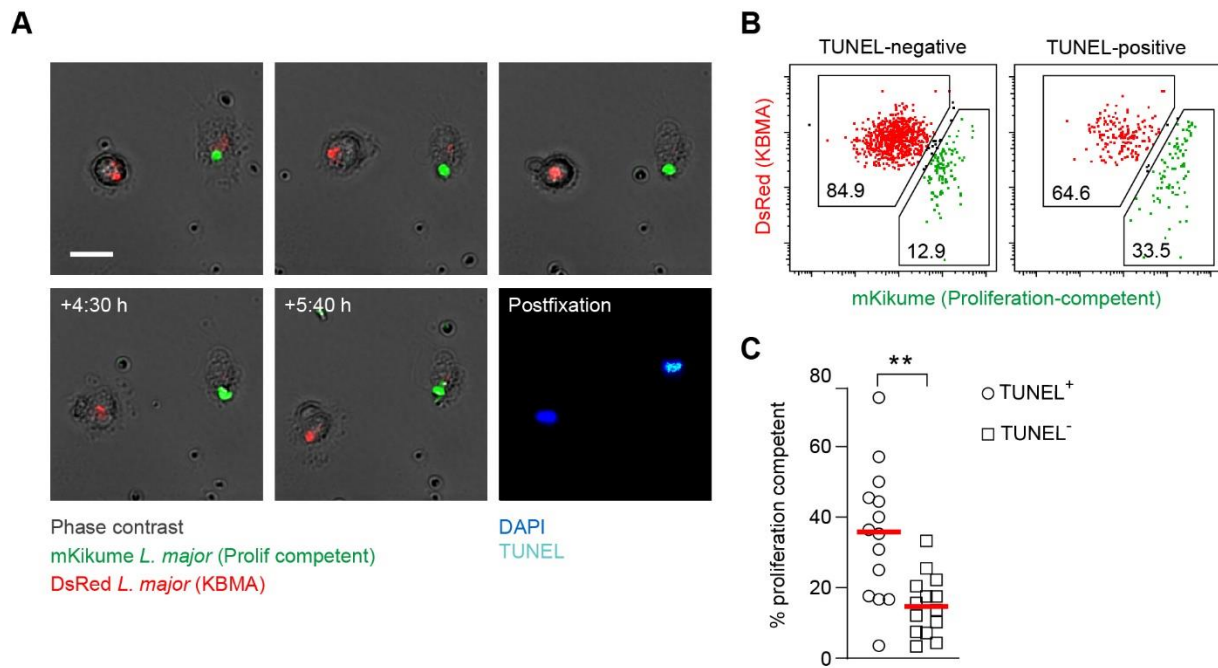


**Figure 3.6.5: Proliferation-competent *L. major* parasites induce cell death in infected macrophages in vitro.** (A) Selected frames from live cell imaging and TUNEL staining after fixation of the same site are shown, revealing TUNEL<sup>+</sup> (cyan) murine peritoneal macrophages co-localising with proliferation-competent (green) but not KBMA proliferation-incompetent (red) parasite. Scale bar, 20  $\mu$ m. (B) Selection of *Lm*<sup>mKikumeGreen</sup> proliferation-competent and *Lm*<sup>DsRed</sup> proliferation-incompetent KBMA parasites in TUNEL<sup>-</sup> (left) and TUNEL<sup>+</sup> (right) cells according to green and red parasite fluorescence. All measured infected cells are shown individually. (C) Quantification of percentage of proliferation-competent parasites in all TUNEL<sup>+</sup> and TUNEL<sup>-</sup> murine peritoneal macrophages. Each symbol shows one field of view imaged over time and relocalised afterwards for TUNEL staining, with at least three TUNEL<sup>+</sup> and at least six TUNEL<sup>-</sup> cells per imaged field analysed according to the criteria shown in (B). Horizontal bars denote the mean. \*\*,  $p < 0.01$  according to paired t test. KBMA, killed but metabolically active.

### 3.7 *L. major* intracellular proliferation rate modifies host cell metabolic pathways

In order to analyse host cellular changes related to infection with proliferation-competent vs. KBMA-parasites, we set up a flow cytometry-based analysis approach. Murine bone marrow-derived macrophages (BMDM) were used for this purpose in order to yield sufficient numbers of host cells for infection and analysis (Figure 3.7.1).

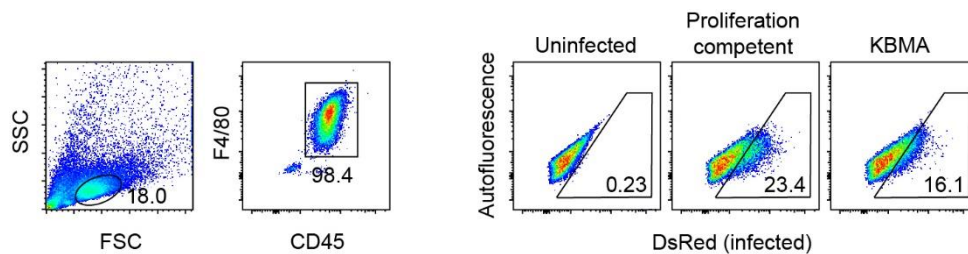


**Figure 3.7.1: Analysis of *Lm*<sup>DsRed</sup>-infected murine bone marrow-derived macrophages.** Gating strategy for live CD45<sup>+</sup>F4/80<sup>+</sup> macrophages (left plots) and DsRed expression (right plots) in uninfected, proliferation-competent-infected and KBMA-infected bone marrow-derived macrophages. Data obtained in collaboration with Dewitz L-A (Institute of Molecular and Clinical Immunology, Medical Faculty, Otto von Guericke University Magdeburg, Magdeburg, Germany).

Cell death analysis via AnnexinV staining (296) 48 h after infection revealed no significant differences between uninfected and KBMA- or proliferation-competent parasite-infected host cells (Figure 3.7.2A–B), probably due to the loss of cellular adherence of dying cells in the course of the experiment. Using murine BMDM infected with proliferation-competent vs. KBMA-parasites did however enable us to measure the impact of *L. major* proliferation capacity on host cellular metabolism on a single cell level.

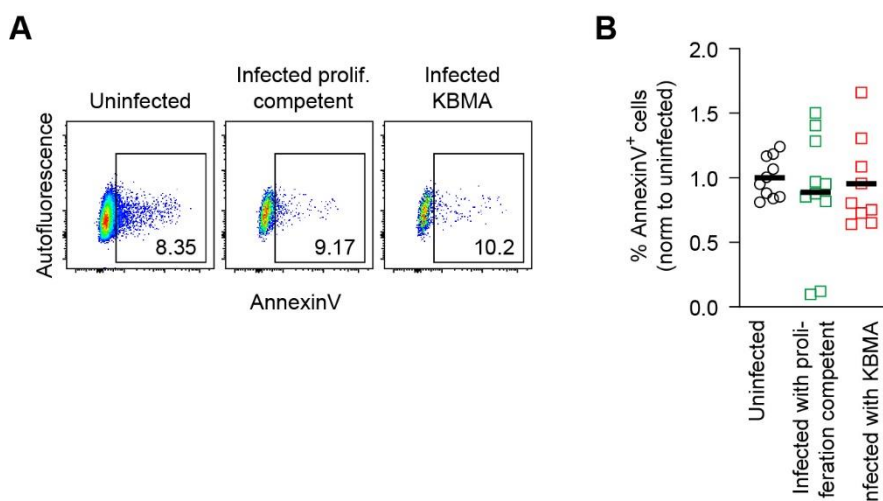


**Figure 3.7.2: AnnexinV staining in murine bone marrow-derived macrophages infected with proliferation-competent and proliferation-incompetent KBMA *Lm*<sup>DsRed</sup> parasites.** (A) Gating strategy for AnnexinV in uninfected, proliferation-competent-infected and KBMA-infected CD45<sup>+</sup>F4/80<sup>+</sup> macrophages. (B) Percent of AnnexinV<sup>+</sup> cells (normalised to uninfected) in uninfected (black), proliferation-competent-infected (green) and KBMA-infected (red) bone marrow-derived macrophages. Each symbol shows one

individual sample. Horizontal bars denote the mean. Data were pooled from three independent experiments. KBMA, killed but metabolically active. No significant differences according to one-way ANOVA. Data obtained in collaboration with Dewitz L-A (Institute of Molecular and Clinical Immunology, Medical Faculty, Otto von Guericke University Magdeburg, Magdeburg, Germany).

To this end, we studied glucose-uptake and transport by the fluorescent tracer 2-NBDG and expression of the glucose transporter 1 (GLUT1). The macrophages infected with either KBMA *L. major* or proliferation-competent *L. major* were compared with non-infected cells using flow cytometry analysis 48 h after infection. While no significant differences were observed in 2-NBDG uptake between uninfected and KBMA-infected macrophages, macrophages infected with proliferation-competent *L. major* exhibited significantly less 2-NBDG uptake as compared to both the uninfected and the KBMA-infected macrophages (Figure 3.7.3A-B). This suggested that infection with proliferating parasites decreases glucose uptake in the host cell.

Remarkably, no significant differences were observed in GLUT1 expression between any of the conditions (Figure 3.7.4A-B), suggesting that the changes in glucose uptake induced by proliferation-competent pathogens are achieved not via marked changes in surface expression of the transporter GLUT1.

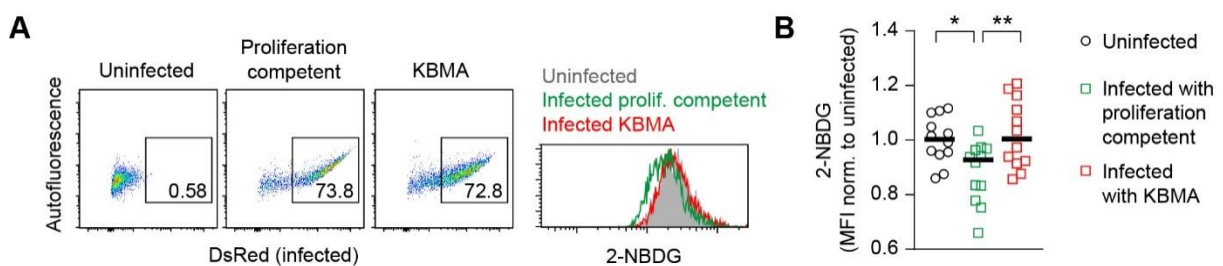


**Figure 3.7.3: Intracellular *L. major* proliferation rate modifies glucose uptake in host macrophages in vitro.** (A-B) Gating (A) and mean fluorescence intensity (normalised to uninfected) (B) for 2-NBDG uptake in uninfected (grey), *Lm*<sup>DsRed</sup> proliferation-competent-infected (green) and *Lm*<sup>DsRed</sup> KBMA-infected (red) bone marrow-derived macrophages. Each symbol shows one individual sample, data pooled from three independent experiments. Horizontal bars denote the mean. \*\*,  $p < 0.01$ ; \*,  $p < 0.05$  according to one-way ANOVA with Bonferroni post-test. KBMA, killed but metabolically active. Data obtained in collaboration with Dewitz L-A (Institute of Molecular and Clinical Immunology, Medical Faculty, Otto von Guericke University Magdeburg, Magdeburg, Germany).

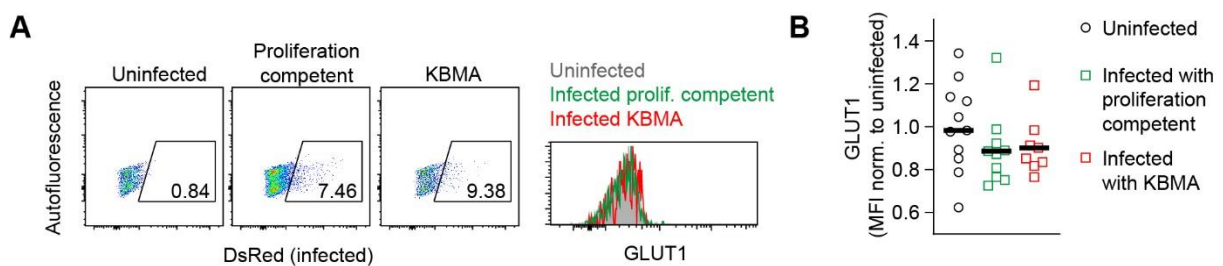


**Figure 3.7.4: Intracellular *L. major* proliferation rate does not affect GLUT1 in host macrophages in vitro.** (A-B) Gating (A) and mean fluorescence intensity (normalised to uninfected) (B) for GLUT1 expression in uninfected (grey), *Lm*<sup>DsRed</sup> proliferation-competent-infected (green) and *Lm*<sup>DsRed</sup> KBMA-infected (red)

bone marrow-derived macrophages. Each symbol shows one individual biological replicate. Horizontal bars denote the mean. Data pooled from three independent experiments. No significant differences according to one-way ANOVA. KBMA, killed but metabolically active. Data obtained in collaboration with Dewitz L-A (Institute of Molecular and Clinical Immunology, Medical Faculty, Otto von Guericke University Magdeburg, Magdeburg, Germany).

In addition to glucose uptake, we analysed the expression of CD36, a membrane glycoprotein involved in high affinity tissue uptake of long chain fatty acids (297, 298). We found that expression of CD36 was significantly increased in macrophages infected with proliferation-competent parasites as compared to both uninfected, as well as KBMA-infected cells (Figure 3.7.5A–B), suggesting that pathogen proliferation might increase CD36 expression in infected macrophages.

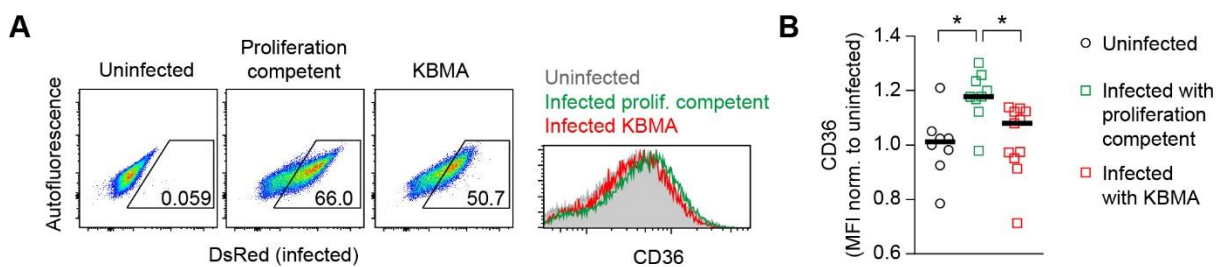


**Figure 3.7.5: Intracellular *L. major* proliferation rate modifies CD36 expression in host macrophages in vitro. (A–B)** Gating (A) and mean fluorescence intensity (normalised to uninfected) (B) for CD36 in uninfected (grey), *Lm*<sup>DsRed</sup> proliferation-competent-infected (green) and *Lm*<sup>DsRed</sup> KBMA-infected (red) bone marrow-derived macrophages. Each symbol shows one individual sample. Data pooled from three independent experiments. Horizontal bars denote the mean. \*,  $p < 0.05$  according to one-way ANOVA with Bonferroni post-test. KBMA, killed but metabolically active. Data obtained in collaboration with Dewitz L-A (Institute of Molecular and Clinical Immunology, Medical Faculty, Otto von Guericke University Magdeburg, Magdeburg, Germany).

To validate these findings in vivo, we analysed intracellular pathogen proliferation and CD36 expression in CD11c<sup>+</sup>Ly6C<sup>hi</sup> and CD11c<sup>+</sup>Ly6C<sup>lo</sup> monocytes isolated from the *Lm*<sup>SWITCH</sup>-infected ear dermis. When we determined pathogen proliferation in vivo, CD11c<sup>+</sup>Ly6C<sup>hi</sup> monocytes exhibited higher intracellular pathogen proliferation than CD11c<sup>+</sup>Ly6C<sup>lo</sup> monocytes (Figure 3.7.6A–B).

Of note, CD36 expression in cells isolated from the infection site was not only generally higher in CD11c<sup>+</sup>Ly6C<sup>hi</sup> monocytes, but also exhibited a substantial increase when comparing infected with non-infected CD11c<sup>+</sup>Ly6C<sup>hi</sup> monocytes. This was, in contrast, not the case for CD11c<sup>+</sup>Ly6C<sup>lo</sup> monocytes (Figure 3.7.7A–B). This suggested that also in vivo, infection with high proliferating pathogen correlated with higher CD36 expression.

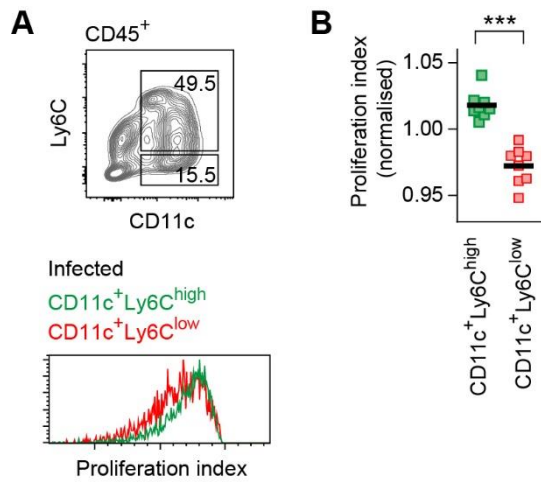


**Figure 3.7.6: Intracellular *L. major* proliferation rate depends on monocyte subtype in vivo.** (A) Gating for CD11c<sup>+</sup>Ly6C<sup>high</sup> and CD11c<sup>+</sup>Ly6C<sup>low</sup> CD45.1<sup>+</sup> monocytes (upper panel) and histogram plots showing proliferation index in infected CD11c<sup>+</sup>Ly6C<sup>high</sup> (green) and CD11c<sup>+</sup>Ly6C<sup>low</sup> (red) CD45.1<sup>+</sup> cells. (B) Quantification of proliferation index normalised to the total proliferation index in each sample (see chapter 2.2.8) in infected CD11c<sup>+</sup>Ly6C<sup>high</sup> (green) and CD11c<sup>+</sup>Ly6C<sup>low</sup> (red) monocytes in newly recruited CD45.1<sup>+</sup> cells analysed according to gating shown in (A). Each symbol represents one mouse ear. Horizontal bars denote the mean. Data pooled from two independent experiments. \*\*\*,  $p < 0.001$  according to paired t-test. Data obtained in collaboration with Fu Y (Institute of Molecular and Clinical Immunology, Medical Faculty, Otto von Guericke University Magdeburg, Magdeburg, Germany).

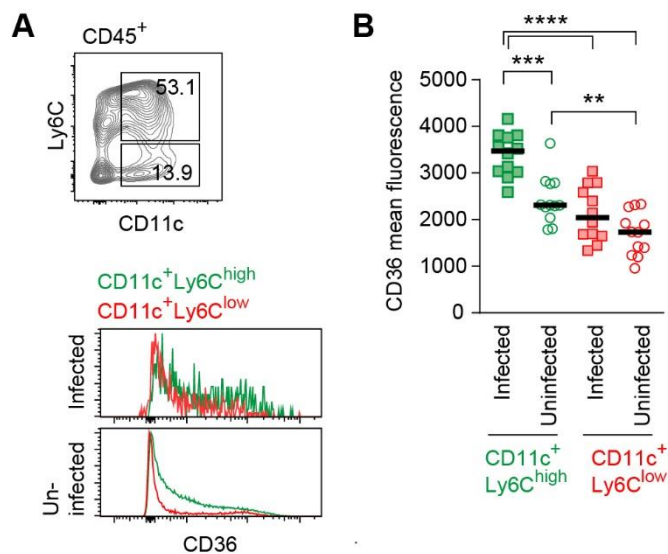


**Figure 3.7.7: Increased CD36 expression in monocyte reservoir associated with high intracellular parasite proliferation in vivo.** (A) Gating for CD11c<sup>+</sup>Ly6C<sup>high</sup> and CD11c<sup>+</sup>Ly6C<sup>low</sup> monocytes (upper panel) and histogram plots showing CD36 expression in infected and uninfected CD11c<sup>+</sup>Ly6C<sup>high</sup> (green) and CD11c<sup>+</sup>Ly6C<sup>low</sup> (red) CD45<sup>+</sup> cells. (B) Mean fluorescence intensity for CD36 expression in infected (squares) and uninfected (dots) CD11c<sup>+</sup>Ly6C<sup>high</sup> (green) and CD11c<sup>+</sup>Ly6C<sup>low</sup> (red) CD45<sup>+</sup> monocytes analysed according to gating shown in (A). Each symbol represents one mouse ear. Horizontal bars denote the mean. Data pooled from two independent experiments. \*\*\*\*,  $p < 0.0001$ ; \*\*\*,  $p < 0.001$ ; \*\*,  $p < 0.01$  according to one-way ANOVA with Bonferroni post-test. Data obtained in collaboration with Fu Y (Institute of Molecular and Clinical Immunology, Medical Faculty, Otto von Guericke University Magdeburg, Magdeburg, Germany).

As CD36 is involved in high affinity tissue uptake of long chain fatty acids (297, 298), we next aimed to evaluate whether differential pathogen proliferation resulted in distinct lipid uptake behaviours in infected cells in vitro. In order to do so, we analysed the uptake of low-density lipoprotein (LDL), long chain (C16) and short-/medium-chain (C1/12) fatty acids into uninfected as well as KBMA and proliferation-competent *L. major*-infected murine BMDM. Both LDL (Figure 3.7.8A–B) and long chain (Figure 3.7.9A–B), but not short chain fatty acid uptake (Figure 3.7.10A–B) was increased upon *L. major* infection. Strikingly, KBMA-infected monocytes showed a higher uptake of LDL (Figure 3.7.8B) and long chain fatty acids (Figure 3.7.9B) as compared to cells infected by proliferation-competent *L. major*. This suggested that the increased CD36 expression might be compensatory as a result of different lipid uptake rates linked with pathogen proliferation (299), and underlined that *L. major* proliferation differentially modulated metabolic pathways in the infected host phagocytes.

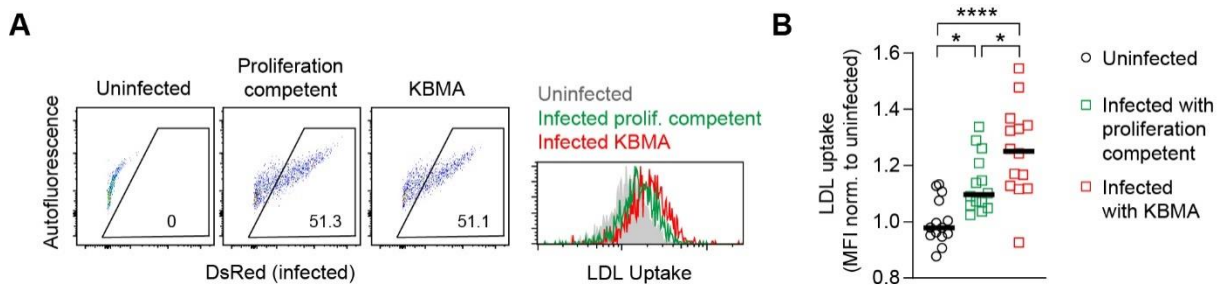


**Figure 3.7.8: Intracellular *L. major* proliferation rate modifies low-density lipoprotein uptake in host macrophages in vitro. (A–B)** Gating (A) and mean fluorescence intensity (normalised to uninfected) (B) for LDL uptake in uninfected (grey), *Lm*<sup>DsRed</sup> proliferation-competent-infected (green) and *Lm*<sup>DsRed</sup> KBMA-infected (red) bone marrow-derived macrophages. Each symbol shows one individual sample, data pooled from three independent experiments. Horizontal bars denote the mean. \*\*\*\*,  $p < 0.0001$ ; \*,  $p < 0.05$  according to one-way ANOVA with Bonferroni post-test. KBMA, killed but metabolically active. LDL, low-density lipoprotein. Data obtained in collaboration with Dewitz L-A (Institute of Molecular and Clinical Immunology, Medical Faculty, Otto von Guericke University Magdeburg, Magdeburg, Germany).

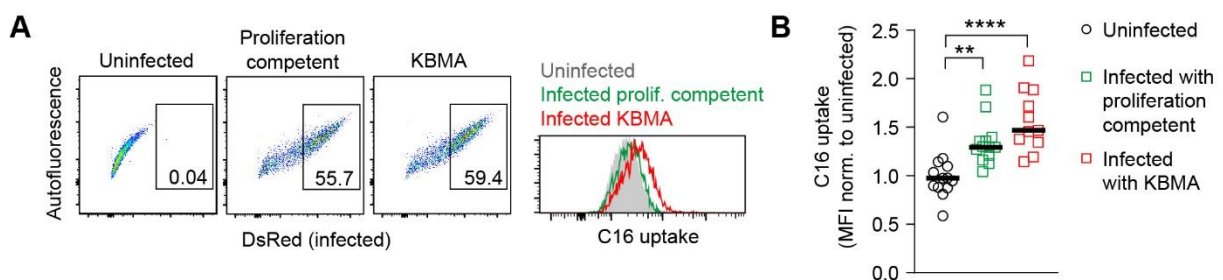


**Figure 3.7.9: Intracellular *L. major* proliferation rate modifies long chain fatty acid uptake in host macrophages in vitro. (A–B)** Gating (A) and mean fluorescence intensity (normalised to uninfected) (B) for C16 uptake in uninfected (grey), *Lm*<sup>DsRed</sup> proliferation-competent-infected (green) and *Lm*<sup>DsRed</sup> KBMA-infected (red) bone marrow-derived macrophages. Each symbol shows one individual sample, data pooled from three independent experiments. Horizontal bars denote the mean. \*\*\*\*,  $p < 0.0001$ ; \*\*,  $p < 0.01$  according to one-way ANOVA with Bonferroni post-test. KBMA, killed but metabolically active. C16, long chain fatty acid. Data obtained in collaboration with Dewitz L-A (Institute of Molecular and Clinical Immunology, Medical Faculty, Otto von Guericke University Magdeburg, Magdeburg, Germany).

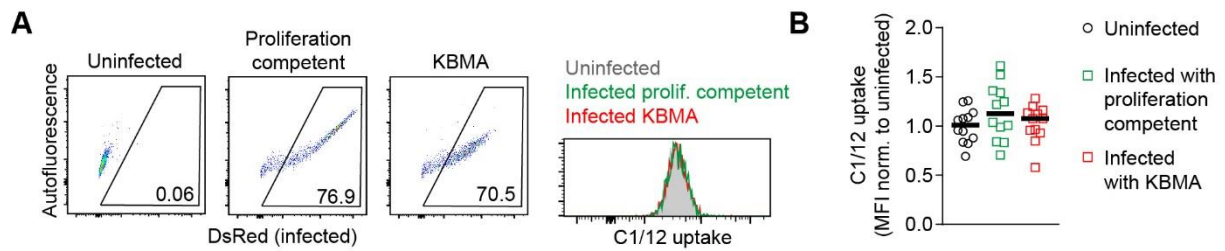


**Figure 3.7.10: Intracellular *L. major* proliferation rate does not affect short-/medium- chain fatty acid uptake in host macrophages in vitro. (A–B) Gating (A) and mean fluorescence intensity (normalised to uninfected) (B) for C1/12 fatty acid uptake in uninfected (grey), *Lm*<sup>DsRed</sup> proliferation-competent-infected (green) and *Lm*<sup>DsRed</sup> KBMA-infected (red) BMDM. Each symbol shows one individual sample. Horizontal bars denote the mean. Data are pooled from at least three independent experiments. KBMA, killed but metabolically active; BMDM, bone marrow-derived macrophages. No significant differences according to one-way ANOVA. KBMA, killed but metabolically active. C1/12, short-/medium chain fatty acid. Data obtained in collaboration with Dewitz L-A (Institute of Molecular and Clinical Immunology, Medical Faculty, Otto von Guericke University Magdeburg, Magdeburg, Germany).**

### 3.8 High proliferating *L. major* parasites more likely reside in close proximity to blood vessels

Having shown that intracellular pathogen proliferation alters the fate of the infected host cell and induces cell-to-cell transfer, we next sought to investigate whether intracellular parasite proliferation might be associated to differences in the microenvironment. We assumed that newly recruited cells, the main reservoir for high proliferating parasites, are more likely to reside in close proximity to the blood vessel. We therefore expected to observe a negative correlation between parasites proliferation and their distance to blood vessels. However, since recent findings suggested that NO-mediated *Leishmania* killing by macrophages might be affected under hypoxic conditions (117, 292, 300, 301), an alternative cause for potential differential pathogen proliferation with respect to blood vessels might be related to differences in oxygen availability. As the production of NO is oxygen dependent (302), proximity to blood vessels might indicate, in contrast to the contribution of newly recruited host cells, an enhanced *L. major* control and thus lower proliferation.

In order to analyse parasite proliferation in relation to blood vessel distance, wild type mice were infected with  $2 \times 10^5$  mKikume-expressing *L. major* ( $Lm^{SWITCH}$ ) for 21 days. Photoconversion of the  $Lm^{SWITCH}$  parasites in the mouse ear was performed 48 h before analysis. In order to visualise the vascularity, mice were injected intravenously with the vascular fluorescent nanoparticle probe AngioSPARK 15 minutes before intravital 2-photon imaging (Figure 3.8.1). To allow analysis of parasite proliferation and the distance to the next blood vessel, acquired intravital imaging data were converted by spectral filtering based on mKikumeRed and far-red fluorescence ratio determined from manually selected *L. major* and autofluorescent shapes as described previously (292) (Figure 3.8.2A–E).

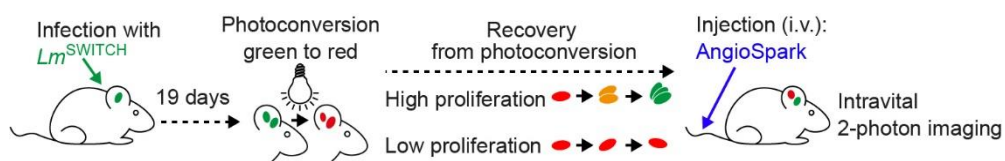


**Figure 3.8.1: Experimental setup for in vivo analysis of parasite proliferation in relation to blood vessel distance.** In vivo analysis of parasite proliferation in relation to blood vessel distance using a photoconversion-based pathogen proliferation biosensor ( $Lm^{SWITCH}$ ), a vascular fluorescent nanoparticle probe (AngioSPARK) and 2-photon intravital imaging.

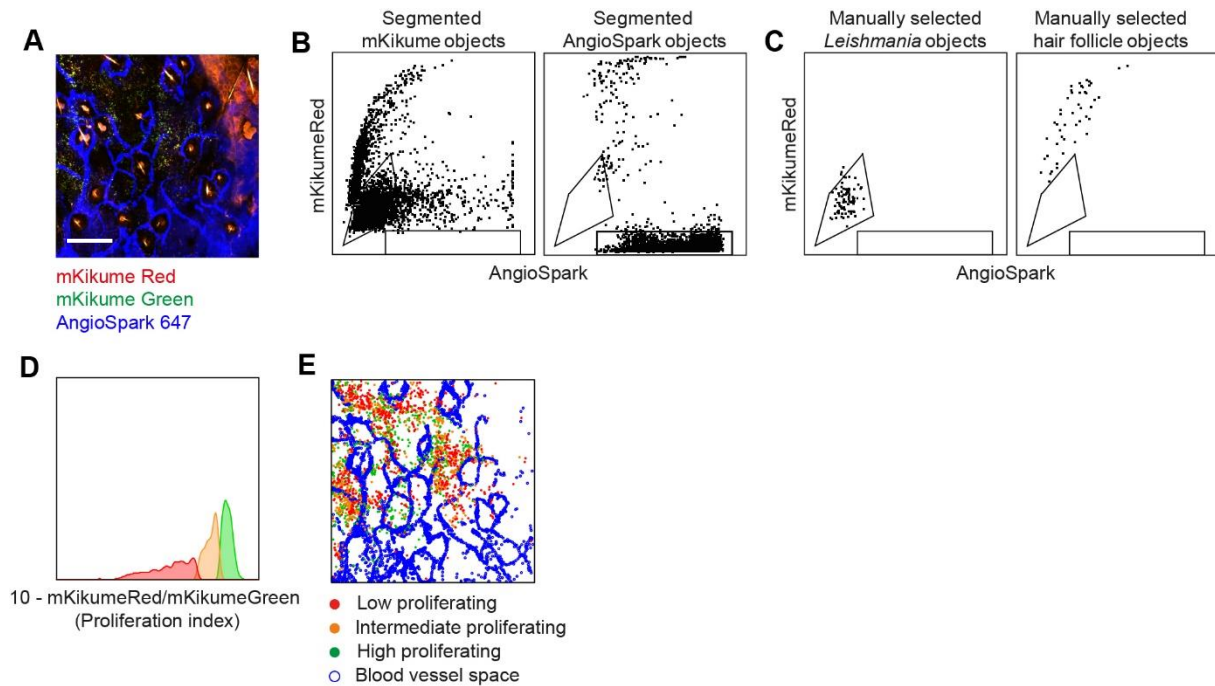


**Figure 3.8.2: Intravital 2-photon imaging of parasite proliferation in relation to blood vessel distance in vivo.** (A) Z-projection of *Lm*<sup>SWITCH</sup>-infected ear dermis displaying low proliferating *Lm*<sup>mKikumeRed</sup>, high proliferating *Lm*<sup>mKikumeGreen</sup> and AngioSpark-stained blood vessels. 18 slices of 3  $\mu$ m-spaced z-stacks taken longitudinally are projected. Scale bar, 1000  $\mu$ m. (B) Gating strategy for segmented mKikume<sup>+</sup> *Leishmania* objects (left panel) and for segmented AngioSpark<sup>+</sup> blood vessel objects (right panel) using Imaris-to-FlowJo converted data. (C) Gating strategy for *Leishmania* (left panel) and for hair follicles (right panel) according to manually selected objects using Imaris software. (D) Histogram plots displaying proliferation index of mKikume<sup>+</sup> objects. (E) Mapped XY positions as determined by spectral filtering; blue, blood vessel; red, low proliferating *L. major*; orange, intermediate proliferating *L. major*; green, high proliferating *L. major*.

When analysing distance to the nearest blood vessel, we observed a negative correlation between parasite proliferation and blood vessel distance (Figure 3.8.3, upper panels and Figure 3.8.4A, left panel). Moreover, this negative correlation was no longer observed when looking at scrambled data in which the pathogen proliferation rates had been assigned arbitrarily (Figure 3.8.3, lower panels and Figure 3.8.4A, right panel). This negative correlation between parasite proliferation and blood vessel distance was also observed when looking at the slopes of correlation for each individual animal, but again was no longer observed when looking at scrambled data (Figure 3.8.4B). Additionally, we observed a positive correlation between vessel distance and absolute mKikume<sup>Red</sup> signal (Figure 3.8.4C), indicating our findings are due to parasite proliferation and not to protein folding kinetics. Thus, our results indicate that high proliferating parasites were more often observed in close proximity to blood vessels as compared to low proliferating parasites, which might be due to reduced control by macrophages or by the increased likelihood of newly recruited monocyte-derived host cells present in this area.

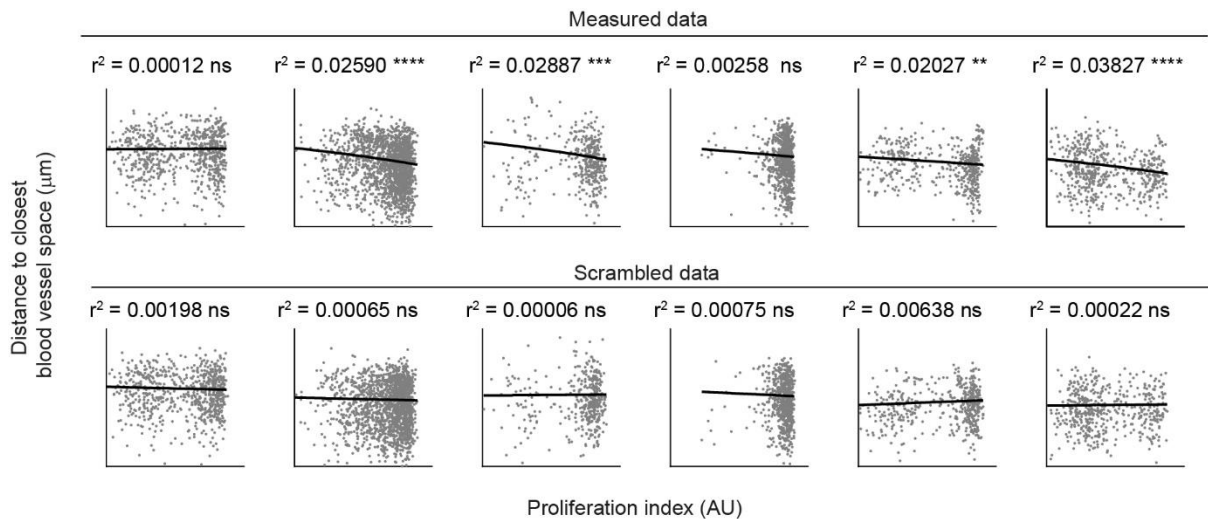


**Figure 3.8.3:** *L. major* proliferation in relation to blood vessels distance in vivo. Correlation plots of measured (upper panels) and scrambled (lower panels) data showing parasite proliferation index in relation to distance to the closest blood vessel of all imaged sites. Each plot indicates one imaged site. Each symbol represents one *Leishmania* object. \*\*\*\*,  $p < 0.0001$ ; \*\*\*,  $p < 0.001$ ; \*\*,  $p < 0.01$ ; ns, not significant according to according to Pearson's correlation coefficient ( $r$ ).

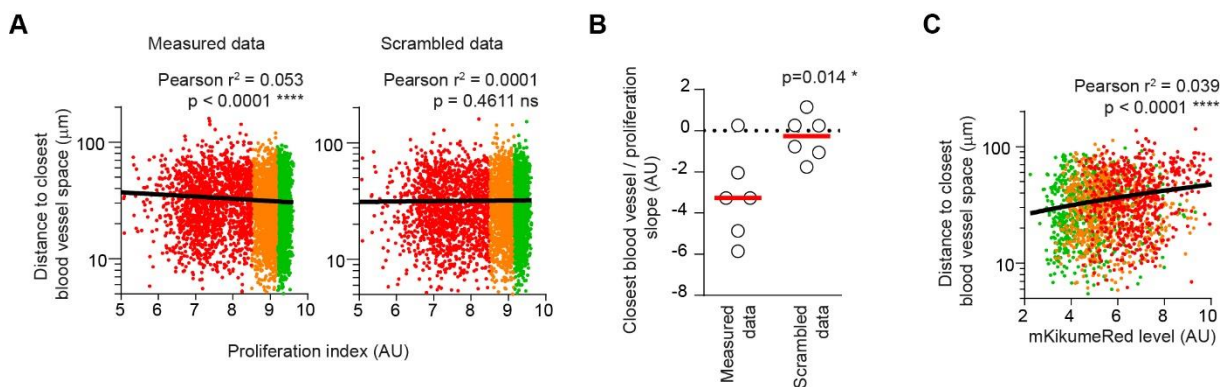


**Figure 3.8.4:** High proliferating *L. major* parasites more likely reside in close proximity to blood vessels in vivo. (A–B) Overlay (A) and quantification (B) of mean values data shown in (Figure 3.8.3). Each symbol pair represents one mouse ear. Horizontal bars denote the mean. (C) Correlation plot of mKikumeRed level in relation to distance to the closest blood vessel of all imaged sites. Data pooled from two independent experiments. \*\*\*\*,  $p < 0.0001$ ; \*,  $p < 0.05$ ; ns, not significant according to according to Pearson's correlation coefficient ( $r$ ) in (A) and (B), and Mann–Whitney test in (C).

Chapter 3.9 published in: Baars I et al., *Interleukin-11 receptor expression on monocytes is dispensable for their recruitment and pathogen uptake during Leishmania major infection*. *Cytokine*. 2021.

### 3.9 Ablation of IL-11 receptor signalling does not significantly influence *Leishmania* infection in monocytes in vivo

IL-11 plays an essential role in bone remodelling by acting on all major cell types involved in bone homeostasis, namely osteoblasts, osteocytes, and osteoclasts and was suggested to affect phagocytic functions in osteoclasts (183, 303). Moreover, IL-11 was shown to reduce myelin phagocytosis by microglia, macrophage-like immune cells of the central nervous system (184). Since we were able to show that IL-11 receptor (IL-11R) is expressed on human monocytes (304), we hypothesised that IL-11 might influence the uptake of *Leishmania* parasites by newly recruited monocytes. Therefore, we sought to investigate *L. major* infection of monocytes upon IL-11R ablation in vivo. We used an adoptive transfer approach in order to compare wild type and IL-11R-deficient monocytes side by side (91). For this, we injected  $2 \times 10^6$  DsRed-labelled *Leishmania* (*Lm*<sup>DsRed</sup>) parasites intradermally into the ear of C57BL/6 mice. 16 days post infection, we injected a 1:1 mixture of either CFSE-labelled CD45.1<sup>+</sup> WT cells and CD45.2<sup>+</sup> IL-11R<sup>-/-</sup> or, as a control, CFSE-labelled CD45.1<sup>+</sup> WT cells and CD45.2<sup>+</sup> IL-11R<sup>+/+</sup> intravenously into the tail vein of the mice. Five days after cell transfer, we analysed cells isolated from the infected ears via flow cytometry (Figure 3.9.1).

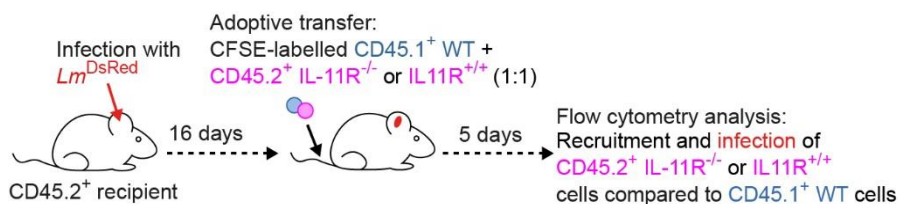


**Figure 3.9.1: Experimental strategy to determine the role of IL-11 receptor signalling during *L. major* infection.** In vivo flow cytometry analysis of CFSE-labelled, newly recruited IL-11R<sup>+/+</sup> or IL-11R<sup>-/-</sup> (CD45.2<sup>+</sup>) and WT control (CD45.1<sup>+</sup>) cells side-by-side.

First, we assessed whether the IL-11R affects monocyte recruitment. For this, we determined, in the CFSE-labelled recruited cell population, the ratio between CD45.1<sup>+</sup> and CD45.2<sup>+</sup> cells for mice adoptively transferred with either IL-11R<sup>+/+</sup> or IL-11R<sup>-/-</sup> CD45.2<sup>+</sup> cells together with CD45.1<sup>+</sup> control cells (Figure 3.9.2A). We observed no significant difference in the recruitment of IL-11R<sup>+/+</sup> versus IL-11R<sup>-/-</sup> cells (Figure 3.9.2B). In order to analyse the proportion of IL-11R<sup>-/-</sup> cells among different monocyte populations, we analysed Ly6C<sup>+</sup>MHC-II<sup>-</sup> (immature), Ly6C<sup>+</sup> MHC-II<sup>+</sup> (semi-mature) and Ly6C<sup>-</sup> MHC-II<sup>+</sup> (mature) monocytes separately (Figure 3.9.3A), yielding no significant differences in case of recently recruited immature monocytes (Figure 3.9.3B). However, a significant reduction in the recruitment of semi-matured Ly6C<sup>+</sup>MHC-II<sup>+</sup> monocytes was observed, suggesting IL-11R signalling might play a role in the recruitment of specific monocyte subsets or might affect maturation of infected monocytes, although no significant changes were observed in case of matured monocytes (Figure 3.9.3B).

Further investigation will be required to determine the exact role of IL-11R signalling in monocyte recruitment during ongoing *Leishmania* infection.

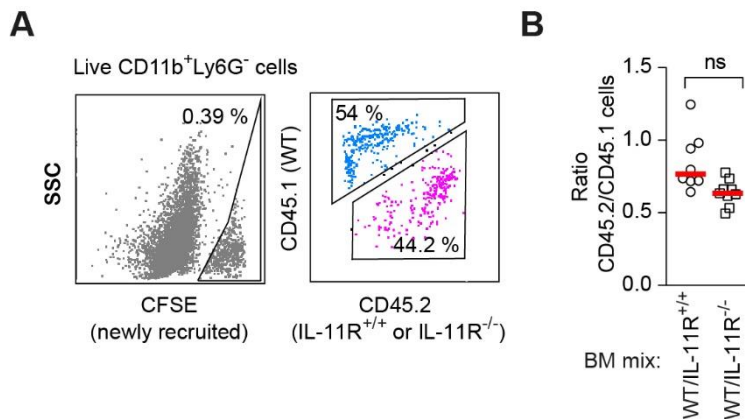


**Figure 3.9.2: IL-11 receptor signalling does not influence monocyte recruitment in the *L. major*-infected murine ear dermis.** (A) Gating strategy to identify CD45.2<sup>+</sup> IL-11R<sup>+/+</sup> (control) or IL-11R<sup>-/-</sup> and CD45.1<sup>+</sup> WT control cells among CFSE<sup>+</sup> newly recruited cells. (B) Ratio of CD45.2<sup>+</sup>/CD45.1<sup>+</sup> cells among newly recruited CFSE<sup>+</sup> cells in WT/IL-11R<sup>+/+</sup> and WT/IL-11R<sup>-/-</sup> mice according to the gating shown in (A). Each dot represents one mouse ear. Horizontal bars in red denote the median. Data pooled from two independent experiments. ns, not significant according to one-way ANOVA with Bonferroni post-test and pairwise comparison. WT, wild type; BM, bone marrow.

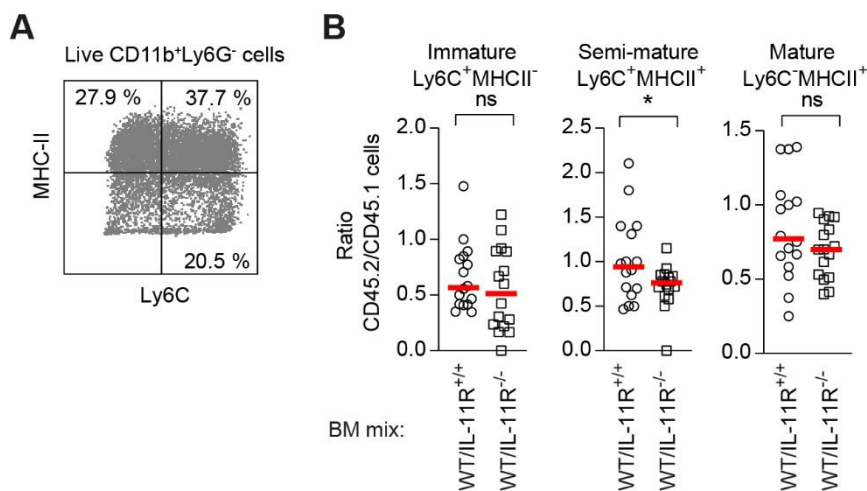


**Figure 3.9.3: Influence of IL-11 receptor signalling on the recruitment of different monocyte subsets in *L. major*-infected murine ear dermis.** (A) Monocytes (CD11b<sup>+</sup>Ly6G<sup>-</sup>) gated with respect to expression of Ly6C and MHC class II in order to identify immature Ly6C<sup>+</sup>MHCII<sup>-</sup>, semi-mature Ly6C<sup>+</sup>MHCII<sup>+</sup> and mature Ly6C<sup>-</sup>MHCII<sup>+</sup> monocytes. (B) Ratio of CD45.2<sup>+</sup>/CD45.1<sup>+</sup> cells among newly recruited CFSE<sup>+</sup> monocytes in WT/IL-11R<sup>+/+</sup> and WT/IL-11R<sup>-/-</sup> mice within the different cell populations shown in (A). Each dot represents one mouse ear. Horizontal bars in red denote the median. Data pooled from two independent experiments. ns, not significant according to one-way ANOVA with Bonferroni post-test and pairwise comparison. WT, wild type; BM, bone marrow.

To determine whether IL-11R signalling affects monocyte infection by *L. major*, we measured the infection rate for the recruited monocytes via *L. major* DsRed fluorescence, and calculated the ratio of infection rates between CD45.1<sup>+</sup> and CD45.2<sup>+</sup> cells for both mouse groups (Figure

3.9.4A). No significant differences were detected, neither for all cells (Figure 3.9.4B), nor for Ly6C<sup>+</sup> MHC-II<sup>-</sup> (immature), Ly6C<sup>+</sup> MHC-II<sup>+</sup> (semi-mature) or Ly6C<sup>-</sup> MHC-II<sup>+</sup> (mature) cells when analysed separately (Figure 3.9.4C). In conclusion, our data argue against a significant role of IL-11R signalling in monocyte recruitment and infection during *L. major* infection in vivo.

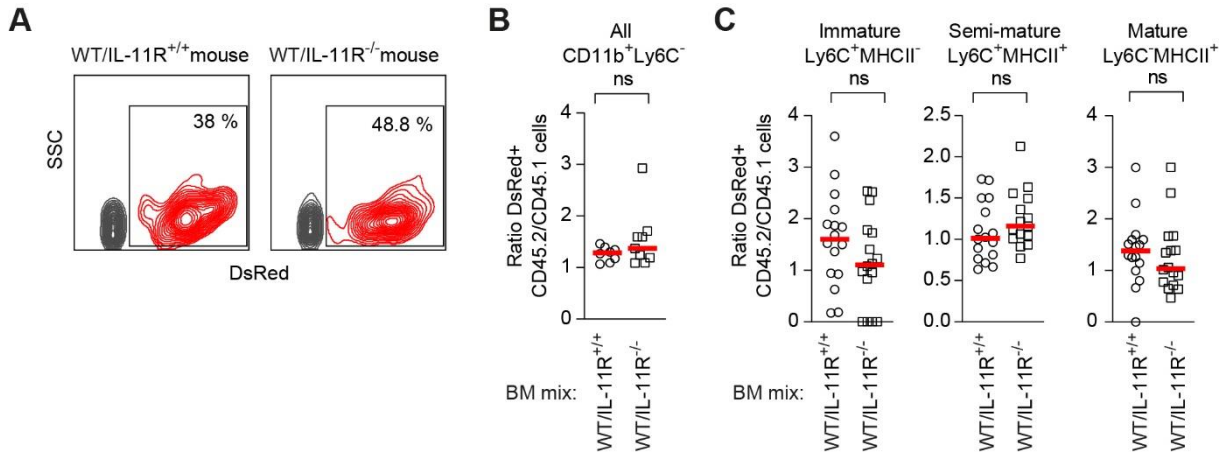


**Figure 3.9.4: IL-11 receptor signalling does not influence infection of monocytes in the *L. major*-infected murine ear dermis.** (A) Gating strategy to identify DsRed<sup>+</sup> infected cells in WT/IL-11R<sup>+/+</sup> and WT/IL-11R<sup>-/-</sup> mice within the different cell populations shown in (Figure 3.9.2A) and (Figure 3.9.3A). (B–C) Ratio of DsRed<sup>+</sup> CD45.2<sup>+</sup>/CD45.1<sup>+</sup> cells among newly recruited CFSE<sup>+</sup> monocytes in WT/IL-11R<sup>+/+</sup> and WT/IL-11R<sup>-/-</sup> mice within all CD11b<sup>+</sup>Ly6G<sup>-</sup> monocytes (B) according to gating shown in (Figure 3.9.2A) and (A) and within the different monocyte subsets (C) according to gating shown in (Figure 3.9.3A) and (A). Each dot represents one mouse ear. Horizontal bars in red denote the median. Data pooled from two independent experiments. ns, not significant according to one-way ANOVA with Bonferroni post-test and pairwise comparison. WT, wild type; BM, bone marrow.

## 4. DISCUSSION

Host cell exit is a critical step in the life-cycle of intracellular pathogens. Similar to cell invasion and intracellular survival, host cell exit represents a well-regulated system that has evolved during host-pathogen co-evolution and relies on intricate host-pathogen dynamics. The main exit strategies employed by pathogens are initiation of programmed cell death, active breaching of host cell-derived membranes and membrane-dependent exit without host cell lysis. The majority of intracellular pathogens utilise more than one of these strategies, depending on life-cycle stage, environmental factors and host cell type (193–197). Although it is well-known that the ability of *L. major* parasites to exit from and to spread among phagocytes are key survival strategies of the parasite, they have hardly been studied during ongoing infection. Elucidating these strategies is however of utmost importance, while this might lead to the identification of novel targets for future treatment approaches.

A possible mechanism involved in *L. major* cell-to-cell transfer among phagocytes is cell death of the infected host cell. Thus far, multiple studies have shown that *Leishmania* parasites can delay apoptosis in infected neutrophils and subsequently use apoptotic neutrophils as “Trojan horses” for silent entry into macrophages without activating their effector mechanisms (68, 81, 82, 305, 306). We hypothesised that *L. major* might employ a similar approach for their transfer among macrophages, although findings regarding macrophage cell death during *Leishmania* infection are inconsistent. Therefore, we aimed to investigate original host cell death in relation to *L. major* exit from and uptake into monocyte-derived phagocytes during ongoing infection in vivo. Additionally, since intracellular proliferation is another major survival strategy of *L. major* parasites and since we have recently shown that high proliferating *L. major* parasites undergo more cell-to-cell transfer as compared to low proliferating parasites (91), we investigated whether pathogen proliferation affects host cell death, thereby enabling the efficient dissemination of the pathogen to new phagocytes. In this study, we show that *L. major* infection modulates host cell metabolism and drives host cell death in vivo depending on intracellular pathogen proliferation rate, thereby enabling the efficient dissemination of the pathogen to new phagocytes.

#### 4.1 The role of CD11c-expressing cells during *Leishmania* infection

When looking at the function of CD11c-expressing *Leishmania*-permissive host cells, our results, based on CD11c<sup>+</sup> cell depletion, indicate that these cells play a dual role in the ongoing infection. That is, CD11c-expressing cells seemed to promote infection by functioning as host cells for the parasite and seemed to control the infection by inducing iNOS production. This is in contrast to previous findings showing that depletion of CD11c<sup>+</sup> cells during ongoing infection dramatically increased iNOS-dependent NO production in splenocytes. However, in line with our current findings indicating that CD11c-expressing cells are an important reservoir for *Leishmania* parasites, the same study showed that depletion of CD11c<sup>+</sup> cells reduced splenic parasite burden (307). Additionally, our findings support previous data showing that CD11c<sup>+</sup> DCs are important for control of the infection by inducing *Leishmania*-specific T cell responses and are the most abundant cell type expressing iNOS (107, 307–311). Of note, the time of CD11c<sup>+</sup> cell differentiation and the efficiency of T cell priming and iNOS production by CD11c<sup>+</sup> cells might depend on the *Leishmania* species causing the infection (312, 313). Our present findings also support our recent data showing that CD11c-expressing monocytes are the main host cell type for efficient *Leishmania* proliferation and for cell-to-cell transmission and support previous findings from others showing that infected CD11c<sup>+</sup> DCs constitute an important reservoir for *L. major* parasites (91, 311, 314). We hypothesise that the increase in parasite burden observed at later stages of CD11c<sup>+</sup> cell depletion could be further enhanced by more efficient phagocyte recruitment due to the decreased iNOS production. This potential increase in phagocyte recruitment could in turn also lead to an increase in intracellular pathogen proliferation, as has previously been postulated by our group (292). Moreover, although we have not looked at DCs in lymph nodes during CD11c<sup>+</sup> cell depletion in ongoing infection, it has been suggested that *Leishmania* parasites might additionally use these cells to migrate to secondary lymphoid organs and peripheral sites (315). This in turn could further promote *Leishmania* dissemination during later stages of the infection. Of note, infected CD11c<sup>+</sup> cells were indicated to have reduced MHC-II-mediated antigen-presenting potential and therefore more likely contribute to the spread rather than to the control of the infection (314, 316, 317). However, findings regarding antigen-presentation ability in CD11c<sup>+</sup> cells are inconsistent, with other studies showing that DCs were able to efficiently present *Leishmania* antigen to T cells (108, 318). Interestingly, inflammatory macrophages, resembling the host cells used in the present study, were shown to successfully capture and kill *L. major* parasites, but did not upregulate MHC-II expression upon infection, suggesting these cells do not actively participate in T cell priming (108). Taken together, these findings indicate that CD11c-expressing cells play distinct roles during *Leishmania* infection, depending on the CD11c<sup>+</sup> cell subpopulation, the *Leishmania* species and strain, the infection site and the infection stage.

Along the same lines, we were able to show that high proliferating *L. major* parasites more likely reside nearby blood vessels. This might be related to the residency of newly recruited

CD11c<sup>+</sup> monocytes, which we have previously shown to preferentially harbour fast proliferating parasites and which migrate via blood vessels, in that area (91). The accumulation of high proliferating parasites around blood vessels might however also be related to altered NO-mediated *Leishmania* killing by macrophages. Although NO is considered to be a critical player in *Leishmania* clearance, the relation between NO-mediated parasite clearance and hypoxia is unclear thus far. That is, previous findings have indicated that hypoxia promotes the control of *L. amazonensis* infection by macrophages (319), while other findings have suggested that hypoxia in *L. major* skin lesions impairs the NO-dependent control of pathogen proliferation by macrophages (320). This second finding would be in line with the implication that NO together with superoxide can form the effective antimicrobial compound peroxynitrite (142), proposing that NO production could be more effective at sites with high oxygen availability and less effective at sites with low oxygen availability. This finding is however contradictory to the findings of the present study. The reason for the contradictory findings regarding hypoxia and *Leishmania* infection might be related to the fact that these previous studies investigated the effect of experimentally-induced hypoxia and not the effect of biologically-induced hypoxia (e.g. by infection or microenvironment). Additionally, during our present studies, we did not look at a direct connection between parasite proliferation and hypoxia, but only at a connection between parasite proliferation and blood vessel distance. Apart from explanations regarding cell niche and oxygen availability, our current findings might also be explained by altered oxygen-dependent parasite proliferation. It however seems unlikely that differences in local oxygen concentration would be the main factor influencing intracellular *Leishmania* amastigote proliferation directly. That is, previous findings suggest that *Leishmania* parasites have developed certain strategies to survive under hypoxic conditions and that mitochondria in *Leishmania* amastigotes are less dependent on respiratory energy as compared to promastigotes, potentially contributing to the survival of amastigotes within phagolysosomes where apparent hypoxic conditions persist (321, 322). We therefore propose that the residency of high proliferating parasites in close proximity to blood vessels might be due to reduced control by macrophages or to the increased likelihood of newly recruited monocyte-derived host cells present in this area.

## 4.2 Cellular dissemination of *Leishmania*

When looking at the spread of *L. major* parasites, we observed that transfer from one host phagocyte to the next is direct, with no extracellular phase detectable in vivo. In line with this, *L. major* transfer among phagocytes was shown to be direct in vitro and cell-to-cell transfer of *L. amazonensis* amastigotes was reported to occur without full exposure to the extracellular milieu (38, 91, 323). Also, in the present study, we observed that the uptake of *L. major* parasites by newly recruited monocytes was accompanied by the uptake of original host cell material, which supports our previous data showing that the original host cell was phagocytosed by the newly infected host cell upon parasite transfer in vitro (91). While the uptake of neutrophil material together with parasites by recruited monocyte-derived macrophages and DCs has been demonstrated in a variety of studies (19, 306, 323–325), the transit between infected monocyte-derived cells in an established infection had been less well elucidated. Our data now show that also the transfer from infected CD11c-expressing cells, most probably inflammatory monocytes (91), involves the uptake of original host cell material. Importantly, we could validate our findings from mice in an in vitro system of human monocytes, illustrating that both in preclinical in vivo and human in vitro systems, uptake of original host cell material is involved in the cell-to-cell transfer of the parasite.

### 4.3 Apoptosis as cellular exit strategy for *Leishmania*

Although intracellular pathogens have developed numerous strategies to delay or inhibit apoptosis in order to establish their intracellular niche, the induction of host cell apoptosis is also one of the main exit strategies employed by pathogens in order to establish pathogen dissemination (326, 327). The significance of host macrophage apoptosis in pathogen spread has previously been shown for *Mycobacterium avium*, as well as for *Mycobacterium tuberculosis* (246, 328). Additionally, apoptosis was found to mediate the spread of *Mycobacterium marinum* among macrophages in granulomas and cell death in macrophages infected with the facultative intracellular fungus *Cryptococcus neoformans* was shown to be associated with apoptotic features (329–333). Interestingly and very much in line with the findings of the present study, *Cryptococcus neoformans*-induced apoptosis was suggested to be related to intracellular growth and cellular escape (331). Furthermore, host cell apoptosis has been shown to play a role during *Chlamydia* infection. However, the exact role of cellular apoptosis in *Chlamydia*-infected cells so far remains unclear with some studies suggesting infection induced apoptosis in host cells (334–336), thereby promoting propagation of the infection, and others suggesting infection inhibited apoptosis (337, 338). Lastly, *Francisella tularensis* and *Salmonella enterica* were shown to induce apoptosis in infected host cells, although this induction in apoptosis was not specifically linked to pathogen dissemination (339–341). In regard to *Leishmania*, host cell death has already been postulated to play a role in egress from neutrophils (19, 82, 342). However, its role for *Leishmania* egress from macrophages thus far remained elusive. We now observed more apoptosis in *L. major*-infected cells as compared to uninfected cells, both by live cell imaging and intravital 2-photon imaging in the living tissue. In contrast, a number of previous studies suggested that *Leishmania* infection inhibits macrophage apoptosis. For example, *L. donovani* infection has been shown to inhibit the programmed cell death-1 (PD-1) receptor and to activate the anti-apoptotic AKT signalling pathway, and the anti-apoptotic Bcl-2 family-related protein myeloid cell leukemia 1 (MCL-1) in macrophages (262–267). In line with this, *L. donovani* and *L. infantum* promastigotes have been suggested to increase anti-apoptotic Bcl-2 in macrophages (268, 269). Moreover, other studies showed that both *L. mexicana* promastigotes and amastigotes downregulate camptothecin-induced apoptosis of monocyte-derived DCs and Akarid and colleagues suggested that *L. major* inhibits apoptosis in murine BMDM (270–275). However, these studies investigated mainly the prevention of experimentally-induced apoptosis in vitro, the effect of short-term *Leishmania* infection or cell death irrespective of the cellular infection status. In line with our findings of the present study, there are also a number of reports showing that *Leishmania* infection induces macrophage apoptosis. DaMata and colleagues demonstrated that *L. amazonensis* induces PS exposure, DNA cleavage into nucleosomal size fragments, and consequent hypodiploidy in macrophages, all indicating apoptosis. In addition, the same study showed that *L. amazonensis*-induced macrophage apoptosis was associated to activation of caspases-3, -8 and -9 (276). Other studies suggested that viable, but not dead, *L. major*, *L.*

*aethiopica* and *L. tropica* promastigotes induced apoptosis in infected macrophages in vitro and that *L. aethiopica*, but not *L. mexicana*, induced cell-to-cell transfer following caspase-3-dependent host macrophage apoptosis in vitro (277, 278). These findings together suggest that host cell apoptosis might be *Leishmania* state and *Leishmania* species or strain dependent. This is in line with another study showing that *Leishmania* infection protects murine macrophages from cycloheximide-induced apoptosis in a species and strain specific manner (279). Also in line with our present findings, we recently showed that *L. major*-infected murine macrophages exhibited signs of apoptosis-associated membrane blebbing shortly before parasite transfer into a new phagocyte, suggesting that the infection of new host cells mainly occurs via cell-to-cell transmission from dying phagocytes in vitro (91). Moreover, multidimensional live imaging of long-term-infected macrophages demonstrated that *L. amazonensis* amastigotes underwent cell-to-cell transfer when the original host macrophage shows signs of imminent apoptosis in vitro, in a process mediated by parasitophorous extrusions (38). Interestingly, increased apoptosis in CD4<sup>+</sup> lymphocytes and monocytes was observed in patients with acute visceral leishmaniasis (280). These data together suggest that *Leishmania* parasites might employ a similar approach for macrophage egress as for neutrophil egress; delaying initial host cell apoptosis until apoptosis is induced in order to promote parasite dissemination among phagocytes.

#### 4.4 Other potential cellular exit strategies for *Leishmania*

Although we employed in vivo and in vitro reporters specific for caspase-3, we are not able to formally exclude an involvement of other regulated cell death pathways, such as necroptosis and pyroptosis, in *L. major* infection and cell-to-cell transfer. Further studies are needed to explore the role of these pathways in *L. major* spread among phagocytes. In this regard, previous studies have demonstrated that necroptosis, more specifically RIPK1-RIPK3-MLKL-associated necroptosis, is important for neutrophil death during *L. infantum* infection and for macrophage death during *L. braziliensis*, *L. amazonensis* and *L. major* infection (220–222). In addition, it was suggested that the inflammasome was important for restriction of parasite replication during infection with *L. amazonensis*, *L. braziliensis*, and *L. infantum chagasi*, but not during *L. major* infection (224). Besides playing a potential role during *Leishmania* infection, host cell necroptosis has also been observed during infections with other pathogens. For example, *Salmonella enterica* serovar Typhimurium, a facultative intracellular gram-negative bacterium, enhanced IFN-induced necroptosis in host macrophages, thereby sustaining infection (343, 344). Additionally, *Mycobacterium tuberculosis* was suggested to induce NLRP3-mediated necroptosis in macrophages and ROS-induced cell death of human *Mycobacterium tuberculosis*-infected neutrophils resembled necroptosis and led to transfer of the bacteria into macrophages (345–347). Necroptosis has also been suggested to play a role during viral infections. For instance, murine cytomegalovirus and influenza A virus infections were shown to induce RIPK1-RIPK3-MLKL-mediated necroptosis and herpes simplex virus infection induced necroptosis in murine cells, but reduced necroptosis in human cells (348–354).

In addition to apoptosis and necroptosis, we and others have shown that host macrophage pyroptosis may contribute to *Leishmania* dissemination (94, 236). On the contrary, other studies suggested that *L. amazonensis* and *L. donovani* infection suppress macrophage pyroptosis (238–241). With regard to other pathogens, a number of studies have indicated that various bacteria, such as *Legionella pneumophila*, *Francisella tularensis*, *Shigella flexneri*, *Salmonella* spp. and *Listeria monocytogenes*, induce pyroptosis (193, 194, 197, 355–366). Moreover, the deletion of caspase-11, a member of the murine caspase family and an important initiator of pyroptosis, makes host cells more susceptible to *Salmonella* and *Legionella pneumophila* infection (367, 368), suggesting pyroptosis might also play a role in antimicrobial functions. In addition, a role for pyroptosis in host cell exit has been proposed for the opportunistic yeast pathogen *Candida albicans*, which induces pyroptosis in macrophages and facilitates release of the pathogen (369). These data together suggest that host cell pyroptosis can both benefit the host by controlling infection and can enable the exit of *Salmonella* spp., *Legionella pneumophila*, *Francisella tularensis* and *Candida albicans* from infected macrophages (193, 356, 358, 370, 371), thereby potentially promoting pathogen spread. It therefore seems plausible that pyroptosis, while involved in the antimicrobial host response, also plays a role in host cell exit of certain pathogens.

These findings together suggest that apoptosis may not be the only form of programmed cell death important for *Leishmania* spread among phagocytes. This is especially of interest since apoptosis, necroptosis, and pyroptosis have recently been shown to be tightly connected and can cross-regulate each other. More specifically, caspase-8 can promote apoptosis, necroptosis, or pyroptosis depending on its posttranslational state and the cell type (372). Also, a recently identified cytoplasmic multimeric protein complex named the PANoptosome, which can engage, in parallel, pyroptosis, apoptosis, and necroptosis, has been shown to play a role during microbial infections. The complex contains Z-DNA-binding protein 1 (ZBP1), NLRP3, ASC, RIPK1, RIPK3, caspase-8, caspase-1 and caspase-6 (373). Since *Leishmania* infection has already been associated to caspase-8-associated apoptosis and to RIPK1-RIPK3-MLKL-associated necroptosis in macrophages (221, 222, 276), it could be well possible that multiple forms of programmed cell death occur simultaneously in these infected cells. It would thus be of interest to study caspase-8 and PANoptosome activity in *L. major*-infected macrophages.

Besides programmed host cell death, other means of host cell exit might play a role in *Leishmania* cell-to-cell transfer. The subcellular localisation of the pathogen within the host cell is a determining factor for egress. Usually, after successful entry into the host cell, pathogens reside within a vacuole inside the host cell cytoplasm. Therefore, pathogens first have to escape their vacuole in order to exit their host cell. In order to do so, many pathogens have been shown to utilise pore toxins and phospholipases to disrupt the vacuolar membrane (374-391). On the contrary, cytolysis, which includes the destruction of both vacuolar membrane and host cell plasma membrane, is often mediated by proteases (392-398). In case of *Leishmania*, leishporin, a pore-forming protein expressed by *L. amazonensis* promastigotes and amastigotes, was shown to be involved in vacuolar escape and lysis of infected macrophages (190-192, 399). Apart from vacuolar escape and cytolysis, pathogens have also developed less destructive means of escape, which are mainly membrane-dependent. One of these escape mechanisms involves actin-mediated protrusion (383, 400-425), which relies on the polymerisation of host cell actin on the microbial surface, protects the pathogen from extracellular defence mechanisms and often results in the transfer to new host cells (426). Some pathogens also employ extrusion or budding (427-434), during which the pathogen is protected by a membrane coat and during which the host cell remains intact, to exit host cells or use exocytosis-like egress (435-451), which involves the transport and fusion of intracellular endosomal vesicles with the plasma membrane and the subsequential release of the pathogen (452, 453). A number of pathogens, such as *Listeria monocytogenes* and *Shigella flexneri*, seem to employ multiple exit strategies. That is, both actin-mediated protrusion and pyroptosis have been suggested to play a role during the cellular escape of these bacteria (360, 361, 366, 383, 403-411, 418-425). Taking all these findings into account, which suggest that pathogens might use various strategies to exit their host cells, it is very well possible that *Leishmania* also exploit different pathways to exit and spread among host cells. While the way of cellular exit might depend on the host organism, immune response, cellular niche, parasite

species and strain, infection site, tissue tropism and infection stage, it seems unlikely that *L. major* parasites employ exit strategies during which parasites are released to the extracellular milieu. Hereof, we have recently shown that parasites were taken up directly from one host cell to the next (91) and our present study suggests that parasites do not undergo an extra-cellular phase during cell-to-cell transmission. Moreover, initiation of host cell apoptosis seems to be a beneficial cellular exit strategy for the pathogen, while employing apoptosis initiation would be a way to facilitate uptake by new host cells without inducing inflammatory responses that are usually associated with necroptosis and pyroptosis.

#### 4.5 Host cell death and intracellular *Leishmania* proliferation

When looking at host cell death in relation to intracellular parasite proliferation, we observed higher parasite proliferation in dying host cells as compared to vital host cells, suggesting that *L. major* proliferation could result in death of the infected phagocyte. Although it would be tempting to assume that the proliferation-dependent initiation of cell death is related to an increased number of intracellular parasites, we have previously shown that high proliferating parasites were present at lower numbers per infected cell (91). This finding was also confirmed in the present study. It therefore seems more probable that the death of cells infected with proliferating parasites is associated with more efficient cellular exit and transfer of these high proliferating *L. major* parasites. This in turn is also in line with earlier data obtained by our group showing that high proliferating *L. major* parasites undergo more cell-to-cell transfer as compared to low proliferating parasites (91). Additionally in support of this hypothesis, our data indeed showed that host cells are only able to survive for more than 72 h post-infection if the proliferation rate of the parasite inside the cell is low, suggesting that long-term residency of *L. major* parasites within macrophages is related to low parasite proliferation. Together with our murine and human data showing more apoptosis in infected compared to uninfected cells, we thus hypothesised that proliferating *L. major* parasites induce cell death of the original host cell, thereby promoting transfer to a new phagocyte. Since we observed high proliferating parasites in close proximity to blood vessels, which we assume might be due to higher numbers of newly recruited monocyte-derived host cells present in this area, it would be interesting to study host cell apoptosis in relation to blood vessel distance.

In order to decipher whether high *Leishmania* proliferation induces or is an effect of cell death of the donor cell, we aimed to study host cell death in macrophages infected with proliferation-modified *Leishmania* parasites. We had shown earlier that inflammatory monocytes are infected by parasites with specifically high pathogen proliferation (91), and that enhanced monocyte recruitment can increase pathogen proliferation (292), suggesting that pathogen proliferation might be at least in part dependent on the availability of newly recruited host cells. With the enhanced cell death in, and pathogen exit from, cells infected with high proliferating *L. major*, it would be possible that the phagocyte subtype is the main determinant for pathogen proliferation capacity, and propensity of cell death. Using KBMA *L. major*, which are proliferation-incompetent parasites, we were able to investigate this question beyond pure correlation between *L. major* proliferation and cell death of the original host cell. Infected host cells displaying signs of cell death were more often associated with proliferation-competent parasites as compared to proliferation-incompetent parasites, suggesting that *L. major* proliferation induces cell death of the infected host. While KBMA parasites most likely reflect only partially the phenotype of low-proliferating pathogens, our data clearly show that modulation of proliferation per se can impact on the probability of host cell death. These data, together

with the implication that *Leishmania* parasites might employ a similar approach for macrophage egress as for neutrophil egress, suggest that the potential initial delay in host cell apoptosis and the eventual initiation of host cell apoptosis might be dependent on intracellular parasite proliferation. To our knowledge, we are the first to show this direct association between *Leishmania* parasite proliferation and host cell death on the cellular level.

#### 4.6 Host cell metabolism and intracellular *Leishmania* proliferation

To further investigate the phagocyte phenotype in relation to intracellular pathogen proliferation, metabolic pathways in *L. major*-infected host cells were analysed. Importantly, phagocytes, including macrophages, adapt their metabolism in response to invading pathogens (454, 455), which plays an important role in cellular defence mechanisms against intracellular pathogens (456). We therefore analysed various metabolic components in *L. major*-infected macrophages. We show that expression of the glucose transporter GLUT1 is not affected by *L. major* infection, which is in contrast to data showing that *L. major* promastigotes increased GLUT1 levels and glycolysis in infected macrophages (457). However, these findings were based on short-term in vitro infection of susceptible murine macrophages, suggesting GLUT1 might be differentially affected depending on infection stage and/or *Leishmania* susceptibility. Also arguing against our current findings, GLUT1-mediated glucose metabolism has been associated with a proinflammatory phenotype and GLUT1 was shown to be highly expressed in inflammatory macrophages (458, 459). While it is possible that *L. major* inhibits the increase in GLUT1 that is normally associated with inflammation, this does not seem to depend on the proliferation rate of the intracellular parasite. Alternatively, other glucose transporters could play a role in enhancing the glucose supply that is suggested to be needed for amastigote proliferation inside macrophages (460–462). In contrast to the latter, we observed reduced 2-NBDG uptake in host macrophages infected with proliferating parasites as compared to non-proliferating parasites, indicating reduced glucose uptake as a result of intracellular pathogen proliferation. This is in contrast to data showing that glucose was an essential nutrient for *Leishmania* amastigotes and that *L. donovani* metacyclic promastigotes increased glycolysis in infected bone marrow-derived macrophages during short-term in vitro infection (460–463). The reduction in glucose uptake we observed in macrophages infected with high proliferators could however be a result of the host cell attempting to contain pathogen proliferation. Alternatively, massive glucose consumption by high proliferating pathogens might result in downstream effects by metabolic products that interfere with efficient glucose uptake (464). Our current findings are however in support of other findings indicating that *L. donovani* parasites, during their differentiation into amastigotes, shift from glucose to fatty acid oxidation as the main source of metabolic energy and in support of findings indicating that macrophages switch from an early glycolytic metabolism to an oxidative phosphorylation during *L. infantum* infection (465, 466). Additionally, it supports the finding that *L. mexicana* amastigotes are characterised by a glucose-sparing metabolism associated with reduced glucose uptake (467). This suggests that *Leishmania* might inhibit the increase in glycolysis that macrophages display during inflammatory activation (468, 469), either in order to avoid a glycolysis-mediated pro-inflammatory response or in order to protect themselves from nutrient overload-induced metabolic stress (470, 471). This would also be in line with earlier findings showing that *Mycobacterium tuberculosis* limits host glycolysis (472), which has been shown to be important

in host defence against the intracellular pathogen (473–475). Therefore, our observations likely pertain beyond *Leishmania* to other intracellular pathogens.

In addition to investigating glucose metabolism in *L. major*-infected macrophages, we also analysed lipid metabolism. We demonstrate increased CD36 expression upon *L. major* infection depending on the proliferation rate of the intracellular parasite. This is in line with previous data showing an increase in CD36 expression upon *L. infantum* and *L. amazonensis* infection (476, 477), but in contrast to findings showing that *L. major* promastigotes actively limited CD36 transcription in macrophages (478). Being a central regulator for lipid metabolism, CD36 has important functions in the uptake of fatty acids, but also serves as a scavenger receptor (479, 480). Evidence for changes in lipid regulation are particularly interesting in the context of *Leishmania* since parasites modulate macrophage membrane cholesterol, as well as gene regulation in cholesterol biosynthetic and trafficking pathways in vitro (481–483). Moreover, *L. amazonensis* has been found to engage CD36 in order to drive maturation of the parasitophorous vacuole (477), where *Leishmania* parasites survive and proliferate (36, 484). In support of this, the lipid accumulation, potentially resulting from increased CD36 expression, observed during *L. major* infection was in close association with the parasitophorous vacuole (457). Alternatively, this accumulation of lipids could be a result of lipid-dependent parasite proliferation inside the parasitophorous vacuole, which would support our current findings showing that increased CD36 expression relates to increased intracellular *Leishmania* proliferation. The assumption that lipid accumulation might benefit pathogens inside the parasitophorous vacuole would also be in line with data showing that cytoplasmic lipid droplets were translocated into the lumen of the parasitophorous vacuole in *Chlamydia* infected cells (485). Of note, we found that the uptake of LDL and long chain fatty acids, whose transport is mediated by CD36 (297, 486), was increased upon *L. major* infection, which is in line with previous findings (457). Interestingly, while infection with proliferation-competent *L. major* increased CD36 expression as compared to KBMA infection, the effect seemed to be opposite for LDL and long chain fatty acid uptake. This suggests that *L. major* proliferation might impact infected cells in a way that decreases the net lipid uptake, but induces compensatory CD36 expression (299) or that lipid uptake reduces during the course of the infection because proliferating parasites have used the lipids as an energy source. While lipid metabolism was also shown to be required for apoptosis initiation (487, 488), it might be possible that the increase in CD36 and the uptake of LDL and long chain fatty acid is related to apoptosis initiation in *L. major*-infected cells. An alternative explanation for increased CD36 surface expression in macrophages infected with proliferation-competent parasites might be the involvement of this receptor in the phagocytosis of apoptotic cells (489–491). Specifically, the enhanced phagocytosis of transferring proliferating parasites by CD36<sup>hi</sup> macrophages could result in the higher signal in the population harbouring proliferation-competent pathogen. Nevertheless, this would again be in favour of our hypothesis that pathogen proliferation drives cell death of the

original host cell and in line with our previous findings that high proliferating *L. major* parasites undergo more cell-to-cell transfer as compared to low proliferating parasites (91).

Since phagocytic receptors have been shown to be involved in phagosomal escape and intracellular pathogen proliferation (492), it would be of interest to investigate whether specific receptors are involved in the spread of high proliferating parasites among phagocytes. In this regard, we were already able to show that IL-11R signalling, which has been suggested to play a role in phagocytosis (183, 493), does not significantly influence monocyte recruitment and infection in a mouse model of cutaneous leishmaniasis. Moreover, other cellular pathways could be affected by or associated with intracellular pathogen proliferation. For example, host arginine metabolism has already been considered important for *Leishmania* proliferation and persistence inside the host cell, although, with L-arginine being a substrate for NO production, it is also essential for parasite elimination by the host (494–496). Interestingly, arginase, the enzyme that converts L-arginine into ornithine and urea, was suggested to play a role in macrophage efferocytosis and internalisation of apoptotic and pyroptotic cells, suggesting that elevated arginase expression in newly recruited monocytes may promote parasite cell-to-cell transfer (497). Therefore, it would be of interest to investigate arginine metabolism in macrophages infected with proliferation-competent and proliferation-incompetent *L. major* parasites. Furthermore, iron was suggested to be critical for *Leishmania* amastigote proliferation within macrophage phagolysosomes and host tryptophan metabolism was associated with increased *L. major* proliferation in infected macrophages (498, 499). When looking at other pathogens, recent data suggested that intracellular *Staphylococcus aureus* induces cytoplasmic calcium overload, which results in apoptotic and/or necrotic cell death and may subsequently facilitate the spread of infection and tissue destruction (500). Taking all these data into account, it seems plausible that *Leishmania* parasites utilise numerous metabolic host cell pathways to allow efficient intracellular survival and proliferation. It would therefore be worthwhile to investigate intracellular *Leishmania* proliferation in relation to other pathways within the infected host cell.

## 4.7 Conclusions and implications

In order to promote pathogen dissemination and disease progression, intracellular pathogens have developed a variety of strategies to escape from and transfer among host cells. It is therefore essential to identify and study these strategies, and it seems as if a limited set of general strategies is utilised among pathogen species, including induced membrane-dependent exit, active host cell lysis, and initiation of different forms of cell death (193, 195, 197). However, especially for *Leishmania*, data on the significance of any of these strategies for cell-to-cell transfer are scarce (40). Taken together, we show here that *L. major* drives host cell death and cell-to-cell transfer among phagocytes. In addition, our findings indicate that increased *L. major* proliferation rate might be involved in these processes. To our knowledge, we are the first to show evidence that *L. major* stimulates dissemination among monocyte-derived phagocytes through parasite proliferation-dependent cell death, which can serve as a starting point for the creation of innovative treatments that can inhibit the establishment of intracellular pathogens at their site of infection. While targeting pathogen exit might not protect from primary infection, it could contribute to control of the infection and disease progression by diminishing pathogen spread among cells and tissues.

## 6. REFERENCES

1. Steinert M, Hentschel U, Hacker J. Symbiosis and pathogenesis: evolution of the microbe–host interaction. *Naturwissenschaften*. 2000;87(1):1–11.
2. Casadevall A, Pirofski LA. Host–pathogen interactions: redefining the basic concepts of virulence and pathogenicity. *Infect Immun*. 1999;67(8):3703–13.
3. Bocca AL, de Almeida Soares CM, Nosanchuk JD, Silva–Pereira I. Intracellular Eukaryotic Pathogens' Virulence Attributes and Their Interplay with Host Immune Defenses. *Mediators Inflamm*. 2017;2017:1264974.
4. Bean B. Antiviral therapy: current concepts and practices. *Clin Microbiol Rev*. 1992;5(2):146–82.
5. Parkman PD, Hopps HE. Viral vaccines and antivirals: current use and future prospects. *Annu Rev Public Health*. 1988;9:203–21.
6. Antimicrobial Resistance C. Global burden of bacterial antimicrobial resistance in 2019: a systematic analysis. *Lancet*. 2022;399(10325):629–55.
7. Fairlamb AH, Gow NA, Matthews KR, Waters AP. Drug resistance in eukaryotic microorganisms. *Nat Microbiol*. 2016;1(7):16092.
8. Singh OP, Tiwary P, Kushwaha AK, Singh SK, Singh DK, Lawyer P, et al. Xenodiagnosis to evaluate the infectiousness of humans to sandflies in an area endemic for visceral leishmaniasis in Bihar, India: a transmission–dynamics study. *Lancet Microbe*. 2021;2(1):e23–e31.
9. Alvar J, Velez ID, Bern C, Herrero M, Desjeux P, Cano J, et al. Leishmaniasis worldwide and global estimates of its incidence. *PLoS One*. 2012;7(5):e35671.
10. Mann S, Frasca K, Scherrer S, Henao–Martinez AF, Newman S, Ramanan P, et al. A Review of Leishmaniasis: Current Knowledge and Future Directions. *Curr Trop Med Rep*. 2021;8(2):121–32.
11. Kane MM, Mosser DM. Leishmania parasites and their ploys to disrupt macrophage activation. *Curr Opin Hematol*. 2000;7(1):26–31.
12. Llanes A, Restrepo CM, Del Vecchio G, Anguizola FJ, Lleonart R. The genome of *Leishmania panamensis*: insights into genomics of the *L. (Viannia)* subgenus. *Sci Rep*. 2015;5:8550.
13. Gupta AK, Das S, Kamran M, Ejazi SA, Ali N. The pathogenicity and virulence of *Leishmania* – interplay of virulence factors with host defenses. *Virulence*. 2022;13(1):903–35.

14. Kebaier C, Louzir H, Chenik M, Ben Salah A, Dellagi K. Heterogeneity of wild *Leishmania major* isolates in experimental murine pathogenicity and specific immune response. *Infect Immun*. 2001;69(8):4906–15.
15. Bretscher PA, Wei G, Menon JN, Bielefeldt–Ohmann H. Establishment of stable, cell–mediated immunity that makes "susceptible" mice resistant to *Leishmania major*. *Science*. 1992;257(5069):539–42.
16. Silva JM, Zacarias DA, de Figueiredo LC, Soares MR, Ishikawa EA, Costa DL, et al. Bone marrow parasite burden among patients with New World kala–azar is associated with disease severity. *Am J Trop Med Hyg*. 2014;90(4):621–6.
17. Abdeladhim M, Kamhawi S, Valenzuela JG. What's behind a sand fly bite? The profound effect of sand fly saliva on host hemostasis, inflammation and immunity. *Infect Genet Evol*. 2014;28:691–703.
18. Ribeiro–Gomes FL, Roma EH, Carneiro MB, Doria NA, Sacks DL, Peters NC. Site–dependent recruitment of inflammatory cells determines the effective dose of *Leishmania major*. *Infect Immun*. 2014;82(7):2713–27.
19. Peters NC, Egen JG, Secundino N, Debrabant A, Kimblin N, Kamhawi S, et al. In vivo imaging reveals an essential role for neutrophils in leishmaniasis transmitted by sand flies. *Science*. 2008;321(5891):970–4.
20. Naik S, Bouladoux N, Wilhelm C, Molloy MJ, Salcedo R, Kastenmuller W, et al. Compartmentalized control of skin immunity by resident commensals. *Science*. 2012;337(6098):1115–9.
21. Gimblet C, Meisel JS, Loesche MA, Cole SD, Horwinski J, Novais FO, et al. Cutaneous Leishmaniasis Induces a Transmissible Dysbiotic Skin Microbiota that Promotes Skin Inflammation. *Cell Host Microbe*. 2017;22(1):13–24 e4.
22. Kelly PH, Bahr SM, Serafim TD, Ajami NJ, Petrosino JF, Meneses C, et al. The Gut Microbiome of the Vector *Lutzomyia longipalpis* Is Essential for Survival of *Leishmania infantum*. *mBio*. 2017;8(1).
23. Dey R, Joshi AB, Oliveira F, Pereira L, Guimaraes–Costa AB, Serafim TD, et al. Gut Microbes Egested during Bites of Infected Sand Flies Augment Severity of Leishmaniasis via Inflammasome–Derived IL–1 $\beta$ . *Cell Host Microbe*. 2018;23(1):134–43 e6.
24. Louradour I, Monteiro CC, Inbar E, Ghosh K, Merkhofer R, Lawyer P, et al. The midgut microbiota plays an essential role in sand fly vector competence for *Leishmania major*. *Cell Microbiol*. 2017;19(10).

25. Scott P, Novais FO. Cutaneous leishmaniasis: immune responses in protection and pathogenesis. *Nat Rev Immunol*. 2016;16(9):581–92.
26. Coutinho De Oliveira B, Duthie MS, Alves Pereira VR. Vaccines for leishmaniasis and the implications of their development for American tegumentary leishmaniasis. *Hum Vaccin Immunother*. 2020;16(4):919–30.
27. Sacks DL. Vaccines against tropical parasitic diseases: a persisting answer to a persisting problem. *Nat Immunol*. 2014;15(5):403–5.
28. Glennie ND, Scott P. Memory T cells in cutaneous leishmaniasis. *Cell Immunol*. 2016;309:50–4.
29. Glennie ND, Yeramilli VA, Beiting DP, Volk SW, Weaver CT, Scott P. Skin-resident memory CD4+ T cells enhance protection against *Leishmania major* infection. *J Exp Med*. 2015;212(9):1405–14.
30. Gupta G, Oghumu S, Satoskar AR. Mechanisms of immune evasion in leishmaniasis. *Adv Appl Microbiol*. 2013;82:155–84.
31. Akhoundi M, Kuhls K, Cannet A, Votycka J, Marty P, Delaunay P, et al. A Historical Overview of the Classification, Evolution, and Dispersion of *Leishmania* Parasites and Sandflies. *PLoS Negl Trop Dis*. 2016;10(3):e0004349.
32. Lainson R, Ryan L, Shaw JJ. Infective stages of *Leishmania* in the sandfly vector and some observations on the mechanism of transmission. *Mem Inst Oswaldo Cruz*. 1987;82(3):421–4.
33. Akopyants NS, Kimblin N, Secundino N, Patrick R, Peters N, Lawyer P, et al. Demonstration of genetic exchange during cyclical development of *Leishmania* in the sand fly vector. *Science*. 2009;324(5924):265–8.
34. Sadlova J, Yeo M, Seblova V, Lewis MD, Mauricio I, Volf P, et al. Visualisation of *Leishmania donovani* fluorescent hybrids during early stage development in the sand fly vector. *PLoS One*. 2011;6(5):e19851.
35. Catta-Preta CMC, Ferreira TR, Ghosh K, Paun A, Sacks D. HOP1 and HAP2 are conserved components of the meiosis-related machinery required for successful mating in *Leishmania*. *Nat Commun*. 2023;14(1):7159.
36. Chang KP, Dwyer DM. Multiplication of a human parasite (*Leishmania donovani*) in phagolysosomes of hamster macrophages in vitro. *Science*. 1976;193(4254):678–80.

37. Antoine JC, Prina E, Lang T, Courret N. The biogenesis and properties of the parasitophorous vacuoles that harbour *Leishmania* in murine macrophages. *Trends Microbiol.* 1998;6(10):392–401.
38. Real F, Florentino PT, Reis LC, Ramos–Sanchez EM, Veras PS, Goto H, et al. Cell–to–cell transfer of *Leishmania amazonensis* amastigotes is mediated by immunomodulatory LAMP–rich parasitophorous extrusions. *Cell Microbiol.* 2014;16(10):1549–64.
39. Esch KJ, Petersen CA. Transmission and epidemiology of zoonotic protozoal diseases of companion animals. *Clin Microbiol Rev.* 2013;26(1):58–85.
40. Flieger A, Frischknecht F, Hacker G, Hornef MW, Pradel G. Pathways of host cell exit by intracellular pathogens. *Microb Cell.* 2018;5(12):525–44.
41. Dunkelberger JR, Song WC. Complement and its role in innate and adaptive immune responses. *Cell Res.* 2010;20(1):34–50.
42. Walport MJ. Complement. First of two parts. *N Engl J Med.* 2001;344(14):1058–66.
43. Walport MJ. Complement. Second of two parts. *N Engl J Med.* 2001;344(15):1140–4.
44. Gurung P, Kanneganti TD. Innate immunity against *Leishmania* infections. *Cell Microbiol.* 2015;17(9):1286–94.
45. Noris M, Remuzzi G. Overview of complement activation and regulation. *Semin Nephrol.* 2013;33(6):479–92.
46. Nylén S, Gautam S. Immunological perspectives of leishmaniasis. *J Glob Infect Dis.* 2010;2(2):135–46.
47. Blackwell JM. Receptors and recognition mechanisms of *Leishmania* species. *Trans R Soc Trop Med Hyg.* 1985;79(5):606–12.
48. Puentes SM, Sacks DL, da Silva RP, Joiner KA. Complement binding by two developmental stages of *Leishmania major* promastigotes varying in expression of a surface lipophosphoglycan. *J Exp Med.* 1988;167(3):887–902.
49. McConville MJ, Turco SJ, Ferguson MA, Sacks DL. Developmental modification of lipophosphoglycan during the differentiation of *Leishmania major* promastigotes to an infectious stage. *EMBO J.* 1992;11(10):3593–600.
50. Brittingham A, Morrison CJ, McMaster WR, McGwire BS, Chang KP, Mosser DM. Role of the *Leishmania* surface protease gp63 in complement fixation, cell adhesion, and resistance to complement–mediated lysis. *J Immunol.* 1995;155(6):3102–11.

51. Verma S, Mandal A, Ansari MY, Kumar A, Abhishek K, Ghosh AK, et al. Leishmania donovani Inhibitor of Serine Peptidases 2 Mediated Inhibition of Lectin Pathway and Upregulation of C5aR Signaling Promote Parasite Survival inside Host. *Front Immunol.* 2018;9:63.
52. Liu D, Uzonna JE. The early interaction of Leishmania with macrophages and dendritic cells and its influence on the host immune response. *Front Cell Infect Microbiol.* 2012;2:83.
53. Halliday A, Bates PA, Chance ML, Taylor MJ. Toll-like receptor 2 (TLR2) plays a role in controlling cutaneous leishmaniasis in vivo, but does not require activation by parasite lipophosphoglycan. *Parasit Vectors.* 2016;9(1):532.
54. Sacramento LA, da Costa JL, de Lima MH, Sampaio PA, Almeida RP, Cunha FQ, et al. Toll-Like Receptor 2 Is Required for Inflammatory Process Development during Leishmania infantum Infection. *Front Microbiol.* 2017;8:262.
55. Becker I, Salaiza N, Aguirre M, Delgado J, Carrillo-Carrasco N, Kobeh LG, et al. Leishmania lipophosphoglycan (LPG) activates NK cells through toll-like receptor-2. *Mol Biochem Parasitol.* 2003;130(2):65-74.
56. Ruiz JH, Becker I. CD8 cytotoxic T cells in cutaneous leishmaniasis. *Parasite Immunol.* 2007;29(12):671-8.
57. de Veer MJ, Curtis JM, Baldwin TM, DiDonato JA, Sexton A, McConville MJ, et al. MyD88 is essential for clearance of Leishmania major: possible role for lipophosphoglycan and Toll-like receptor 2 signaling. *Eur J Immunol.* 2003;33(10):2822-31.
58. Srivastav S, Kar S, Chande AG, Mukhopadhyaya R, Das PK. Leishmania donovani exploits host deubiquitinating enzyme A20, a negative regulator of TLR signaling, to subvert host immune response. *J Immunol.* 2012;189(2):924-34.
59. Jafarzadeh A, Nemati M, Sharifi I, Nair A, Shukla D, Chauhan P, et al. Leishmania species-dependent functional duality of toll-like receptor 2. *IUBMB Life.* 2019;71(11):1685-700.
60. Schleicher U, Liese J, Knippertz I, Kurzmann C, Hesse A, Heit A, et al. NK cell activation in visceral leishmaniasis requires TLR9, myeloid DCs, and IL-12, but is independent of plasmacytoid DCs. *J Exp Med.* 2007;204(4):893-906.
61. Liese J, Schleicher U, Bogdan C. TLR9 signaling is essential for the innate NK cell response in murine cutaneous leishmaniasis. *Eur J Immunol.* 2007;37(12):3424-34.
62. Sacramento L, Trevelin SC, Nascimento MS, Lima-Junior DS, Costa DL, Almeida RP, et al. Toll-like receptor 9 signaling in dendritic cells regulates neutrophil recruitment to

- inflammatory foci following *Leishmania infantum* infection. *Infect Immun*. 2015;83(12):4604–16.
63. Pearson RD, Steigbigel RT. Phagocytosis and killing of the protozoan *Leishmania donovani* by human polymorphonuclear leukocytes. *J Immunol*. 1981;127(4):1438–43.
64. Chang KP. Leishmanicidal mechanisms of human polymorphonuclear phagocytes. *Am J Trop Med Hyg*. 1981;30(2):322–33.
65. Guimaraes-Costa AB, Nascimento MT, Froment GS, Soares RP, Morgado FN, Conceicao-Silva F, et al. *Leishmania amazonensis* promastigotes induce and are killed by neutrophil extracellular traps. *Proc Natl Acad Sci U S A*. 2009;106(16):6748–53.
66. Charmoy M, Brunner-Agten S, Aebischer D, Auderset F, Launois P, Milon G, et al. Neutrophil-derived CCL3 is essential for the rapid recruitment of dendritic cells to the site of *Leishmania major* inoculation in resistant mice. *PLoS Pathog*. 2010;6(2):e1000755.
67. Scapini P, Lapinet-Vera JA, Gasperini S, Calzetti F, Bazzoni F, Cassatella MA. The neutrophil as a cellular source of chemokines. *Immunol Rev*. 2000;177:195–203.
68. Sarkar A, Aga E, Bussmeyer U, Bhattacharyya A, Moller S, Hellberg L, et al. Infection of neutrophil granulocytes with *Leishmania major* activates ERK 1/2 and modulates multiple apoptotic pathways to inhibit apoptosis. *Med Microbiol Immunol*. 2013;202(1):25–35.
69. Brinkmann V, Reichard U, Goosmann C, Fauler B, Uhlemann Y, Weiss DS, et al. Neutrophil extracellular traps kill bacteria. *Science*. 2004;303(5663):1532–5.
70. Fuchs TA, Abed U, Goosmann C, Hurwitz R, Schulze I, Wahn V, et al. Novel cell death program leads to neutrophil extracellular traps. *J Cell Biol*. 2007;176(2):231–41.
71. Kirchner T, Moller S, Klinger M, Solbach W, Laskay T, Behnen M. The impact of various reactive oxygen species on the formation of neutrophil extracellular traps. *Mediators Inflamm*. 2012;2012:849136.
72. Pilszczek FH, Salina D, Poon KK, Fahey C, Yipp BG, Sibley CD, et al. A novel mechanism of rapid nuclear neutrophil extracellular trap formation in response to *Staphylococcus aureus*. *J Immunol*. 2010;185(12):7413–25.
73. Rochael NC, Guimaraes-Costa AB, Nascimento MT, DeSouza-Vieira TS, Oliveira MP, Garcia e Souza LF, et al. Classical ROS-dependent and early/rapid ROS-independent release of Neutrophil Extracellular Traps triggered by *Leishmania* parasites. *Sci Rep*. 2015;5:18302.

74. Gabriel C, McMaster WR, Girard D, Descoteaux A. *Leishmania donovani* promastigotes evade the antimicrobial activity of neutrophil extracellular traps. *J Immunol.* 2010;185(7):4319–27.
75. Guimaraes–Costa AB, DeSouza–Vieira TS, Paletta–Silva R, Freitas–Mesquita AL, Meyer–Fernandes JR, Saraiva EM. 3'-nucleotidase/nuclease activity allows *Leishmania* parasites to escape killing by neutrophil extracellular traps. *Infect Immun.* 2014;82(4):1732–40.
76. Chagas AC, Oliveira F, Debrabant A, Valenzuela JG, Ribeiro JM, Calvo E. Lundep, a sand fly salivary endonuclease increases *Leishmania* parasite survival in neutrophils and inhibits Xlla contact activation in human plasma. *PLoS Pathog.* 2014;10(2):e1003923.
77. Barrientos L, Bignon A, Gueguen C, de Chaisemartin L, Gorges R, Sandre C, et al. Neutrophil extracellular traps downregulate lipopolysaccharide–induced activation of monocyte–derived dendritic cells. *J Immunol.* 2014;193(11):5689–98.
78. Guimaraes–Costa AB, Rochael NC, Oliveira F, Echevarria–Lima J, Saraiva EM. Neutrophil Extracellular Traps Reprogram IL–4/GM–CSF–Induced Monocyte Differentiation to Anti-inflammatory Macrophages. *Front Immunol.* 2017;8:523.
79. Salei N, Hellberg L, Kohl J, Laskay T. Enhanced survival of *Leishmania major* in neutrophil granulocytes in the presence of apoptotic cells. *PLoS One.* 2017;12(2):e0171850.
80. Ghersetich I, Menchini G, Teofoli P, Lotti T. Immune response to *Leishmania* infection in human skin. *Clin Dermatol.* 1999;17(3):333–8.
81. Laskay T, van Zandbergen G, Solbach W. Neutrophil granulocytes—Trojan horses for *Leishmania major* and other intracellular microbes? *Trends Microbiol.* 2003;11(5):210–4.
82. van Zandbergen G, Klinger M, Mueller A, Dannenberg S, Gebert A, Solbach W, et al. Cutting edge: neutrophil granulocyte serves as a vector for *Leishmania* entry into macrophages. *J Immunol.* 2004;173(11):6521–5.
83. Ritter U, Frischknecht F, van Zandbergen G. Are neutrophils important host cells for *Leishmania* parasites? *Trends Parasitol.* 2009;25(11):505–10.
84. Gagnon E, Duclos S, Rondeau C, Chevet E, Cameron PH, Steele–Mortimer O, et al. Endoplasmic reticulum–mediated phagocytosis is a mechanism of entry into macrophages. *Cell.* 2002;110(1):119–31.
85. Vinet AF, Fukuda M, Turco SJ, Descoteaux A. The *Leishmania donovani* lipophosphoglycan excludes the vesicular proton–ATPase from phagosomes by impairing the recruitment of synaptotagmin V. *PLoS Pathog.* 2009;5(10):e1000628.

86. Forestier CL, Machu C, Loussert C, Pescher P, Spath GF. Imaging host cell–Leishmania interaction dynamics implicates parasite motility, lysosome recruitment, and host cell wounding in the infection process. *Cell Host Microbe*. 2011;9(4):319–30.
87. Ueno N, Bratt CL, Rodriguez NE, Wilson ME. Differences in human macrophage receptor usage, lysosomal fusion kinetics and survival between logarithmic and metacyclic *Leishmania infantum* chagasi promastigotes. *Cell Microbiol*. 2009;11(12):1827–41.
88. Wozencraft AO, Blackwell JM. Increased infectivity of stationary–phase promastigotes of *Leishmania donovani*: correlation with enhanced C3 binding capacity and CR3–mediated attachment to host macrophages. *Immunology*. 1987;60(4):559–63.
89. Tamoutounour S, Guilliams M, Montanana Sanchis F, Liu H, Terhorst D, Malosse C, et al. Origins and functional specialization of macrophages and of conventional and monocyte–derived dendritic cells in mouse skin. *Immunity*. 2013;39(5):925–38.
90. Romano A, Carneiro MBH, Doria NA, Roma EH, Ribeiro–Gomes FL, Inbar E, et al. Divergent roles for Ly6C+CCR2+CX3CR1+ inflammatory monocytes during primary or secondary infection of the skin with the intra–phagosomal pathogen *Leishmania major*. *PLoS Pathog*. 2017;13(6):e1006479.
91. Heyde S, Philipsen L, Formaglio P, Fu Y, Baars I, Hobbel G, et al. CD11c–expressing Ly6C+CCR2+ monocytes constitute a reservoir for efficient *Leishmania* proliferation and cell–to–cell transmission. *PLoS Pathog*. 2018;14(10):e1007374.
92. Rossi M, Fasel N. How to master the host immune system? *Leishmania* parasites have the solutions! *Int Immunol*. 2018;30(3):103–11.
93. Olivier M, Atayde VD, Isnard A, Hassani K, Shio MT. *Leishmania* virulence factors: focus on the metalloprotease GP63. *Microbes Infect*. 2012;14(15):1377–89.
94. Rosazza T, Lecoer H, Blisnick T, Moya–Nilges M, Pescher P, Bastin P, et al. Dynamic imaging reveals surface exposure of virulent *Leishmania* amastigotes during pyroptosis of infected macrophages. *J Cell Sci*. 2020;134(5).
95. Desjardins M, Descoteaux A. Inhibition of phagolysosomal biogenesis by the *Leishmania* lipophosphoglycan. *J Exp Med*. 1997;185(12):2061–8.
96. Lodge R, Descoteaux A. Modulation of phagolysosome biogenesis by the lipophosphoglycan of *Leishmania*. *Clin Immunol*. 2005;114(3):256–65.
97. Duclos S, Desjardins M. Subversion of a young phagosome: the survival strategies of intracellular pathogens. *Cell Microbiol*. 2000;2(5):365–77.

98. Miller MA, McGowan SE, Gantt KR, Champion M, Novick SL, Andersen KA, et al. Inducible resistance to oxidant stress in the protozoan *Leishmania chagasi*. *J Biol Chem*. 2000;275(43):33883–9.
99. Rodriguez NE, Gaur U, Wilson ME. Role of caveolae in *Leishmania chagasi* phagocytosis and intracellular survival in macrophages. *Cell Microbiol*. 2006;8(7):1106–20.
100. Carvalhal DG, Barbosa A, Jr., D'El-Rei Hermida M, Clarencio J, Pinheiro NF, Jr., Veras PS, et al. The modelling of mononuclear phagocyte–connective tissue adhesion in vitro: application to disclose a specific inhibitory effect of *Leishmania* infection. *Exp Parasitol*. 2004;107(3–4):189–99.
101. Steigerwald M, Moll H. *Leishmania major* modulates chemokine and chemokine receptor expression by dendritic cells and affects their migratory capacity. *Infect Immun*. 2005;73(4):2564–7.
102. Gordon S. Phagocytosis: An Immunobiologic Process. *Immunity*. 2016;44(3):463–75.
103. Banchereau J, Steinman RM. Dendritic cells and the control of immunity. *Nature*. 1998;392(6673):245–52.
104. Fonteneau JF, Kavanagh DG, Lirvall M, Sanders C, Cover TL, Bhardwaj N, et al. Characterization of the MHC class I cross–presentation pathway for cell–associated antigens by human dendritic cells. *Blood*. 2003;102(13):4448–55.
105. Kalinski P, Hilkens CM, Wierenga EA, Kapsenberg ML. T–cell priming by type–1 and type–2 polarized dendritic cells: the concept of a third signal. *Immunol Today*. 1999;20(12):561–7.
106. Gorak PM, Engwerda CR, Kaye PM. Dendritic cells, but not macrophages, produce IL–12 immediately following *Leishmania donovani* infection. *Eur J Immunol*. 1998;28(2):687–95.
107. Leon B, Lopez–Bravo M, Ardavin C. Monocyte–derived dendritic cells formed at the infection site control the induction of protective T helper 1 responses against *Leishmania*. *Immunity*. 2007;26(4):519–31.
108. von Stebut E, Belkaid Y, Jakob T, Sacks DL, Udey MC. Uptake of *Leishmania major* amastigotes results in activation and interleukin 12 release from murine skin–derived dendritic cells: implications for the initiation of anti–*Leishmania* immunity. *J Exp Med*. 1998;188(8):1547–52.
109. Althwaiqeb SA, Bordoni B. Histology, B Cell Lymphocyte. *StatPearls*. Treasure Island (FL)2024.

110. Jawed JJ, Dutta S, Majumdar S. Functional aspects of T cell diversity in visceral leishmaniasis. *Biomed Pharmacother.* 2019;117:109098.
111. Zhu J, Paul WE. CD4 T cells: fates, functions, and faults. *Blood.* 2008;112(5):1557–69.
112. Luckheeram RV, Zhou R, Verma AD, Xia B. CD4(+)T cells: differentiation and functions. *Clin Dev Immunol.* 2012;2012:925135.
113. Fallon PG, Jolin HE, Smith P, Emson CL, Townsend MJ, Fallon R, et al. IL-4 induces characteristic Th2 responses even in the combined absence of IL-5, IL-9, and IL-13. *Immunity.* 2002;17(1):7–17.
114. Scott P, Natovitz P, Coffman RL, Pearce E, Sher A. Immunoregulation of cutaneous leishmaniasis. T cell lines that transfer protective immunity or exacerbation belong to different T helper subsets and respond to distinct parasite antigens. *J Exp Med.* 1988;168(5):1675–84.
115. Mosmann TR, Coffman RL. TH1 and TH2 cells: different patterns of lymphokine secretion lead to different functional properties. *Annu Rev Immunol.* 1989;7:145–73.
116. Green SJ, Crawford RM, Hockmeyer JT, Meltzer MS, Nacy CA. *Leishmania major* amastigotes initiate the L-arginine-dependent killing mechanism in IFN- $\gamma$ -stimulated macrophages by induction of tumor necrosis factor- $\alpha$ . *J Immunol.* 1990;145(12):4290–7.
117. Liew FY, Millott S, Parkinson C, Palmer RM, Moncada S. Macrophage killing of *Leishmania* parasite in vivo is mediated by nitric oxide from L-arginine. *J Immunol.* 1990;144(12):4794–7.
118. Liew FY, Li Y, Millott S. Tumor necrosis factor- $\alpha$  synergizes with IFN- $\gamma$  in mediating killing of *Leishmania major* through the induction of nitric oxide. *J Immunol.* 1990;145(12):4306–10.
119. Chatzigeorgiou A, Lyberi M, Chatzilymperis G, Nezos A, Kamper E. CD40/CD40L signaling and its implication in health and disease. *Biofactors.* 2009;35(6):474–83.
120. Carneiro MB, Lopes ME, Hohman LS, Romano A, David BA, Kratofil R, et al. Th1–Th2 Cross-Regulation Controls Early *Leishmania* Infection in the Skin by Modulating the Size of the Permissive Monocytic Host Cell Reservoir. *Cell Host Microbe.* 2020;27(5):752–68 e7.
121. Gantt KR, Goldman TL, McCormick ML, Miller MA, Jeronimo SM, Nascimento ET, et al. Oxidative responses of human and murine macrophages during phagocytosis of *Leishmania chagasi*. *J Immunol.* 2001;167(2):893–901.

122. Bacellar O, Lessa H, Schriefer A, Machado P, Ribeiro de Jesus A, Dutra WO, et al. Up-regulation of Th1-type responses in mucosal leishmaniasis patients. *Infect Immun.* 2002;70(12):6734–40.
123. Chakraborty D, Banerjee S, Sen A, Banerjee KK, Das P, Roy S. Leishmania donovani affects antigen presentation of macrophage by disrupting lipid rafts. *J Immunol.* 2005;175(5):3214–24.
124. Meier CL, Svensson M, Kaye PM. Leishmania-induced inhibition of macrophage antigen presentation analyzed at the single-cell level. *J Immunol.* 2003;171(12):6706–13.
125. Matheoud D, Moradin N, Bellemare-Pelletier A, Shio MT, Hong WJ, Olivier M, et al. Leishmania evades host immunity by inhibiting antigen cross-presentation through direct cleavage of the SNARE VAMP8. *Cell Host Microbe.* 2013;14(1):15–25.
126. Muller AJ, Filipe-Santos O, Eberl G, Aebischer T, Spath GF, Bousso P. CD4+ T cells rely on a cytokine gradient to control intracellular pathogens beyond sites of antigen presentation. *Immunity.* 2012;37(1):147–57.
127. Peters NC, Pagan AJ, Lawyer PG, Hand TW, Henrique Roma E, Stamper LW, et al. Chronic parasitic infection maintains high frequencies of short-lived Ly6C+CD4+ effector T cells that are required for protection against re-infection. *PLoS Pathog.* 2014;10(12):e1004538.
128. Mandell MA, Beverley SM. Continual renewal and replication of persistent Leishmania major parasites in concomitantly immune hosts. *Proc Natl Acad Sci U S A.* 2017;114(5):E801–E10.
129. Akkaya B, Shevach EM. Regulatory T cells: Master thieves of the immune system. *Cell Immunol.* 2020;355:104160.
130. Belkaid Y, Piccirillo CA, Mendez S, Shevach EM, Sacks DL. CD4+CD25+ regulatory T cells control Leishmania major persistence and immunity. *Nature.* 2002;420(6915):502–7.
131. Okwor I, Liu D, Beverley SM, Uzonna JE. Inoculation of killed Leishmania major into immune mice rapidly disrupts immunity to a secondary challenge via IL-10-mediated process. *Proc Natl Acad Sci U S A.* 2009;106(33):13951–6.
132. Mendez S, Reckling SK, Piccirillo CA, Sacks D, Belkaid Y. Role for CD4(+) CD25(+) regulatory T cells in reactivation of persistent leishmaniasis and control of concomitant immunity. *J Exp Med.* 2004;200(2):201–10.
133. Tabbara KS, Peters NC, Afrin F, Mendez S, Bertholet S, Belkaid Y, et al. Conditions influencing the efficacy of vaccination with live organisms against Leishmania major infection. *Infect Immun.* 2005;73(8):4714–22.

134. Peters N, Sacks D. Immune privilege in sites of chronic infection: Leishmania and regulatory T cells. *Immunol Rev.* 2006;213:159–79.
135. Maspi N, Abdoli A, Ghaffarifar F. Pro- and anti-inflammatory cytokines in cutaneous leishmaniasis: a review. *Pathog Glob Health.* 2016;110(6):247–60.
136. Guler ML, Gorham JD, Hsieh CS, Mackey AJ, Steen RG, Dietrich WF, et al. Genetic susceptibility to Leishmania: IL-12 responsiveness in TH1 cell development. *Science.* 1996;271(5251):984–7.
137. Arango Duque G, Descoteaux A. Macrophage cytokines: involvement in immunity and infectious diseases. *Front Immunol.* 2014;5:491.
138. Tomiotto-Pellissier F, Bortoleti B, Assolini JP, Goncalves MD, Carlotto ACM, Miranda-Sapla MM, et al. Macrophage Polarization in Leishmaniasis: Broadening Horizons. *Front Immunol.* 2018;9:2529.
139. Stamler JS, Singel DJ, Loscalzo J. Biochemistry of nitric oxide and its redox-activated forms. *Science.* 1992;258(5090):1898–902.
140. Stuehr DJ. Mammalian nitric oxide synthases. *Biochim Biophys Acta.* 1999;1411(2–3):217–30.
141. Liew FY, Li Y, Millott S. Tumour necrosis factor (TNF- $\alpha$ ) in leishmaniasis. II. TNF- $\alpha$ -induced macrophage leishmanicidal activity is mediated by nitric oxide from L-arginine. *Immunology.* 1990;71(4):556–9.
142. Radi R. Nitric oxide, oxidants, and protein tyrosine nitration. *Proc Natl Acad Sci U S A.* 2004;101(12):4003–8.
143. Gordon S, Martinez FO. Alternative activation of macrophages: mechanism and functions. *Immunity.* 2010;32(5):593–604.
144. Muxel SM, Aoki JI, Fernandes JCR, Laranjeira-Silva MF, Zampieri RA, Acuna SM, et al. Arginine and Polyamines Fate in Leishmania Infection. *Front Microbiol.* 2017;8:2682.
145. Pessenda G, da Silva JS. Arginase and its mechanisms in Leishmania persistence. *Parasite Immunol.* 2020;42(7):e12722.
146. Akilov OE, Kosaka S, O'Riordan K, Hasan T. Parasiticidal effect of delta-aminolevulinic acid-based photodynamic therapy for cutaneous leishmaniasis is indirect and mediated through the killing of the host cells. *Exp Dermatol.* 2007;16(8):651–60.
147. de Lima VM, Peiro JR, de Oliveira Vasconcelos R. IL-6 and TNF- $\alpha$  production during active canine visceral leishmaniasis. *Vet Immunol Immunopathol.* 2007;115(1–2):189–93.

148. Santos IK, Costa CH, Krieger H, Feitosa MF, Zurakowski D, Fardin B, et al. Mannan-binding lectin enhances susceptibility to visceral leishmaniasis. *Infect Immun.* 2001;69(8):5212–5.
149. Karam MC, Hamdan HG, Abi Chedid NA, Bodman-Smith KB, Baroody GM. Interleukin-10 reduces hyperalgesia and the level of Interleukin-1beta in BALB/c mice infected with *Leishmania major* with no major effect on the level of Interleukin-6. *J Neuroimmunol.* 2007;183(1–2):43–9.
150. Satoskar AR, Bozza M, Rodriguez Sosa M, Lin G, David JR. Migration-inhibitory factor gene-deficient mice are susceptible to cutaneous *Leishmania major* infection. *Infect Immun.* 2001;69(2):906–11.
151. Wilson ME, Sandor M, Blum AM, Young BM, Metwali A, Elliott D, et al. Local suppression of IFN-gamma in hepatic granulomas correlates with tissue-specific replication of *Leishmania chagasi*. *J Immunol.* 1996;156(6):2231–9.
152. Ansari NA, Saluja S, Salotra P. Elevated levels of interferon-gamma, interleukin-10, and interleukin-6 during active disease in Indian kala azar. *Clin Immunol.* 2006;119(3):339–45.
153. Ansari NA, Ramesh V, Salotra P. Interferon (IFN)-gamma, tumor necrosis factor-alpha, interleukin-6, and IFN-gamma receptor 1 are the major immunological determinants associated with post-kala azar dermal leishmaniasis. *J Infect Dis.* 2006;194(7):958–65.
154. Caceres-Dittmar G, Tapia FJ, Sanchez MA, Yamamura M, Uyemura K, Modlin RL, et al. Determination of the cytokine profile in American cutaneous leishmaniasis using the polymerase chain reaction. *Clin Exp Immunol.* 1993;91(3):500–5.
155. Castellucci L, Menezes E, Oliveira J, Magalhaes A, Guimaraes LH, Lessa M, et al. IL6 – 174 G/C promoter polymorphism influences susceptibility to mucosal but not localized cutaneous leishmaniasis in Brazil. *J Infect Dis.* 2006;194(4):519–27.
156. Cenini P, Berhe N, Hailu A, McGinnes K, Frommel D. Mononuclear cell subpopulations and cytokine levels in human visceral leishmaniasis before and after chemotherapy. *J Infect Dis.* 1993;168(4):986–93.
157. Galindo-Sevilla N, Soto N, Mancilla J, Cerbulo A, Zambrano E, Chavira R, et al. Low serum levels of dehydroepiandrosterone and cortisol in human diffuse cutaneous leishmaniasis by *Leishmania mexicana*. *Am J Trop Med Hyg.* 2007;76(3):566–72.
158. Kocyigit A, Gur S, Gurel MS, Bulut V, Ulukanligil M. Antimonial therapy induces circulating proinflammatory cytokines in patients with cutaneous leishmaniasis. *Infect Immun.* 2002;70(12):6589–91.

159. Louzir H, Melby PC, Ben Salah A, Marrakchi H, Aoun K, Ben Ismail R, et al. Immunologic determinants of disease evolution in localized cutaneous leishmaniasis due to *Leishmania major*. *J Infect Dis*. 1998;177(6):1687–95.
160. Melby PC, Andrade–Narvaez FJ, Darnell BJ, Valencia–Pacheco G, Tryon VV, Palomo–Cetina A. Increased expression of proinflammatory cytokines in chronic lesions of human cutaneous leishmaniasis. *Infect Immun*. 1994;62(3):837–42.
161. Peruhype–Magalhaes V, Martins–Filho OA, Prata A, Silva Lde A, Rabello A, Teixeira–Carvalho A, et al. Mixed inflammatory/regulatory cytokine profile marked by simultaneous raise of interferon–gamma and interleukin–10 and low frequency of tumour necrosis factor–alpha(+) monocytes are hallmarks of active human visceral Leishmaniasis due to *Leishmania chagasi* infection. *Clin Exp Immunol*. 2006;146(1):124–32.
162. Stager S, Maroof A, Zubairi S, Sanos SL, Kopf M, Kaye PM. Distinct roles for IL–6 and IL–12p40 in mediating protection against *Leishmania donovani* and the expansion of IL–10+ CD4+ T cells. *Eur J Immunol*. 2006;36(7):1764–71.
163. Wu W, Weigand L, Belkaid Y, Mendez S. Immunomodulatory effects associated with a live vaccine against *Leishmania major* containing CpG oligodeoxynucleotides. *Eur J Immunol*. 2006;36(12):3238–47.
164. Hatzigeorgiou DE, He S, Sobel J, Grabstein KH, Hafner A, Ho JL. IL–6 down–modulates the cytokine–enhanced antileishmanial activity in human macrophages. *J Immunol*. 1993;151(7):3682–92.
165. Saha B, Saini A, Germond R, Perrin PJ, Harlan DM, Davis TA. Susceptibility or resistance to *Leishmania* infection is dictated by the macrophages evolved under the influence of IL–3 or GM–CSF. *Eur J Immunol*. 1999;29(7):2319–29.
166. Murray HW. Accelerated control of visceral *Leishmania donovani* infection in interleukin–6–deficient mice. *Infect Immun*. 2008;76(9):4088–91.
167. Moskowitz NH, Brown DR, Reiner SL. Efficient immunity against *Leishmania major* in the absence of interleukin–6. *Infect Immun*. 1997;65(6):2448–50.
168. Titus RG, DeKrey GK, Morris RV, Soares MB. Interleukin–6 deficiency influences cytokine expression in susceptible BALB mice infected with *Leishmania major* but does not alter the outcome of disease. *Infect Immun*. 2001;69(8):5189–92.
169. Garbers C, Hermanns HM, Schaper F, Muller–Newen G, Grotzinger J, Rose–John S, et al. Plasticity and cross–talk of interleukin 6–type cytokines. *Cytokine Growth Factor Rev*. 2012;23(3):85–97.

170. Garbers C, Scheller J. Interleukin-6 and interleukin-11: same same but different. *Biol Chem*. 2013;394(9):1145-61.
171. Lokau J, Nitz R, Agthe M, Monhasery N, Aparicio-Siegmund S, Schumacher N, et al. Proteolytic Cleavage Governs Interleukin-11 Trans-signaling. *Cell Rep*. 2016;14(7):1761-73.
172. Du XX, Doerschuk CM, Orazi A, Williams DA. A bone marrow stromal-derived growth factor, interleukin-11, stimulates recovery of small intestinal mucosal cells after cytoreductive therapy. *Blood*. 1994;83(1):33-7.
173. Du X, Liu Q, Yang Z, Orazi A, Rescorla FJ, Grosfeld JL, et al. Protective effects of interleukin-11 in a murine model of ischemic bowel necrosis. *Am J Physiol*. 1997;272(3 Pt 1):G545-52.
174. Waxman AB, Mahboubi K, Knickelbein RG, Mantell LL, Manzo N, Pober JS, et al. Interleukin-11 and interleukin-6 protect cultured human endothelial cells from H<sub>2</sub>O<sub>2</sub>-induced cell death. *Am J Respir Cell Mol Biol*. 2003;29(4):513-22.
175. Teramura M, Kobayashi S, Hoshino S, Oshimi K, Mizoguchi H. Interleukin-11 enhances human megakaryocytopoiesis in vitro. *Blood*. 1992;79(2):327-31.
176. Xu DH, Zhu Z, Wakefield MR, Xiao H, Bai Q, Fang Y. The role of IL-11 in immunity and cancer. *Cancer Lett*. 2016;373(2):156-63.
177. Bartz H, Buning-Pfaue F, Turkel O, Schauer U. Respiratory syncytial virus induces prostaglandin E<sub>2</sub>, IL-10 and IL-11 generation in antigen presenting cells. *Clin Exp Immunol*. 2002;129(3):438-45.
178. Kernacki KA, Goebel DJ, Poosch MS, Hazlett LD. Early cytokine and chemokine gene expression during *Pseudomonas aeruginosa* corneal infection in mice. *Infect Immun*. 1998;66(1):376-9.
179. Wang DQ, Ding XP, Yin S, Mao YD. Role of the IL-11/STAT3 signaling pathway in human chronic atrophic gastritis and gastric cancer. *Genet Mol Res*. 2016;15(2).
180. Zhang X, Putoczki T, Markovic-Plese S. IL-11 in multiple sclerosis. *Oncotarget*. 2015;6(32):32297-8.
181. Shepelkova G, Evstifeev V, Majorov K, Bocharova I, Apt A. Therapeutic Effect of Recombinant Mutated Interleukin 11 in the Mouse Model of Tuberculosis. *J Infect Dis*. 2016;214(3):496-501.

182. Metcalfe RD, Putoczki TL, Griffin MDW. Structural Understanding of Interleukin 6 Family Cytokine Signaling and Targeted Therapies: Focus on Interleukin 11. *Front Immunol.* 2020;11:1424.
183. Kespohl B, Schumertl T, Bertrand J, Lokau J, Garbers C. The cytokine interleukin-11 crucially links bone formation, remodeling and resorption. *Cytokine Growth Factor Rev.* 2021;60:18-27.
184. Maheshwari A, Janssens K, Bogie J, Van Den Haute C, Struys T, Lambrechts I, et al. Local overexpression of interleukin-11 in the central nervous system limits demyelination and enhances remyelination. *Mediators Inflamm.* 2013;2013:685317.
185. Li XP, Chen GY, Jin Q, Lou FR, Liu BJ, Zhang J, et al. CsIL-11, a teleost interleukin-11, is involved in promoting phagocytosis and antibacterial immune defense. *Int J Biol Macromol.* 2021;192:1021-8.
186. Galgamuwa LS, Sumanasena B, Iddawela D, Wickramasinghe S, Yatawara L. Assessment of intralesional cytokine profile of cutaneous leishmaniasis caused by *Leishmania donovani* in Sri Lanka. *BMC Microbiol.* 2019;19(1):14.
187. Handman E, Spira DT. Growth of *Leishmania* amastigotes in macrophages from normal and immune mice. *Z Parasitenkd.* 1977;53(1):75-81.
188. Rittig MG, Schroppel K, Seack KH, Sander U, N'Diaye EN, Maridonneau-Parini I, et al. Coiling phagocytosis of trypanosomatids and fungal cells. *Infect Immun.* 1998;66(9):4331-9.
189. Rittig MG, Bogdan C. *Leishmania*-host-cell interaction: complexities and alternative views. *Parasitol Today.* 2000;16(7):292-7.
190. Noronha FS, Cruz JS, Beirao PS, Horta MF. Macrophage damage by *Leishmania amazonensis* cytolyisin: evidence of pore formation on cell membrane. *Infect Immun.* 2000;68(8):4578-84.
191. Noronha FS, Ramalho-Pinto FJ, Horta MF. Cytolytic activity in the genus *Leishmania*: involvement of a putative pore-forming protein. *Infect Immun.* 1996;64(10):3975-82.
192. Almeida-Campos FR, Noronha FS, Horta MF. The multitalented pore-forming proteins of intracellular pathogens. *Microbes Infect.* 2002;4(7):741-50.
193. Hybiske K, Stephens RS. Exit strategies of intracellular pathogens. *Nat Rev Microbiol.* 2008;6(2):99-110.
194. Hybiske K, Stephens R. Cellular Exit Strategies of Intracellular Bacteria. *Microbiol Spectr.* 2015;3(6).

195. Friedrich N, Hagedorn M, Soldati-Favre D, Soldati T. Prison break: pathogens' strategies to egress from host cells. *Microbiol Mol Biol Rev.* 2012;76(4):707–20.
196. Wirth CC, Pradel G. Molecular mechanisms of host cell egress by malaria parasites. *Int J Med Microbiol.* 2012;302(4–5):172–8.
197. Traven A, Naderer T. Microbial egress: a hitchhiker's guide to freedom. *PLoS Pathog.* 2014;10(7):e1004201.
198. Jorgensen I, Rayamajhi M, Miao EA. Programmed cell death as a defence against infection. *Nat Rev Immunol.* 2017;17(3):151–64.
199. Lockshin RA, Zakeri Z. Apoptosis, autophagy, and more. *Int J Biochem Cell Biol.* 2004;36(12):2405–19.
200. Kerr JF, Wyllie AH, Currie AR. Apoptosis: a basic biological phenomenon with wide-ranging implications in tissue kinetics. *Br J Cancer.* 1972;26(4):239–57.
201. Kirkin V. History of the Selective Autophagy Research: How Did It Begin and Where Does It Stand Today? *J Mol Biol.* 2020;432(1):3–27.
202. Gatica D, Lahiri V, Klionsky DJ. Cargo recognition and degradation by selective autophagy. *Nat Cell Biol.* 2018;20(3):233–42.
203. Shen S, Kepp O, Kroemer G. The end of autophagic cell death? *Autophagy.* 2012;8(1):1–3.
204. Glick D, Barth S, Macleod KF. Autophagy: cellular and molecular mechanisms. *J Pathol.* 2010;221(1):3–12.
205. Veras PST, de Menezes JPB, Dias BRS. Deciphering the Role Played by Autophagy in Leishmania Infection. *Front Immunol.* 2019;10:2523.
206. Cyrino LT, Araujo AP, Joazeiro PP, Vicente CP, Giorgio S. In vivo and in vitro Leishmania amazonensis infection induces autophagy in macrophages. *Tissue Cell.* 2012;44(6):401–8.
207. Franco LH, Fleuri AKA, Pellison NC, Quirino GFS, Horta CV, de Carvalho RVH, et al. Autophagy downstream of endosomal Toll-like receptor signaling in macrophages is a key mechanism for resistance to Leishmania major infection. *J Biol Chem.* 2017;292(32):13087–96.
208. Thomas SA, Nandan D, Kass J, Reiner NE. Countervailing, time-dependent effects on host autophagy promotes intracellular survival of Leishmania. *J Biol Chem.* 2018;293(7):2617–30.

209. Dias BRS, de Souza CS, Almeida NJ, Lima JGB, Fukutani KF, Dos Santos TBS, et al. Autophagic Induction Greatly Enhances *Leishmania major* Intracellular Survival Compared to *Leishmania amazonensis* in CBA/j-Infected Macrophages. *Front Microbiol.* 2018;9:1890.
210. Matte C, Casgrain PA, Seguin O, Moradin N, Hong WJ, Descoteaux A. *Leishmania major* Promastigotes Evade LC3-Associated Phagocytosis through the Action of GP63. *PLoS Pathog.* 2016;12(6):e1005690.
211. Mitroulis I, Kourtzelis I, Papadopoulos VP, Mimidis K, Speletas M, Ritis K. In vivo induction of the autophagic machinery in human bone marrow cells during *Leishmania donovani* complex infection. *Parasitol Int.* 2009;58(4):475-7.
212. Frank B, Marcu A, de Oliveira Almeida Petersen AL, Weber H, Stigloher C, Mottram JC, et al. Autophagic digestion of *Leishmania major* by host macrophages is associated with differential expression of BNIP3, CTSE, and the miRNAs miR-101c, miR-129, and miR-210. *Parasit Vectors.* 2015;8:404.
213. Pitale DM, Gendalur NS, Descoteaux A, Shaha C. *Leishmania donovani* Induces Autophagy in Human Blood-Derived Neutrophils. *J Immunol.* 2019;202(4):1163-75.
214. Crauwels P, Bohn R, Thomas M, Gottwalt S, Jackel F, Kramer S, et al. Apoptotic-like *Leishmania* exploit the host's autophagy machinery to reduce T-cell-mediated parasite elimination. *Autophagy.* 2015;11(2):285-97.
215. Ruffolo PR. The Pathogenesis of Necrosis. I. Correlated Light and Electron Microscopic Observations of the Myocardial Necrosis Induced by the Intravenous Injection of Papain. *Am J Pathol.* 1964;45(5):741-56.
216. Sarhan M, Land WG, Tonnus W, Hugo CP, Linkermann A. Origin and Consequences of Necroinflammation. *Physiol Rev.* 2018;98(2):727-80.
217. Green DR, Llamby F. Cell Death Signaling. *Cold Spring Harb Perspect Biol.* 2015;7(12).
218. Elmore SA, Dixon D, Hailey JR, Harada T, Herbert RA, Maronpot RR, et al. Recommendations from the INHAND Apoptosis/Necrosis Working Group. *Toxicol Pathol.* 2016;44(2):173-88.
219. Nikolettou V, Markaki M, Palikaras K, Tavernarakis N. Crosstalk between apoptosis, necrosis and autophagy. *Biochim Biophys Acta.* 2013;1833(12):3448-59.
220. Barbosa LA, Fiuza PP, Borges LJ, Rolim FA, Andrade MB, Luz NF, et al. RIPK1-RIPK3-MLKL-Associated Necroptosis Drives *Leishmania infantum* Killing in Neutrophils. *Front Immunol.* 2018;9:1818.

221. Farias Luz N, Balaji S, Okuda K, Barreto AS, Bertin J, Gough PJ, et al. RIPK1 and PGAM5 Control Leishmania Replication through Distinct Mechanisms. *J Immunol*. 2016;196(12):5056–63.
222. Luz NF, Khouri R, Van Weyenbergh J, Zanette DL, Fiuza PP, Noronha A, et al. Leishmania braziliensis Subverts Necroptosis by Modulating RIPK3 Expression. *Front Microbiol*. 2018;9:2283.
223. Nazarian–Samani Z, Sewell RDE, Rafieian–Kopaei M. Inflammasome Signaling and Other Factors Implicated in Atherosclerosis Development and Progression. *Curr Pharm Des*. 2020;26(22):2583–90.
224. Lima–Junior DS, Costa DL, Carregaro V, Cunha LD, Silva AL, Mineo TW, et al. Inflammasome–derived IL–1beta production induces nitric oxide–mediated resistance to Leishmania. *Nat Med*. 2013;19(7):909–15.
225. Fink SL, Cookson BT. Apoptosis, pyroptosis, and necrosis: mechanistic description of dead and dying eukaryotic cells. *Infect Immun*. 2005;73(4):1907–16.
226. Hersh D, Monack DM, Smith MR, Ghori N, Falkow S, Zychlinsky A. The Salmonella invasin SipB induces macrophage apoptosis by binding to caspase–1. *Proc Natl Acad Sci U S A*. 1999;96(5):2396–401.
227. He WT, Wan H, Hu L, Chen P, Wang X, Huang Z, et al. Gasdermin D is an executor of pyroptosis and required for interleukin–1beta secretion. *Cell Res*. 2015;25(12):1285–98.
228. Fink SL, Cookson BT. Caspase–1–dependent pore formation during pyroptosis leads to osmotic lysis of infected host macrophages. *Cell Microbiol*. 2006;8(11):1812–25.
229. Kufer TA, Sansonetti PJ. Sensing of bacteria: NOD a lonely job. *Curr Opin Microbiol*. 2007;10(1):62–9.
230. Broz P, Dixit VM. Inflammasomes: mechanism of assembly, regulation and signalling. *Nat Rev Immunol*. 2016;16(7):407–20.
231. Faustin B, Lartigue L, Bruey JM, Luciano F, Sergienko E, Bailly–Maitre B, et al. Reconstituted NALP1 inflammasome reveals two–step mechanism of caspase–1 activation. *Mol Cell*. 2007;25(5):713–24.
232. Fernandes–Alnemri T, Wu J, Yu JW, Datta P, Miller B, Jankowski W, et al. The pyroptosome: a supramolecular assembly of ASC dimers mediating inflammatory cell death via caspase–1 activation. *Cell Death Differ*. 2007;14(9):1590–604.

233. Martinon F, Tschopp J. Inflammatory caspases and inflammasomes: master switches of inflammation. *Cell Death Differ*. 2007;14(1):10–22.
234. Evavold CL, Ruan J, Tan Y, Xia S, Wu H, Kagan JC. The Pore-Forming Protein Gasdermin D Regulates Interleukin-1 Secretion from Living Macrophages. *Immunity*. 2018;48(1):35–44 e6.
235. Heilig R, Dick MS, Sborgi L, Meunier E, Hiller S, Broz P. The Gasdermin-D pore acts as a conduit for IL-1beta secretion in mice. *Eur J Immunol*. 2018;48(4):584–92.
236. Volkmar K, Jaedtka M, Baars I, Walber B, Philipp MS, Bagola K, et al. Investigating pyroptosis as a mechanism of L. major cell-to-cell spread in the human BLaER1 infection model. *Mol Microbiol*. 2023.
237. de Sa KSG, Amaral LA, Rodrigues TS, Ishimoto AY, de Andrade WAC, de Almeida L, et al. Gasdermin-D activation promotes NLRP3 activation and host resistance to Leishmania infection. *Nat Commun*. 2023;14(1):1049.
238. Giraud E, Rouault E, Fiette L, Colle JH, Smirlis D, Melanitou E. Osteopontin in the host response to Leishmania amazonensis. *BMC Microbiol*. 2019;19(1):32.
239. Saha G, Khamar BM, Prerna K, Kumar M, Dubey VK. BLIMP-1 Plays Important Role in the Regulation of Macrophage Pyroptosis for the Growth and Multiplication of Leishmania donovani. *ACS Infect Dis*. 2019;5(12):2087–95.
240. Saha G, Khamar BM, Singh OP, Sundar S, Dubey VK. Leishmania donovani evades Caspase 1 dependent host defense mechanism during infection. *Int J Biol Macromol*. 2019;126:392–401.
241. Saha G, Chiranjivi AK, Khamar BM, Prerna K, Kumar M, Dubey VK. BLIMP-1 Mediated Downregulation of TAK1 and p53 Molecules Is Crucial in the Pathogenesis of Kala-Azar. *Front Cell Infect Microbiol*. 2020;10:594431.
242. Galluzzi L, Brenner C, Morselli E, Touat Z, Kroemer G. Viral control of mitochondrial apoptosis. *PLoS Pathog*. 2008;4(5):e1000018.
243. Oberhammer FA, Hochegger K, Froschl G, Tiefenbacher R, Pavelka M. Chromatin condensation during apoptosis is accompanied by degradation of lamin A+B, without enhanced activation of cdc2 kinase. *J Cell Biol*. 1994;126(4):827–37.
244. Tounekti O, Belehradek J, Jr., Mir LM. Relationships between DNA fragmentation, chromatin condensation, and changes in flow cytometry profiles detected during apoptosis. *Exp Cell Res*. 1995;217(2):506–16.

245. Daniel PT, Sturm I, Ritschel S, Friedrich K, Dorken B, Bendzko P, et al. Detection of genomic DNA fragmentation during apoptosis (DNA ladder) and the simultaneous isolation of RNA from low cell numbers. *Anal Biochem.* 1999;266(1):110–5.
246. Martin CJ, Booty MG, Rosebrock TR, Nunes–Alves C, Desjardins DM, Keren I, et al. Efferocytosis is an innate antibacterial mechanism. *Cell Host Microbe.* 2012;12(3):289–300.
247. Galluzzi L, Vitale I, Abrams JM, Alnemri ES, Baehrecke EH, Blagosklonny MV, et al. Molecular definitions of cell death subroutines: recommendations of the Nomenclature Committee on Cell Death 2012. *Cell Death Differ.* 2012;19(1):107–20.
248. Ghavami S, Kerkhoff C, Los M, Hashemi M, Sorg C, Karami–Tehrani F. Mechanism of apoptosis induced by S100A8/A9 in colon cancer cell lines: the role of ROS and the effect of metal ions. *J Leukoc Biol.* 2004;76(1):169–75.
249. Jan R, Chaudhry GE. Understanding Apoptosis and Apoptotic Pathways Targeted Cancer Therapeutics. *Adv Pharm Bull.* 2019;9(2):205–18.
250. Brenner D, Mak TW. Mitochondrial cell death effectors. *Curr Opin Cell Biol.* 2009;21(6):871–7.
251. Kim R. Recent advances in understanding the cell death pathways activated by anticancer therapy. *Cancer.* 2005;103(8):1551–60.
252. Ghobrial IM, Witzig TE, Adjei AA. Targeting apoptosis pathways in cancer therapy. *CA Cancer J Clin.* 2005;55(3):178–94.
253. Sica A, Wang JM, Colotta F, Dejana E, Mantovani A, Oppenheim JJ, et al. Monocyte chemotactic and activating factor gene expression induced in endothelial cells by IL–1 and tumor necrosis factor. *J Immunol.* 1990;144(8):3034–8.
254. Oppenheim RW, Flavell RA, Vinsant S, Prevette D, Kuan CY, Rakic P. Programmed cell death of developing mammalian neurons after genetic deletion of caspases. *J Neurosci.* 2001;21(13):4752–60.
255. Bredesen DE, Rao RV, Mehlen P. Cell death in the nervous system. *Nature.* 2006;443(7113):796–802.
256. Sankari SL, Masthan KM, Babu NA, Bhattacharjee T, Elumalai M. Apoptosis in cancer— an update. *Asian Pac J Cancer Prev.* 2012;13(10):4873–8.
257. Boatright KM, Renatus M, Scott FL, Sperandio S, Shin H, Pedersen IM, et al. A unified model for apical caspase activation. *Mol Cell.* 2003;11(2):529–41.

258. Parrish AB, Freel CD, Kornbluth S. Cellular mechanisms controlling caspase activation and function. *Cold Spring Harb Perspect Biol.* 2013;5(6).
259. Slee EA, Harte MT, Kluck RM, Wolf BB, Casiano CA, Newmeyer DD, et al. Ordering the cytochrome c-initiated caspase cascade: hierarchical activation of caspases-2, -3, -6, -7, -8, and -10 in a caspase-9-dependent manner. *J Cell Biol.* 1999;144(2):281-92.
260. Martinvalet D, Zhu P, Lieberman J. Granzyme A induces caspase-independent mitochondrial damage, a required first step for apoptosis. *Immunity.* 2005;22(3):355-70.
261. Poon IK, Lucas CD, Rossi AG, Ravichandran KS. Apoptotic cell clearance: basic biology and therapeutic potential. *Nat Rev Immunol.* 2014;14(3):166-80.
262. Roy S, Gupta P, Palit S, Basu M, Ukil A, Das PK. The role of PD-1 in regulation of macrophage apoptosis and its subversion by *Leishmania donovani*. *Clin Transl Immunology.* 2017;6(5):e137.
263. Ruhland A, Leal N, Kima PE. *Leishmania* promastigotes activate PI3K/Akt signalling to confer host cell resistance to apoptosis. *Cell Microbiol.* 2007;9(1):84-96.
264. Gupta P, Srivastav S, Saha S, Das PK, Ukil A. *Leishmania donovani* inhibits macrophage apoptosis and pro-inflammatory response through AKT-mediated regulation of beta-catenin and FOXO-1. *Cell Death Differ.* 2016;23(11):1815-26.
265. Abhishek K, Das S, Kumar A, Kumar A, Kumar V, Saini S, et al. *Leishmania donovani* induced Unfolded Protein Response delays host cell apoptosis in PERK dependent manner. *PLoS Negl Trop Dis.* 2018;12(7):e0006646.
266. Das S, Ghosh AK, Singh S, Saha B, Ganguly A, Das P. Unmethylated CpG motifs in the *L. donovani* DNA regulate TLR9-dependent delay of programmed cell death in macrophages. *J Leukoc Biol.* 2015;97(2):363-78.
267. Giri J, Srivastav S, Basu M, Palit S, Gupta P, Ukil A. *Leishmania donovani* Exploits Myeloid Cell Leukemia 1 (MCL-1) Protein to Prevent Mitochondria-dependent Host Cell Apoptosis. *J Biol Chem.* 2016;291(7):3496-507.
268. Pandey RK, Mehrotra S, Sharma S, Gudde RS, Sundar S, Shaha C. *Leishmania donovani*-Induced Increase in Macrophage Bcl-2 Favors Parasite Survival. *Front Immunol.* 2016;7:456.
269. Cianciulli A, Porro C, Calvello R, Trotta T, Panaro MA. Resistance to apoptosis in *Leishmania infantum*-infected human macrophages: a critical role for anti-apoptotic Bcl-2 protein and cellular IAP1/2. *Clin Exp Med.* 2018;18(2):251-61.

270. Rodriguez-Gonzalez J, Wilkins-Rodriguez A, Argueta-Donohue J, Aguirre-Garcia M, Gutierrez-Kobeh L. *Leishmania mexicana* promastigotes down regulate JNK and p-38 MAPK activation: Role in the inhibition of camptothecin-induced apoptosis of monocyte-derived dendritic cells. *Exp Parasitol*. 2016;163:57-67.
271. Rodriguez-Gonzalez J, Wilkins-Rodriguez AA, Gutierrez-Kobeh L. Role of glutathione, ROS, and Bcl-xL in the inhibition of apoptosis of monocyte-derived dendritic cells by *Leishmania mexicana* promastigotes. *Parasitol Res*. 2018;117(4):1225-35.
272. Valdes-Reyes L, Argueta J, Moran J, Salaiza N, Hernandez J, Berzunza M, et al. *Leishmania mexicana*: inhibition of camptothecin-induced apoptosis of monocyte-derived dendritic cells. *Exp Parasitol*. 2009;121(3):199-207.
273. Gutierrez-Kobeh L, de Oyarzabal E, Argueta J, Wilkins A, Salaiza N, Fernandez E, et al. Inhibition of dendritic cell apoptosis by *Leishmania mexicana* amastigotes. *Parasitol Res*. 2013;112(4):1755-62.
274. Vazquez-Lopez R, Argueta-Donohue J, Wilkins-Rodriguez A, Escalona-Montano A, Aguirre-Garcia M, Gutierrez-Kobeh L. *Leishmania mexicana* amastigotes inhibit p38 and JNK and activate PI3K/AKT: role in the inhibition of apoptosis of dendritic cells. *Parasite Immunol*. 2015;37(11):579-89.
275. Akarid K, Arnoult D, Micic-Polianski J, Sif J, Estaquier J, Ameisen JC. *Leishmania major*-mediated prevention of programmed cell death induction in infected macrophages is associated with the repression of mitochondrial release of cytochrome c. *J Leukoc Biol*. 2004;76(1):95-103.
276. DaMata JP, Mendes BP, Maciel-Lima K, Menezes CA, Dutra WO, Sousa LP, et al. Distinct Macrophage Fates after in vitro Infection with Different Species of *Leishmania*: Induction of Apoptosis by *Leishmania (Leishmania) amazonensis*, but Not by *Leishmania (Viannia) guyanensis*. *PLoS One*. 2015;10(10):e0141196.
277. Getti GT, Cheke RA, Humber DP. Induction of apoptosis in host cells: a survival mechanism for *Leishmania* parasites? *Parasitology*. 2008;135(12):1391-9.
278. Ranatunga M, Rai R, Richardson SCW, Dyer P, Harbige L, Deacon A, et al. *Leishmania aethiopica* cell-to-cell spreading involves caspase-3, Akt, and NF-kappaB but not PKC-delta activation and involves uptake of LAMP-1-positive bodies containing parasites. *FEBS J*. 2020;287(9):1777-97.
279. Donovan MJ, Maciuba BZ, Mahan CE, McDowell MA. *Leishmania* infection inhibits cycloheximide-induced macrophage apoptosis in a strain-dependent manner. *Exp Parasitol*. 2009;123(1):58-64.

280. Potestio M, D'Agostino P, Romano GC, Milano S, Ferlazzo V, Aquino A, et al. CD4+ CCR5+ and CD4+ CCR3+ lymphocyte subset and monocyte apoptosis in patients with acute visceral leishmaniasis. *Immunology*. 2004;113(2):260–8.
281. Nandurkar HH, Robb L, Tarlinton D, Barnett L, Kontgen F, Begley CG. Adult mice with targeted mutation of the interleukin-11 receptor (IL11Ra) display normal hematopoiesis. *Blood*. 1997;90(6):2148–59.
282. Muller AJ, Aeschlimann S, Olekhovitch R, Dacher M, Spath GF, Bousso P. Photoconvertible pathogen labeling reveals nitric oxide control of *Leishmania major* infection in vivo via dampening of parasite metabolism. *Cell Host Microbe*. 2013;14(4):460–7.
283. Misslitz A, Mottram JC, Overath P, Aebischer T. Targeted integration into a rRNA locus results in uniform and high level expression of transgenes in *Leishmania amastigotes*. *Mol Biochem Parasitol*. 2000;107(2):251–61.
284. Sorensen M, Lippuner C, Kaiser T, Misslitz A, Aebischer T, Bumann D. Rapidly maturing red fluorescent protein variants with strongly enhanced brightness in bacteria. *FEBS Lett*. 2003;552(2–3):110–4.
285. Wenzel UA, Bank E, Florian C, Forster S, Zimara N, Steinacker J, et al. *Leishmania major* parasite stage-dependent host cell invasion and immune evasion. *FASEB J*. 2012;26(1):29–39.
286. Tyas L, Brophy VA, Pope A, Rivett AJ, Tavares JM. Rapid caspase-3 activation during apoptosis revealed using fluorescence-resonance energy transfer. *EMBO Rep*. 2000;1(3):266–70.
287. Breart B, Lemaitre F, Celli S, Bousso P. Two-photon imaging of intratumoral CD8+ T cell cytotoxic activity during adoptive T cell therapy in mice. *J Clin Invest*. 2008;118(4):1390–7.
288. Garrod KR, Moreau HD, Garcia Z, Lemaitre F, Bouvier I, Albert ML, et al. Dissecting T cell contraction in vivo using a genetically encoded reporter of apoptosis. *Cell Rep*. 2012;2(5):1438–47.
289. Rossmann L, Bagola K, Stephen T, Gerards AL, Walber B, Ullrich A, et al. Distinct single-component adjuvants steer human DC-mediated T-cell polarization via Toll-like receptor signaling toward a potent antiviral immune response. *Proc Natl Acad Sci U S A*. 2021;118(39).
290. Yoshioka K, Takahashi H, Homma T, Saito M, Oh KB, Nemoto Y, et al. A novel fluorescent derivative of glucose applicable to the assessment of glucose uptake activity of *Escherichia coli*. *Biochim Biophys Acta*. 1996;1289(1):5–9.

291. Moreau HD, Lemaitre F, Terriac E, Azar G, Piel M, Lennon-Dumenil AM, et al. Dynamic in situ cytometry uncovers T cell receptor signaling during immunological synapses and kinapses in vivo. *Immunity*. 2012;37(2):351–63.
292. Formaglio P, Alabdullah M, Siokis A, Handschuh J, Sauerland I, Fu Y, et al. Nitric oxide controls proliferation of *Leishmania major* by inhibiting the recruitment of permissive host cells. *Immunity*. 2021;54(12):2724–39 e10.
293. Lin L, Cook DN, Wieseahn GP, Alfonso R, Behrman B, Cimino GD, et al. Photochemical inactivation of viruses and bacteria in platelet concentrates by use of a novel psoralen and long-wavelength ultraviolet light. *Transfusion*. 1997;37(4):423–35.
294. Belanger KJ, Kelly DJ, Mettillie FC, Hanson CV, Lippert LE. Psoralen photochemical inactivation of *Orientia tsutsugamushi* in platelet concentrates. *Transfusion*. 2000;40(12):1503–7.
295. Seiss EA, Krone A, Formaglio P, Goldmann O, Engelmann S, Schraven B, et al. Longitudinal proliferation mapping in vivo reveals NADPH oxidase-mediated dampening of *Staphylococcus aureus* growth rates within neutrophils. *Sci Rep*. 2019;9(1):5703.
296. Tait JF, Gibson D, Fujikawa K. Phospholipid binding properties of human placental anticoagulant protein-I, a member of the lipocortin family. *J Biol Chem*. 1989;264(14):7944–9.
297. Abumrad NA, el-Maghrabi MR, Amri EZ, Lopez E, Grimaldi PA. Cloning of a rat adipocyte membrane protein implicated in binding or transport of long-chain fatty acids that is induced during preadipocyte differentiation. Homology with human CD36. *J Biol Chem*. 1993;268(24):17665–8.
298. Baillie AG, Coburn CT, Abumrad NA. Reversible binding of long-chain fatty acids to purified FAT, the adipose CD36 homolog. *J Membr Biol*. 1996;153(1):75–81.
299. Drury J, Rychahou PG, He D, Jafari N, Wang C, Lee EY, et al. Inhibition of Fatty Acid Synthase Upregulates Expression of CD36 to Sustain Proliferation of Colorectal Cancer Cells. *Front Oncol*. 2020;10:1185.
300. Mael J, Ransijn A, Buchmuller-Rouiller Y. Killing of *Leishmania* parasites in activated murine macrophages is based on an L-arginine-dependent process that produces nitrogen derivatives. *J Leukoc Biol*. 1991;49(1):73–82.
301. Olekhnovitch R, Ryffel B, Muller AJ, Bousso P. Collective nitric oxide production provides tissue-wide immunity during *Leishmania* infection. *J Clin Invest*. 2014;124(4):1711–22.

302. Hickok JR, Vasudevan D, Jablonski K, Thomas DD. Oxygen dependence of nitric oxide-mediated signaling. *Redox Biol.* 2013;1(1):203–9.
303. Sims NA, Jenkins BJ, Nakamura A, Quinn JM, Li R, Gillespie MT, et al. Interleukin-11 receptor signaling is required for normal bone remodeling. *J Bone Miner Res.* 2005;20(7):1093–102.
304. Baars I, Lokau J, Sauerland I, Muller AJ, Garbers C. Interleukin-11 receptor expression on monocytes is dispensable for their recruitment and pathogen uptake during *Leishmania major* infection. *Cytokine.* 2021;148:155699.
305. Aga E, Katschinski DM, van Zandbergen G, Laufs H, Hansen B, Muller K, et al. Inhibition of the spontaneous apoptosis of neutrophil granulocytes by the intracellular parasite *Leishmania major*. *J Immunol.* 2002;169(2):898–905.
306. Laskay T, van Zandbergen G, Solbach W. Neutrophil granulocytes as host cells and transport vehicles for intracellular pathogens: apoptosis as infection-promoting factor. *Immunobiology.* 2008;213(3–4):183–91.
307. Owens BM, Beattie L, Moore JW, Brown N, Mann JL, Dalton JE, et al. IL-10-producing Th1 cells and disease progression are regulated by distinct CD11c(+) cell populations during visceral leishmaniasis. *PLoS Pathog.* 2012;8(7):e1002827.
308. Brewig N, Kissenpfennig A, Malissen B, Veit A, Bickert T, Fleischer B, et al. Priming of CD8+ and CD4+ T cells in experimental leishmaniasis is initiated by different dendritic cell subtypes. *J Immunol.* 2009;182(2):774–83.
309. Vargas-Inchaustegui DA, Xin L, Soong L. *Leishmania braziliensis* infection induces dendritic cell activation, ISG15 transcription, and the generation of protective immune responses. *J Immunol.* 2008;180(11):7537–45.
310. Dey S, Mukherjee D, Sultana SS, Mallick S, Dutta A, Ghosh J, et al. Combination of *Mycobacterium indicus pranii* and Heat-Induced Promastigotes Cures Drug-Resistant *Leishmania* Infection: Critical Role of Interleukin-6-Producing Classical Dendritic Cells. *Infect Immun.* 2020;88(6).
311. De Trez C, Magez S, Akira S, Ryffel B, Carlier Y, Muraille E. iNOS-producing inflammatory dendritic cells constitute the major infected cell type during the chronic *Leishmania major* infection phase of C57BL/6 resistant mice. *PLoS Pathog.* 2009;5(6):e1000494.
312. Xin L, Li Y, Soong L. Role of interleukin-1beta in activating the CD11c(high) CD45RB-dendritic cell subset and priming *Leishmania amazonensis*-specific CD4+ T cells in vitro and in vivo. *Infect Immun.* 2007;75(10):5018–26.

313. Carvalho AK, Silveira FT, Passero LF, Gomes CM, Corbett CE, Laurenti MD. *Leishmania* (V.) *braziliensis* and *L. (L.) amazonensis* promote differential expression of dendritic cells and cellular immune response in murine model. *Parasite Immunol.* 2012;34(8-9):395-403.
314. Muraille E, De Trez C, Pajak B, Torrentera FA, De Baetselier P, Leo O, et al. Amastigote load and cell surface phenotype of infected cells from lesions and lymph nodes of susceptible and resistant mice infected with *Leishmania major*. *Infect Immun.* 2003;71(5):2704-15.
315. Hurdayal R, Nieuwenhuizen NE, Khutlang R, Brombacher F. Inflammatory Dendritic Cells, Regulated by IL-4 Receptor Alpha Signaling, Control Replication, and Dissemination of *Leishmania major* in Mice. *Front Cell Infect Microbiol.* 2019;9:479.
316. Antoine JC, Lang T, Prina E, Courret N, Hellio R. H-2M molecules, like MHC class II molecules, are targeted to parasitophorous vacuoles of *Leishmania*-infected macrophages and internalized by amastigotes of *L. amazonensis* and *L. mexicana*. *J Cell Sci.* 1999;112 ( Pt 15):2559-70.
317. Flohe S, Lang T, Moll H. Synthesis, stability, and subcellular distribution of major histocompatibility complex class II molecules in Langerhans cells infected with *Leishmania major*. *Infect Immun.* 1997;65(8):3444-50.
318. Basu A, Chakrabarti G, Saha A, Bandyopadhyay S. Modulation of CD11C<sup>+</sup> splenic dendritic cell functions in murine visceral leishmaniasis: correlation with parasite replication in the spleen. *Immunology.* 2000;99(2):305-13.
319. Degrossoli A, Arrais-Silva WW, Colhone MC, Gadelha FR, Joazeiro PP, Giorgio S. The influence of low oxygen on macrophage response to *Leishmania* infection. *Scand J Immunol.* 2011;74(2):165-75.
320. Mahnke A, Meier RJ, Schatz V, Hofmann J, Castiglione K, Schleicher U, et al. Hypoxia in *Leishmania major* skin lesions impairs the NO-dependent leishmanicidal activity of macrophages. *J Invest Dermatol.* 2014;134(9):2339-46.
321. Sen Santara S, Roy J, Mukherjee S, Bose M, Saha R, Adak S. Globin-coupled heme containing oxygen sensor soluble adenylate cyclase in *Leishmania* prevents cell death during hypoxia. *Proc Natl Acad Sci U S A.* 2013;110(42):16790-5.
322. Chakraborty B, Biswas S, Mondal S, Bera T. Stage specific developmental changes in the mitochondrial and surface membrane associated redox systems of *Leishmania donovani* promastigote and amastigote. *Biochemistry (Mosc).* 2010;75(4):494-518.
323. Ribeiro-Gomes FL, Romano A, Lee S, Roffe E, Peters NC, Debrabant A, et al. Apoptotic cell clearance of *Leishmania major*-infected neutrophils by dendritic cells inhibits CD8(+) T-

cell priming in vitro by Mer tyrosine kinase-dependent signaling. *Cell Death Dis.* 2015;6(12):e2018.

324. Kleinholz CL, Riek-Burchardt M, Seiss EA, Amore J, Gintschel P, Philipsen L, et al. Ly6G deficiency alters the dynamics of neutrophil recruitment and pathogen capture during *Leishmania* major skin infection. *Sci Rep.* 2021;11(1):15071.

325. Ribeiro-Gomes FL, Peters NC, Debrabant A, Sacks DL. Efficient capture of infected neutrophils by dendritic cells in the skin inhibits the early anti-*leishmania* response. *PLoS Pathog.* 2012;8(2):e1002536.

326. Weinrauch Y, Zychlinsky A. The induction of apoptosis by bacterial pathogens. *Annu Rev Microbiol.* 1999;53:155–87.

327. Gao LY, Kwai YA. The modulation of host cell apoptosis by intracellular bacterial pathogens. *Trends Microbiol.* 2000;8(7):306–13.

328. Early J, Fischer K, Bermudez LE. *Mycobacterium avium* uses apoptotic macrophages as tools for spreading. *Microb Pathog.* 2011;50(2):132–9.

329. Davis JM, Ramakrishnan L. The role of the granuloma in expansion and dissemination of early tuberculous infection. *Cell.* 2009;136(1):37–49.

330. De Leon-Rodriguez CM, Rossi DCP, Fu MS, Dragotakes Q, Coelho C, Guerrero Ros I, et al. The Outcome of the *Cryptococcus neoformans*–Macrophage Interaction Depends on Phagolysosomal Membrane Integrity. *J Immunol.* 2018;201(2):583–603.

331. Tucker SC, Casadevall A. Replication of *Cryptococcus neoformans* in macrophages is accompanied by phagosomal permeabilization and accumulation of vesicles containing polysaccharide in the cytoplasm. *Proc Natl Acad Sci U S A.* 2002;99(5):3165–70.

332. Villena SN, Pinheiro RO, Pinheiro CS, Nunes MP, Takiya CM, DosReis GA, et al. Capsular polysaccharides galactoxylomannan and glucuronoxylomannan from *Cryptococcus neoformans* induce macrophage apoptosis mediated by Fas ligand. *Cell Microbiol.* 2008;10(6):1274–85.

333. Ben-Abdallah M, Sturny-Leclere A, Ave P, Louise A, Moyrand F, Weih F, et al. Fungal-induced cell cycle impairment, chromosome instability and apoptosis via differential activation of NF- $\kappa$ B. *PLoS Pathog.* 2012;8(3):e1002555.

334. Perfettini JL, Hospital V, Stahl L, Jungas T, Verbeke P, Ojcius DM. Cell death and inflammation during infection with the obligate intracellular pathogen, *Chlamydia*. *Biochimie.* 2003;85(8):763–9.

335. Matsuo J, Haga S, Hashimoto K, Okubo T, Ozawa T, Ozaki M, et al. Activation of caspase-3 during *Chlamydia trachomatis*-induced apoptosis at a late stage. *Can J Microbiol.* 2019;65(2):135-43.
336. Huang Y, Li S, He S, Li Y, He Q, Wu Y. *Chlamydia psittaci* inclusion membrane protein CPSIT\_0842 induces macrophage apoptosis through MAPK/ERK-mediated autophagy. *Int J Biochem Cell Biol.* 2023;157:106376.
337. Miyairi I, Byrne GI. *Chlamydia* and programmed cell death. *Curr Opin Microbiol.* 2006;9(1):102-8.
338. Waguia Kontchou C, Gentle IE, Weber A, Schoeniger A, Edlich F, Hacker G. *Chlamydia trachomatis* inhibits apoptosis in infected cells by targeting the pro-apoptotic proteins Bax and Bak. *Cell Death Differ.* 2022;29(10):2046-59.
339. Lai XH, Golovliov I, Sjostedt A. *Francisella tularensis* induces cytopathogenicity and apoptosis in murine macrophages via a mechanism that requires intracellular bacterial multiplication. *Infect Immun.* 2001;69(7):4691-4.
340. Lai XH, Sjostedt A. Delineation of the molecular mechanisms of *Francisella tularensis*-induced apoptosis in murine macrophages. *Infect Immun.* 2003;71(8):4642-6.
341. Paesold G, Guiney DG, Eckmann L, Kagnoff MF. Genes in the *Salmonella* pathogenicity island 2 and the *Salmonella* virulence plasmid are essential for *Salmonella*-induced apoptosis in intestinal epithelial cells. *Cell Microbiol.* 2002;4(11):771-81.
342. van Zandbergen G, Solbach W, Laskay T. Apoptosis driven infection. *Autoimmunity.* 2007;40(4):349-52.
343. Lindgren SW, Stojiljkovic I, Heffron F. Macrophage killing is an essential virulence mechanism of *Salmonella typhimurium*. *Proc Natl Acad Sci U S A.* 1996;93(9):4197-201.
344. Robinson N, McComb S, Mulligan R, Dudani R, Krishnan L, Sad S. Type I interferon induces necroptosis in macrophages during infection with *Salmonella enterica* serovar Typhimurium. *Nat Immunol.* 2012;13(10):954-62.
345. Wong KW, Jacobs WR, Jr. Critical role for NLRP3 in necrotic death triggered by *Mycobacterium tuberculosis*. *Cell Microbiol.* 2011;13(9):1371-84.
346. Divangahi M, Chen M, Gan H, Desjardins D, Hickman TT, Lee DM, et al. *Mycobacterium tuberculosis* evades macrophage defenses by inhibiting plasma membrane repair. *Nat Immunol.* 2009;10(8):899-906.

347. Dallenga T, Repnik U, Corleis B, Eich J, Reimer R, Griffiths GW, et al. M. tuberculosis–Induced Necrosis of Infected Neutrophils Promotes Bacterial Growth Following Phagocytosis by Macrophages. *Cell Host Microbe*. 2017;22(4):519–30 e3.
348. Upton JW, Kaiser WJ, Mocarski ES. Virus inhibition of RIP3–dependent necrosis. *Cell Host Microbe*. 2010;7(4):302–13.
349. Upton JW, Kaiser WJ, Mocarski ES. DAI/ZBP1/DLM–1 complexes with RIP3 to mediate virus–induced programmed necrosis that is targeted by murine cytomegalovirus vIRA. *Cell Host Microbe*. 2012;11(3):290–7.
350. Nogusa S, Thapa RJ, Dillon CP, Liedmann S, Oguin TH, 3rd, Ingram JP, et al. RIPK3 Activates Parallel Pathways of MLKL–Driven Necroptosis and FADD–Mediated Apoptosis to Protect against Influenza A Virus. *Cell Host Microbe*. 2016;20(1):13–24.
351. Thapa RJ, Ingram JP, Ragan KB, Nogusa S, Boyd DF, Benitez AA, et al. DAI Senses Influenza A Virus Genomic RNA and Activates RIPK3–Dependent Cell Death. *Cell Host Microbe*. 2016;20(5):674–81.
352. Wang X, Li Y, Liu S, Yu X, Li L, Shi C, et al. Direct activation of RIP3/MLKL–dependent necrosis by herpes simplex virus 1 (HSV–1) protein ICP6 triggers host antiviral defense. *Proc Natl Acad Sci U S A*. 2014;111(43):15438–43.
353. Huang Z, Wu SQ, Liang Y, Zhou X, Chen W, Li L, et al. RIP1/RIP3 binding to HSV–1 ICP6 initiates necroptosis to restrict virus propagation in mice. *Cell Host Microbe*. 2015;17(2):229–42.
354. Guo H, Kaiser WJ, Mocarski ES. Manipulation of apoptosis and necroptosis signaling by herpesviruses. *Med Microbiol Immunol*. 2015;204(3):439–48.
355. Ren T, Zamboni DS, Roy CR, Dietrich WF, Vance RE. Flagellin–deficient Legionella mutants evade caspase–1– and Naip5–mediated macrophage immunity. *PLoS Pathog*. 2006;2(3):e18.
356. Molofsky AB, Byrne BG, Whitfield NN, Madigan CA, Fuse ET, Tateda K, et al. Cytosolic recognition of flagellin by mouse macrophages restricts Legionella pneumophila infection. *J Exp Med*. 2006;203(4):1093–104.
357. Gavrillin MA, Bouakl IJ, Knatz NL, Duncan MD, Hall MW, Gunn JS, et al. Internalization and phagosome escape required for Francisella to induce human monocyte IL–1beta processing and release. *Proc Natl Acad Sci U S A*. 2006;103(1):141–6.
358. Mariathasan S, Weiss DS, Dixit VM, Monack DM. Innate immunity against Francisella tularensis is dependent on the ASC/caspase–1 axis. *J Exp Med*. 2005;202(8):1043–9.

359. Fernandes-Alnemri T, Yu JW, Juliana C, Solorzano L, Kang S, Wu J, et al. The AIM2 inflammasome is critical for innate immunity to *Francisella tularensis*. *Nat Immunol*. 2010;11(5):385–93.
360. Suzuki T, Franchi L, Toma C, Ashida H, Ogawa M, Yoshikawa Y, et al. Differential regulation of caspase-1 activation, pyroptosis, and autophagy via Ipaf and ASC in *Shigella*-infected macrophages. *PLoS Pathog*. 2007;3(8):e111.
361. Hilbi H, Moss JE, Hersh D, Chen Y, Arondel J, Banerjee S, et al. *Shigella*-induced apoptosis is dependent on caspase-1 which binds to Ipab. *J Biol Chem*. 1998;273(49):32895–900.
362. Franchi L, Amer A, Body-Malapel M, Kanneganti TD, Ozoren N, Jagirdar R, et al. Cytosolic flagellin requires Ipaf for activation of caspase-1 and interleukin 1beta in salmonella-infected macrophages. *Nat Immunol*. 2006;7(6):576–82.
363. Miao EA, Alpuche-Aranda CM, Dors M, Clark AE, Bader MW, Miller SI, et al. Cytoplasmic flagellin activates caspase-1 and secretion of interleukin 1beta via Ipaf. *Nat Immunol*. 2006;7(6):569–75.
364. Brennan MA, Cookson BT. Salmonella induces macrophage death by caspase-1-dependent necrosis. *Mol Microbiol*. 2000;38(1):31–40.
365. Fink SL, Cookson BT. Pyroptosis and host cell death responses during Salmonella infection. *Cell Microbiol*. 2007;9(11):2562–70.
366. Ozoren N, Masumoto J, Franchi L, Kanneganti TD, Body-Malapel M, Erturk I, et al. Distinct roles of TLR2 and the adaptor ASC in IL-1beta/IL-18 secretion in response to *Listeria monocytogenes*. *J Immunol*. 2006;176(7):4337–42.
367. Knodler LA, Crowley SM, Sham HP, Yang H, Wrande M, Ma C, et al. Noncanonical inflammasome activation of caspase-4/caspase-11 mediates epithelial defenses against enteric bacterial pathogens. *Cell Host Microbe*. 2014;16(2):249–56.
368. Akhter A, Caution K, Abu Khweek A, Tazi M, Abdulrahman BA, Abdelaziz DH, et al. Caspase-11 promotes the fusion of phagosomes harboring pathogenic bacteria with lysosomes by modulating actin polymerization. *Immunity*. 2012;37(1):35–47.
369. Uwamahoro N, Verma-Gaur J, Shen HH, Qu Y, Lewis R, Lu J, et al. The pathogen *Candida albicans* hijacks pyroptosis for escape from macrophages. *mBio*. 2014;5(2):e00003–14.
370. Lara-Tejero M, Sutterwala FS, Ogura Y, Grant EP, Bertin J, Coyle AJ, et al. Role of the caspase-1 inflammasome in *Salmonella typhimurium* pathogenesis. *J Exp Med*. 2006;203(6):1407–12.

371. Raupach B, Peuschel SK, Monack DM, Zychlinsky A. Caspase-1-mediated activation of interleukin-1beta (IL-1beta) and IL-18 contributes to innate immune defenses against *Salmonella enterica* serovar Typhimurium infection. *Infect Immun*. 2006;74(8):4922-6.
372. Bertheloot D, Latz E, Franklin BS. Necroptosis, pyroptosis and apoptosis: an intricate game of cell death. *Cell Mol Immunol*. 2021;18(5):1106-21.
373. Samir P, Malireddi RKS, Kanneganti TD. The PANoptosome: A Deadly Protein Complex Driving Pyroptosis, Apoptosis, and Necroptosis (PANoptosis). *Front Cell Infect Microbiol*. 2020;10:238.
374. Gaillard JL, Berche P, Mounier J, Richard S, Sansonetti P. In vitro model of penetration and intracellular growth of *Listeria monocytogenes* in the human enterocyte-like cell line Caco-2. *Infect Immun*. 1987;55(11):2822-9.
375. Bielecki J, Youngman P, Connelly P, Portnoy DA. *Bacillus subtilis* expressing a haemolysin gene from *Listeria monocytogenes* can grow in mammalian cells. *Nature*. 1990;345(6271):175-6.
376. Kayal S, Charbit A. Listeriolysin O: a key protein of *Listeria monocytogenes* with multiple functions. *FEMS Microbiol Rev*. 2006;30(4):514-29.
377. High N, Mounier J, Prevost MC, Sansonetti PJ. IpaB of *Shigella flexneri* causes entry into epithelial cells and escape from the phagocytic vacuole. *EMBO J*. 1992;11(5):1991-9.
378. Page AL, Ohayon H, Sansonetti PJ, Parsot C. The secreted IpaB and IpaC invasins and their cytoplasmic chaperone IpgC are required for intercellular dissemination of *Shigella flexneri*. *Cell Microbiol*. 1999;1(2):183-93.
379. Hayward RD, Cain RJ, McGhie EJ, Phillips N, Garner MJ, Koronakis V. Cholesterol binding by the bacterial type III translocon is essential for virulence effector delivery into mammalian cells. *Mol Microbiol*. 2005;56(3):590-603.
380. Picking WL, Nishioka H, Hearn PD, Baxter MA, Harrington AT, Blocker A, et al. IpaD of *Shigella flexneri* is independently required for regulation of Ipa protein secretion and efficient insertion of IpaB and IpaC into host membranes. *Infect Immun*. 2005;73(3):1432-40.
381. Andrews NW, Abrams CK, Slatin SL, Griffiths G. A *T. cruzi*-secreted protein immunologically related to the complement component C9: evidence for membrane pore-forming activity at low pH. *Cell*. 1990;61(7):1277-87.
382. Hall BF, Webster P, Ma AK, Joiner KA, Andrews NW. Desialylation of lysosomal membrane glycoproteins by *Trypanosoma cruzi*: a role for the surface neuraminidase in facilitating parasite entry into the host cell cytoplasm. *J Exp Med*. 1992;176(2):313-25.

383. Smith GA, Marquis H, Jones S, Johnston NC, Portnoy DA, Goldfine H. The two distinct phospholipases C of *Listeria monocytogenes* have overlapping roles in escape from a vacuole and cell-to-cell spread. *Infect Immun*. 1995;63(11):4231–7.
384. Marquis H, Hager EJ. pH-regulated activation and release of a bacteria-associated phospholipase C during intracellular infection by *Listeria monocytogenes*. *Mol Microbiol*. 2000;35(2):289–98.
385. Camilli A, Tilney LG, Portnoy DA. Dual roles of *plcA* in *Listeria monocytogenes* pathogenesis. *Mol Microbiol*. 1993;8(1):143–57.
386. Vazquez-Boland JA, Kocks C, Dramsi S, Ohayon H, Geoffroy C, Mengaud J, et al. Nucleotide sequence of the lecithinase operon of *Listeria monocytogenes* and possible role of lecithinase in cell-to-cell spread. *Infect Immun*. 1992;60(1):219–30.
387. Winkler HH, Miller ET. Phospholipase A and the interaction of *Rickettsia prowazekii* and mouse fibroblasts (L-929 cells). *Infect Immun*. 1982;38(1):109–13.
388. Silverman DJ, Santucci LA, Meyers N, Sekeyova Z. Penetration of host cells by *Rickettsia rickettsii* appears to be mediated by a phospholipase of rickettsial origin. *Infect Immun*. 1992;60(7):2733–40.
389. Walker DH, Feng HM, Popov VL. Rickettsial phospholipase A2 as a pathogenic mechanism in a model of cell injury by typhus and spotted fever group rickettsiae. *Am J Trop Med Hyg*. 2001;65(6):936–42.
390. Renesto P, Dehoux P, Gouin E, Touqui L, Cossart P, Raoult D. Identification and characterization of a phospholipase D-superfamily gene in rickettsiae. *J Infect Dis*. 2003;188(9):1276–83.
391. Cummings BS, McHowat J, Schnellmann RG. Phospholipase A(2)s in cell injury and death. *J Pharmacol Exp Ther*. 2000;294(3):793–9.
392. Sevick EM, Lakowicz JR, Szmanski H, Nowaczyk K, Johnson ML. Frequency domain imaging of absorbers obscured by scattering. *J Photochem Photobiol B*. 1992;16(2):169–85.
393. Hybiske K, Stephens RS. Mechanisms of host cell exit by the intracellular bacterium *Chlamydia*. *Proc Natl Acad Sci U S A*. 2007;104(27):11430–5.
394. Blackman MJ. Malarial proteases and host cell egress: an 'emerging' cascade. *Cell Microbiol*. 2008;10(10):1925–34.
395. Rosenthal PJ. Falcipains and other cysteine proteases of malaria parasites. *Adv Exp Med Biol*. 2011;712:30–48.

396. Yeoh S, O'Donnell RA, Koussis K, Dluzewski AR, Ansell KH, Osborne SA, et al. Subcellular discharge of a serine protease mediates release of invasive malaria parasites from host erythrocytes. *Cell*. 2007;131(6):1072–83.
397. Arastu–Kapur S, Ponder EL, Fonovic UP, Yeoh S, Yuan F, Fonovic M, et al. Identification of proteases that regulate erythrocyte rupture by the malaria parasite *Plasmodium falciparum*. *Nat Chem Biol*. 2008;4(3):203–13.
398. Thomas JA, Tan MSY, Bisson C, Borg A, Umrekar TR, Hackett F, et al. A protease cascade regulates release of the human malaria parasite *Plasmodium falciparum* from host red blood cells. *Nat Microbiol*. 2018;3(4):447–55.
399. Castro–Gomes T, Almeida–Campos FR, Calzavara–Silva CE, da Silva RA, Frezard F, Horta MF. Membrane binding requirements for the cytolytic activity of *Leishmania amazonensis* leishporin. *FEBS Lett*. 2009;583(19):3209–14.
400. Kespichayawattana W, Rattanachetkul S, Wanun T, Utaisincharoen P, Sirisinha S. *Burkholderia pseudomallei* induces cell fusion and actin–associated membrane protrusion: a possible mechanism for cell–to–cell spreading. *Infect Immun*. 2000;68(9):5377–84.
401. French CT, Toesca IJ, Wu TH, Teslaa T, Beaty SM, Wong W, et al. Dissection of the *Burkholderia* intracellular life cycle using a photothermal nanoblade. *Proc Natl Acad Sci U S A*. 2011;108(29):12095–100.
402. Stevens MP, Stevens JM, Jeng RL, Taylor LA, Wood MW, Hawes P, et al. Identification of a bacterial factor required for actin–based motility of *Burkholderia pseudomallei*. *Mol Microbiol*. 2005;56(1):40–53.
403. Tilney LG, Portnoy DA. Actin filaments and the growth, movement, and spread of the intracellular bacterial parasite, *Listeria monocytogenes*. *J Cell Biol*. 1989;109(4 Pt 1):1597–608.
404. Portnoy DA, Auerbuch V, Glomski IJ. The cell biology of *Listeria monocytogenes* infection: the intersection of bacterial pathogenesis and cell–mediated immunity. *J Cell Biol*. 2002;158(3):409–14.
405. Robbins JR, Barth AI, Marquis H, de Hostos EL, Nelson WJ, Theriot JA. *Listeria monocytogenes* exploits normal host cell processes to spread from cell to cell. *J Cell Biol*. 1999;146(6):1333–50.
406. Rajabian T, Gavicherla B, Heisig M, Muller–Altrock S, Goebel W, Gray–Owen SD, et al. The bacterial virulence factor InlC perturbs apical cell junctions and promotes cell–to–cell spread of *Listeria*. *Nat Cell Biol*. 2009;11(10):1212–8.

407. Fattouh R, Kwon H, Czuczman MA, Copeland JW, Pelletier L, Quinlan ME, et al. The diaphanous-related formins promote protrusion formation and cell-to-cell spread of *Listeria monocytogenes*. *J Infect Dis*. 2015;211(7):1185–95.
408. Pust S, Morrison H, Wehland J, Sechi AS, Herrlich P. *Listeria monocytogenes* exploits ERM protein functions to efficiently spread from cell to cell. *EMBO J*. 2005;24(6):1287–300.
409. Chong R, Squires R, Swiss R, Agaisse H. RNAi screen reveals host cell kinases specifically involved in *Listeria monocytogenes* spread from cell to cell. *PLoS One*. 2011;6(8):e23399.
410. Gedde MM, Higgins DE, Tilney LG, Portnoy DA. Role of listeriolysin O in cell-to-cell spread of *Listeria monocytogenes*. *Infect Immun*. 2000;68(2):999–1003.
411. Grundling A, Gonzalez MD, Higgins DE. Requirement of the *Listeria monocytogenes* broad-range phospholipase PC-PLC during infection of human epithelial cells. *J Bacteriol*. 2003;185(21):6295–307.
412. Stamm LM, Pak MA, Morisaki JH, Snapper SB, Rottner K, Lommel S, et al. Role of the WASP family proteins for *Mycobacterium marinum* actin tail formation. *Proc Natl Acad Sci U S A*. 2005;102(41):14837–42.
413. Stamm LM, Morisaki JH, Gao LY, Jeng RL, McDonald KL, Roth R, et al. *Mycobacterium marinum* escapes from phagosomes and is propelled by actin-based motility. *J Exp Med*. 2003;198(9):1361–8.
414. Reed SCO, Lamason RL, Risca VI, Abernathy E, Welch MD. *Rickettsia* actin-based motility occurs in distinct phases mediated by different actin nucleators. *Curr Biol*. 2014;24(1):98–103.
415. Haglund CM, Choe JE, Skau CT, Kovar DR, Welch MD. *Rickettsia Sca2* is a bacterial formin-like mediator of actin-based motility. *Nat Cell Biol*. 2010;12(11):1057–63.
416. Kleba B, Clark TR, Lutter EI, Ellison DW, Hackstadt T. Disruption of the *Rickettsia rickettsii Sca2* autotransporter inhibits actin-based motility. *Infect Immun*. 2010;78(5):2240–7.
417. Lamason RL, Bastounis E, Kafai NM, Serrano R, Del Alamo JC, Theriot JA, et al. *Rickettsia Sca4* Reduces Vinculin-Mediated Intercellular Tension to Promote Spread. *Cell*. 2016;167(3):670–83 e10.
418. Bernardini ML, Mounier J, d'Hauteville H, Coquis-Rondon M, Sansonetti PJ. Identification of *icsA*, a plasmid locus of *Shigella flexneri* that governs bacterial intra- and

intercellular spread through interaction with F-actin. *Proc Natl Acad Sci U S A*. 1989;86(10):3867–71.

419. Leung Y, Ally S, Goldberg MB. Bacterial actin assembly requires toca-1 to relieve N-wasp autoinhibition. *Cell Host Microbe*. 2008;3(1):39–47.

420. Sansonetti PJ, Mounier J, Prevost MC, Mege RM. Cadherin expression is required for the spread of *Shigella flexneri* between epithelial cells. *Cell*. 1994;76(5):829–39.

421. Bishai EA, Sidhu GS, Li W, Dhillon J, Bohil AB, Cheney RE, et al. Myosin-X facilitates *Shigella*-induced membrane protrusions and cell-to-cell spread. *Cell Microbiol*. 2013;15(3):353–67.

422. Heindl JE, Saran I, Yi CR, Lesser CF, Goldberg MB. Requirement for formin-induced actin polymerization during spread of *Shigella flexneri*. *Infect Immun*. 2010;78(1):193–203.

423. Yoshida S, Handa Y, Suzuki T, Ogawa M, Suzuki M, Tamai A, et al. Microtubule-severing activity of *Shigella* is pivotal for intercellular spreading. *Science*. 2006;314(5801):985–9.

424. Germane KL, Ohi R, Goldberg MB, Spiller BW. Structural and functional studies indicate that *Shigella* VirA is not a protease and does not directly destabilize microtubules. *Biochemistry*. 2008;47(39):10241–3.

425. Fukumatsu M, Ogawa M, Arakawa S, Suzuki M, Nakayama K, Shimizu S, et al. *Shigella* targets epithelial tricellular junctions and uses a noncanonical clathrin-dependent endocytic pathway to spread between cells. *Cell Host Microbe*. 2012;11(4):325–36.

426. Welch MD, Way M. Arp2/3-mediated actin-based motility: a tail of pathogen abuse. *Cell Host Microbe*. 2013;14(3):242–55.

427. Volceanov L, Herbst K, Biniossek M, Schilling O, Haller D, Nolke T, et al. Septins arrange F-actin-containing fibers on the *Chlamydia trachomatis* inclusion and are required for normal release of the inclusion by extrusion. *mBio*. 2014;5(5):e01802–14.

428. Lutter EI, Barger AC, Nair V, Hackstadt T. *Chlamydia trachomatis* inclusion membrane protein CT228 recruits elements of the myosin phosphatase pathway to regulate release mechanisms. *Cell Rep*. 2013;3(6):1921–31.

429. Chin E, Kirker K, Zuck M, James G, Hybiske K. Actin recruitment to the *Chlamydia* inclusion is spatiotemporally regulated by a mechanism that requires host and bacterial factors. *PLoS One*. 2012;7(10):e46949.

430. Sturm A, Amino R, van de Sand C, Regen T, Retzlaff S, Rennenberg A, et al. Manipulation of host hepatocytes by the malaria parasite for delivery into liver sinusoids. *Science*. 2006;313(5791):1287–90.
431. Tarun AS, Baer K, Dumpit RF, Gray S, Lejarcegui N, Frevert U, et al. Quantitative isolation and in vivo imaging of malaria parasite liver stages. *Int J Parasitol*. 2006;36(12):1283–93.
432. Graewe S, Rankin KE, Lehmann C, Deschermeier C, Hecht L, Froehlke U, et al. Hostile takeover by Plasmodium: reorganization of parasite and host cell membranes during liver stage egress. *PLoS Pathog*. 2011;7(9):e1002224.
433. Kim MJ, Kim MK, Kang JS. Involvement of lipid rafts in the budding-like exit of *Orientia tsutsugamushi*. *Microb Pathog*. 2013;63:37–43.
434. Urakami H, Tsuruhara T, Tamura A. Electron microscopic studies on intracellular multiplication of *Rickettsia tsutsugamushi* in L cells. *Microbiol Immunol*. 1984;28(11):1191–201.
435. Chen J, de Felipe KS, Clarke M, Lu H, Anderson OR, Segal G, et al. Legionella effectors that promote nonlytic release from protozoa. *Science*. 2004;303(5662):1358–61.
436. Chen J, Reyes M, Clarke M, Shuman HA. Host cell-dependent secretion and translocation of the LepA and LepB effectors of *Legionella pneumophila*. *Cell Microbiol*. 2007;9(7):1660–71.
437. de Felipe KS, Glover RT, Charpentier X, Anderson OR, Reyes M, Pericone CD, et al. Legionella eukaryotic-like type IV substrates interfere with organelle trafficking. *PLoS Pathog*. 2008;4(8):e1000117.
438. Gomez-Valero L, Rusniok C, Cazalet C, Buchrieser C. Comparative and functional genomics of legionella identified eukaryotic like proteins as key players in host-pathogen interactions. *Front Microbiol*. 2011;2:208.
439. Shi X, Halder P, Yavuz H, Jahn R, Shuman HA. Direct targeting of membrane fusion by SNARE mimicry: Convergent evolution of Legionella effectors. *Proc Natl Acad Sci U S A*. 2016;113(31):8807–12.
440. Takeuchi H, Furuta N, Morisaki I, Amano A. Exit of intracellular *Porphyromonas gingivalis* from gingival epithelial cells is mediated by endocytic recycling pathway. *Cell Microbiol*. 2011;13(5):677–91.
441. Yilmaz O, Verbeke P, Lamont RJ, Ojcius DM. Intercellular spreading of *Porphyromonas gingivalis* infection in primary gingival epithelial cells. *Infect Immun*. 2006;74(1):703–10.

442. Takeuchi H, Furuta N, Amano A. Cell entry and exit by periodontal pathogen via recycling pathway. *Commun Integr Biol.* 2011;4(5):587–9.
443. Nolan SJ, Fu MS, Coppens I, Casadevall A. Lipids Affect the *Cryptococcus neoformans*–Macrophage Interaction and Promote Nonlytic Exocytosis. *Infect Immun.* 2017;85(12).
444. Alvarez M, Casadevall A. Phagosome extrusion and host–cell survival after *Cryptococcus neoformans* phagocytosis by macrophages. *Curr Biol.* 2006;16(21):2161–5.
445. Ma H, Croudace JE, Lammas DA, May RC. Expulsion of live pathogenic yeast by macrophages. *Curr Biol.* 2006;16(21):2156–60.
446. Johnston SA, May RC. The human fungal pathogen *Cryptococcus neoformans* escapes macrophages by a phagosome emptying mechanism that is inhibited by Arp2/3 complex–mediated actin polymerisation. *PLoS Pathog.* 2010;6(8):e1001041.
447. Chayakulkeeree M, Johnston SA, Oei JB, Lev S, Williamson PR, Wilson CF, et al. SEC14 is a specific requirement for secretion of phospholipase B1 and pathogenicity of *Cryptococcus neoformans*. *Mol Microbiol.* 2011;80(4):1088–101.
448. Nicola AM, Robertson EJ, Albuquerque P, Derengowski Lda S, Casadevall A. Nonlytic exocytosis of *Cryptococcus neoformans* from macrophages occurs in vivo and is influenced by phagosomal pH. *mBio.* 2011;2(4).
449. Alvarez M, Casadevall A. Cell–to–cell spread and massive vacuole formation after *Cryptococcus neoformans* infection of murine macrophages. *BMC Immunol.* 2007;8:16.
450. Stukes SA, Cohen HW, Casadevall A. Temporal kinetics and quantitative analysis of *Cryptococcus neoformans* nonlytic exocytosis. *Infect Immun.* 2014;82(5):2059–67.
451. Johnston SA, May RC. *Cryptococcus* interactions with macrophages: evasion and manipulation of the phagosome by a fungal pathogen. *Cell Microbiol.* 2013;15(3):403–11.
452. Sudhof TC, Rizo J. Synaptic vesicle exocytosis. *Cold Spring Harb Perspect Biol.* 2011;3(12).
453. Ireton K, Van Ngo H, Bhalla M. Interaction of microbial pathogens with host exocytic pathways. *Cell Microbiol.* 2018;20(8):e12861.
454. Russell DG, Huang L, VanderVen BC. Immunometabolism at the interface between macrophages and pathogens. *Nat Rev Immunol.* 2019;19(5):291–304.
455. O'Neill LA, Pearce EJ. Immunometabolism governs dendritic cell and macrophage function. *J Exp Med.* 2016;213(1):15–23.

456. Escoll P, Buchrieser C. Metabolic reprogramming: an innate cellular defence mechanism against intracellular bacteria? *Curr Opin Immunol.* 2019;60:117–23.
457. Rabhi I, Rabhi S, Ben-Othman R, Rasche A, Daskalaki A, Trentin B, et al. Transcriptomic signature of *Leishmania* infected mice macrophages: a metabolic point of view. *PLoS Negl Trop Dis.* 2012;6(8):e1763.
458. Freerman AJ, Johnson AR, Sacks GN, Milner JJ, Kirk EL, Troester MA, et al. Metabolic reprogramming of macrophages: glucose transporter 1 (GLUT1)-mediated glucose metabolism drives a proinflammatory phenotype. *J Biol Chem.* 2014;289(11):7884–96.
459. Cho H, Kwon HY, Sharma A, Lee SH, Liu X, Miyamoto N, et al. Visualizing inflammation with an M1 macrophage selective probe via GLUT1 as the gating target. *Nat Commun.* 2022;13(1):5974.
460. McConville MJ, Saunders EC, Kloehn J, Dagley MJ. *Leishmania* carbon metabolism in the macrophage phagolysosome– feast or famine? *F1000Res.* 2015;4(F1000 Faculty Rev):938.
461. Saunders EC, McConville MJ. Immunometabolism of *Leishmania* granulomas. *Immunol Cell Biol.* 2020;98(10):832–44.
462. Burchmore RJ, Rodriguez-Contreras D, McBride K, Merkel P, Barrett MP, Modi G, et al. Genetic characterization of glucose transporter function in *Leishmania mexicana*. *Proc Natl Acad Sci U S A.* 2003;100(7):3901–6.
463. Acevedo Ospina H, Guay-Vincent MM, Descoteaux A. Macrophage Mitochondrial Biogenesis and Metabolic Reprogramming Induced by *Leishmania donovani* Require Lipophosphoglycan and Type I Interferon Signaling. *mBio.* 2022;13(6):e0257822.
464. Locasale JW. New concepts in feedback regulation of glucose metabolism. *Curr Opin Syst Biol.* 2018;8:32–8.
465. Rosenzweig D, Smith D, Opperdoes F, Stern S, Olafson RW, Zilberstein D. Retooling *Leishmania* metabolism: from sand fly gut to human macrophage. *FASEB J.* 2008;22(2):590–602.
466. Moreira D, Rodrigues V, Abengoza M, Rivas L, Rial E, Laforge M, et al. *Leishmania infantum* modulates host macrophage mitochondrial metabolism by hijacking the SIRT1–AMPK axis. *PLoS Pathog.* 2015;11(3):e1004684.
467. Saunders EC, Ng WW, Kloehn J, Chambers JM, Ng M, McConville MJ. Induction of a stringent metabolic response in intracellular stages of *Leishmania mexicana* leads to increased dependence on mitochondrial metabolism. *PLoS Pathog.* 2014;10(1):e1003888.

468. Jha AK, Huang SC, Sergushichev A, Lampropoulou V, Ivanova Y, Loginicheva E, et al. Network integration of parallel metabolic and transcriptional data reveals metabolic modules that regulate macrophage polarization. *Immunity*. 2015;42(3):419–30.
469. Rodriguez-Prados JC, Traves PG, Cuenca J, Rico D, Aragonés J, Martín-Sanz P, et al. Substrate fate in activated macrophages: a comparison between innate, classic, and alternative activation. *J Immunol*. 2010;185(1):605–14.
470. Soto-Herederó G, Gomez de Las Heras MM, Gabande-Rodríguez E, Oller J, Mittelbrunn M. Glycolysis – a key player in the inflammatory response. *FEBS J*. 2020;287(16):3350–69.
471. Teodoro JS, Rolo AP, Palmeira CM. The NAD ratio redox paradox: why does too much reductive power cause oxidative stress? *Toxicol Mech Methods*. 2013;23(5):297–302.
472. Hackett EE, Charles-Messance H, O'Leary SM, Gleeson LE, Muñoz-Wolf N, Case S, et al. Mycobacterium tuberculosis Limits Host Glycolysis and IL-1β by Restriction of PFK-M via MicroRNA-21. *Cell Rep*. 2020;30(1):124–36 e4.
473. Gleeson LE, Sheedy FJ, Palsson-McDermott EM, Triglia D, O'Leary SM, O'Sullivan MP, et al. Cutting Edge: Mycobacterium tuberculosis Induces Aerobic Glycolysis in Human Alveolar Macrophages That Is Required for Control of Intracellular Bacillary Replication. *J Immunol*. 2016;196(6):2444–9.
474. Gleeson LE, O'Leary SM, Ryan D, McLaughlin AM, Sheedy FJ, Keane J. Cigarette Smoking Impairs the Bioenergetic Immune Response to Mycobacterium tuberculosis Infection. *Am J Respir Cell Mol Biol*. 2018;59(5):572–9.
475. Huang L, Nazarova EV, Tan S, Liu Y, Russell DG. Growth of Mycobacterium tuberculosis in vivo segregates with host macrophage metabolism and ontogeny. *J Exp Med*. 2018;215(4):1135–52.
476. Gatto M, Borim PA, Wolf IR, Fukuta da Cruz T, Ferreira Mota GA, Marques Braz AM, et al. Transcriptional analysis of THP-1 cells infected with Leishmania infantum indicates no activation of the inflammasome platform. *PLoS Negl Trop Dis*. 2020;14(1):e0007949.
477. Okuda K, Tong M, Dempsey B, Moore KJ, Gazzinelli RT, Silverman N. Leishmania amazonensis Engages CD36 to Drive Parasitophorous Vacuole Maturation. *PLoS Pathog*. 2016;12(6):e1005669.
478. Bichiou H, Rabhi S, Ben Hamda C, Bouabid C, Belghith M, Piquemal D, et al. Leishmania Parasites Differently Regulate Antioxidant Genes in Macrophages Derived From Resistant and Susceptible Mice. *Front Cell Infect Microbiol*. 2021;11:748738.

479. Prabhudas M, Bowdish D, Drickamer K, Febbraio M, Herz J, Kobzik L, et al. Standardizing scavenger receptor nomenclature. *J Immunol*. 2014;192(5):1997–2006.
480. Glatz JFC, Nabben M, Luiken J. CD36 (SR-B2) as master regulator of cellular fatty acid homeostasis. *Curr Opin Lipidol*. 2022;33(2):103–11.
481. Semini G, Paape D, Paterou A, Schroeder J, Barrios-Llerena M, Aebischer T. Changes to cholesterol trafficking in macrophages by *Leishmania* parasites infection. *Microbiologyopen*. 2017;6(4).
482. Rub A, Dey R, Jadhav M, Kamat R, Chakkaramakkil S, Majumdar S, et al. Cholesterol depletion associated with *Leishmania major* infection alters macrophage CD40 signalosome composition and effector function. *Nat Immunol*. 2009;10(3):273–80.
483. Mukherjee M, Basu Ball W, Das PK. *Leishmania donovani* activates SREBP2 to modulate macrophage membrane cholesterol and mitochondrial oxidants for establishment of infection. *Int J Biochem Cell Biol*. 2014;55:196–208.
484. Antoine JC, Prina E, Jouanne C, Bongrand P. Parasitophorous vacuoles of *Leishmania amazonensis*-infected macrophages maintain an acidic pH. *Infect Immun*. 1990;58(3):779–87.
485. Cocchiari JL, Kumar Y, Fischer ER, Hackstadt T, Valdivia RH. Cytoplasmic lipid droplets are translocated into the lumen of the *Chlamydia trachomatis* parasitophorous vacuole. *Proc Natl Acad Sci U S A*. 2008;105(27):9379–84.
486. Ding Z, Liu S, Wang X, Theus S, Deng X, Fan Y, et al. PCSK9 regulates expression of scavenger receptors and ox-LDL uptake in macrophages. *Cardiovasc Res*. 2018;114(8):1145–53.
487. Agmon E, Stockwell BR. Lipid homeostasis and regulated cell death. *Curr Opin Chem Biol*. 2017;39:83–9.
488. Flores-Romero H, Ros U, Garcia-Saez AJ. A lipid perspective on regulated cell death. *Int Rev Cell Mol Biol*. 2020;351:197–236.
489. Pennathur S, Pasichnyk K, Bahrami NM, Zeng L, Febbraio M, Yamaguchi I, et al. The macrophage phagocytic receptor CD36 promotes fibrogenic pathways on removal of apoptotic cells during chronic kidney injury. *Am J Pathol*. 2015;185(8):2232–45.
490. Woo MS, Yang J, Beltran C, Cho S. Cell Surface CD36 Protein in Monocyte/Macrophage Contributes to Phagocytosis during the Resolution Phase of Ischemic Stroke in Mice. *J Biol Chem*. 2016;291(45):23654–61.

491. Chen Y, Zhang J, Cui W, Silverstein RL. CD36, a signaling receptor and fatty acid transporter that regulates immune cell metabolism and fate. *J Exp Med*. 2022;219(6).
492. Geier H, Celli J. Phagocytic receptors dictate phagosomal escape and intracellular proliferation of *Francisella tularensis*. *Infect Immun*. 2011;79(6):2204–14.
493. Airapetov MI, Eresko SO, Ignatova PD, Lebedev AA, Bychkov ER, Shabanov PD. Interleukin-11 in Pathologies of the Nervous System. *Mol Biol*. 2023;57(1):1–6.
494. Iniesta V, Carcelen J, Molano I, Peixoto PM, Redondo E, Parra P, et al. Arginase I induction during *Leishmania major* infection mediates the development of disease. *Infect Immun*. 2005;73(9):6085–90.
495. Kropf P, Fuentes JM, Fahrnich E, Arpa L, Herath S, Weber V, et al. Arginase and polyamine synthesis are key factors in the regulation of experimental leishmaniasis in vivo. *FASEB J*. 2005;19(8):1000–2.
496. Munder M, Choi BS, Rogers M, Kropf P. L-arginine deprivation impairs *Leishmania major*-specific T-cell responses. *Eur J Immunol*. 2009;39(8):2161–72.
497. Puleston DJ, Pearce EL. Appetite for Arginine: Metabolic Control of Macrophage Hunger. *Cell Metab*. 2020;31(3):441–2.
498. Huynh C, Sacks DL, Andrews NW. A *Leishmania amazonensis* ZIP family iron transporter is essential for parasite replication within macrophage phagolysosomes. *J Exp Med*. 2006;203(10):2363–75.
499. Rodrigues V, Andre S, Maksouri H, Mouttaki T, Chiheb S, Riyad M, et al. Transcriptional Analysis of Human Skin Lesions Identifies Tryptophan-2,3-Deoxygenase as a Restriction Factor for Cutaneous *Leishmania*. *Front Cell Infect Microbiol*. 2019;9:338.
500. Stelzner K, Winkler AC, Liang C, Boyny A, Ade CP, Dandekar T, et al. Intracellular *Staphylococcus aureus* Perturbs the Host Cell Ca<sup>2+</sup> Homeostasis To Promote Cell Death. *mBio*. 2020;11(6).

## 7. APPENDIX

### 7.1 Macro for vessel distance analysis

```
waitForUser("Import the .xls file containing the blood vessel positions with the File/Import/Results pathway then click OK");
```

```
VesselCount=nResults();
```

```
VesselX=newArray(VesselCount);
```

```
VesselY=newArray(VesselCount);
```

```
VesselZ=newArray(VesselCount);
```

```
for (i=0; i<VesselCount; i++) {
```

```
    VesselX[i]=getResult("X", i);
```

```
    VesselY[i]=getResult("Y", i);
```

```
    VesselZ[i]=getResult("Z", i);
```

```
    //print(i, LeishX[i], LeishY[i]);
```

```
}
```

```
//imports all blood vessel positions from a microscopy dataset and generates a data array with x, y, z positions
```

```
waitForUser("Import the xls file containing the Leishmania positions with the File/Import/Results pathway then click OK");
```

```
//opens a results file with Leishmania x, y, z positions and fluorescence values
```

```
LeishmaniaCount=nResults();
```

```
for (j=0; j<LeishmaniaCount; j++) {  
  
    dLeishMin= 13000000;  
  
    for (k=0; k<VesselCount; k++) {  
  
        Xpos=getResult("X", j);  
        Ypos=getResult("Y", j);  
        Zpos=getResult("Z", j);  
  
        dLeish=sqrt(((Xpos-VesselX[k])*(Xpos-VesselX[k]))+((Ypos-VesselY[k])*(Ypos-VesselY[k]))+((Zpos-VesselZ[k])*(Zpos-VesselZ[k])));  
  
        if (dLeish<dLeishMin) {  
  
            dLeishMin=dLeish;  
  
        }  
  
    }  
  
    setResult ("MinVesselDist", j, round(dLeishMin));  
  
}
```

//calculates for each Leishmania object the distance to the closest blood vessel object and stores the calculates distance with the Leishmania object